8-2012

# Absorber Geometry Optimization for a New Wave Energy Converter

Durren

ABSORBER GEOMETRY OPTIMIZATION FOR A
NEW WAVE ENERGY CONVERTOR

by

Rachel A. Durren

A Thesis
Submitted to the
Faculty of The Graduate College
in partial fulfillment of the
requirements for the
Degree of Master of Science in Engineering (Mechanical)
Department of Mechanical and Aeronautical Engineering
Advisor: Parviz Merati, Ph.D.

Western Michigan University
Kalamazoo, Michigan
August 2012

THE GRADUATE COLLEGE
WESTERN MICHIGAN UNIVERSITY
KALAMAZOO, MICHIGAN

Date _____ 7/9/12 _____

WE HEREBY APPROVE THE THESIS SUBMITTED BY

_____ Rachel A. Durren _____

ENTITLED _ABSORBER GEOMETRY OPTIMIZATION FOR A NEW WAVE_____

ENERGY CONVERTOR_____

AS PARTIAL FULFILLMENT OF THE REQUIREMENTS FOR THE

DEGREE OF ____Master of Science in Engineering (Mechanical)_____

Mechanical and Aeronautical Engineering_____
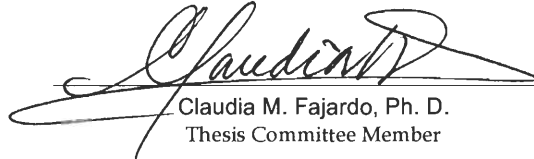             (Department)

Parviz Merati, Ph.D.
Thesis Committee Chair

Mechanical Engineering_____
             (Program)

Claudia M. Fajardo, Ph. D.
Thesis Committee Member

Tianshu Liu, Ph.D.
Thesis Committee Member

APPROVED

_____
Dean of The Graduate College

Date _____August 2012_____

ABSORBER GEOMETRY OPTIMIZATION FOR A
NEW WAVE ENERGY CONVERTOR

Rachel A. Durren, M.S.E.

Western Michigan University, 2012

Alternative energy technologies are on the forefront of research due to the rising costs of oil and natural gas. One relatively under development source of energy is ocean waves. In order to make the use of ocean waves economically viable, the amount of energy absorbed by wave energy convertors (WEC) must be optimized. The research within presents a new conceptual design, "Aqua Fly", for a WEC with emphasis on maximizing the amount of energy absorbed. The energy absorption component of the "Aqua Fly" was isolated and a small scale 2-D study of energy absorption. First, the amount of energy in the wave was increased by adding a reflection to the system and creating a standing wave in the tank.. It was found that by placing the trailing edge of the wing in an anti-node the maximum amount of energy can be absorbed. The geometry of the wing was then varied to find the optimum configuration of reflection plate location and wing geometry for energy absorption. It was found that using a wing with a 90° downward bend into the water and a reflection plate placed at 0 wavelengths from the trailing edge of the wing allowed for the optimum energy absorption.

# ACKNOWLEDGMENTS

TABLE OF CONTENTS

Table of Contents-Continued

CHAPTER

LIST OF TABLES

LIST OF FIGURES

# CHAPTER 1

# INTRODUCTION

## Ocean Waves

All waves are produced by some form of resonating force. There are many different resonating forces which produce waves in the ocean. These include capillary waves, wind waves, tsunamis, internal waves, storm surges, tides, and planetary waves. The most common wave in the ocean is wind waves (Mei, 1989).

Wind waves can be classified as two different types. The first is wind seas which are created by the forcing of local wind. The wavelengths of wind seas can vary from a few meters to 500m depending on the magnitude of the wind. The second is produced from storms and spread across the ocean with little energy loss. This type of wave is called swells and has wavelengths between 100- 500m. These two types of waves can exist on their own or in combination with each other (Mei, 1989).

Wind waves are created at the air water interface and can be classified as a form of concentrated solar energy (Brekken, 2009). Waves have an increased intensity on the order of 30 times that of solar energy and six times that of wind (Falnes, 2007). The uneven solar heating of the earth's surface creates wind and the wind interaction with the ocean surface creates the waves. These waves travel in the direction of the local wind and can travel for thousands of miles with little attenuation (Brekken, 2009).

In the entire open ocean, there are approximately 8000-80000TWh/yr or 1-10 TW per year of available energy. This is comparable with the current amount of energy consumed per year on earth (Falnes, 2007).

Not all locations are ideal climates for wave energy. Generally, locations on the west coast of land masses at latitudes above 40° north and south of the equator is where the wave energy is the greatest. Since most weather patterns move from west to east, regions on the west coast of land masses are more conducive to wave energy production. These regions include Scotland, Northern Canada, Southern Africa, and the Northwestern United States (US Department of Energy, 2009).

Even in the optimal locations, wave energy varies throughout the year with about six times more available energy in the winter compared to the summer months. However, waves can be predicted several days in advance and are continuous. An average wave transmits energy on the order of 10-50 kW/m in the open ocean (Falnes, 2007). As a wave approaches land the available energy decreases due to frictional loss from the ocean floor (Twidell, Weir, 2007).

The total energy of the wave is split between kinetic and potential energy with equal proportion (Twidell, Weir, 2007). The kinetic energy is due to the wave motion, while the potential energy, is due to the mechanical work being performed to produce the elevation difference at the water surface. The pressure differential between the wave peak and wave trough causes the increase of wave elevation which is governed by the Bernoulli principle (Brekken, 2009).

Motion of a particle in a wind wave.
A = At deep water. The orbital motion of fluid particles decreases rapidly with increasing depth below the surface.
B = At shallow water (sea floor is now at B). The elliptical movement of a fluid particle flattens with decreasing depth.
1 = Propagation direction.
2 = Wave crest.
3 = Wave trough.
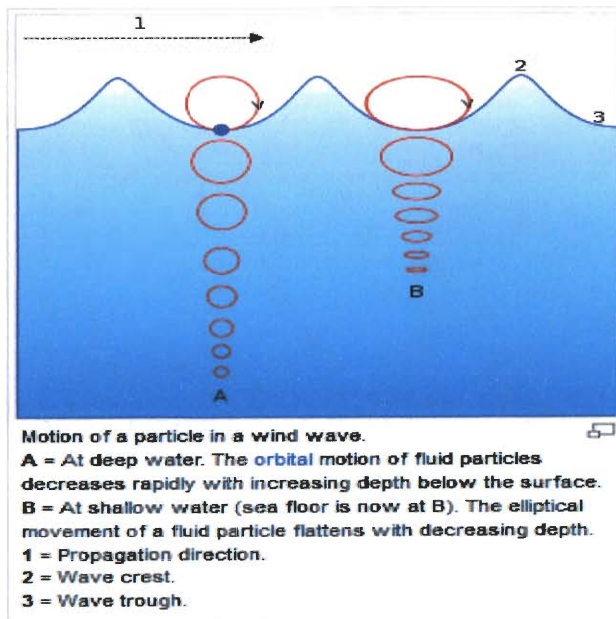
**Figure 1.1 Wave particle motion in both shallow and deep water (Spinka, 2008)**

The depth of the ocean bottom in relationship to the wavelength of the wave has a direct effect on the motion of the wave particles (Twidell, Weir, 2007). The motion and energy of wave particles decrease with the depth of the water (Figure 1.1). When the water depth is greater than or equal to half the wavelength of the wave, the water is considered deep. For deep water, the particle motion takes on a circular path that decreases in amplitude with the depth of the water. However, in shallow water the path becomes elliptical and some to the energy is absorbed by the friction of the ocean floor (Twidell, Weir, 2007).

There are two main components to wave motion. The first is velocity field of the wave; the velocity of a wave is at a maximum near its crest and decreases with depth. The trajectory of this motion is mainly in the direction of the wave front also known as surge. The heaving or up down velocity is minimal at the wave crest. Based on this, the largest kinetic energy of the wave is at its crest and decreases with depth.

The second important component of wave motion is the wave particle motion. Wave particles move in a circular path near the surface of the water. They have motion in both the surge and heave directions (Figure 1.2). The diameter of the circular path decreases with depth so the largest potential energy is at the surface of the wave. Based on the understanding of both the wave velocity field and particle motion, a more efficient wave energy device can be designed. It should capture both the surge and heave of the wave at the surface where the energy is greatest.
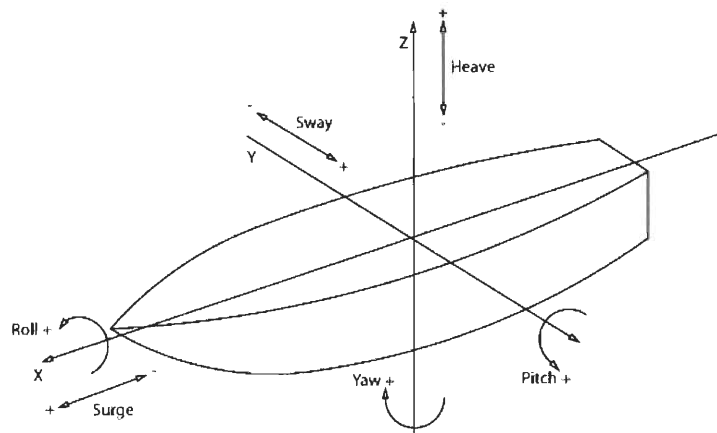


**Figure 1.2 Definition of surge and heave (Ship Motion Control)**

**Wave Energy Conversion**

The harnessing of wave energy is relatively underdeveloped; however the concept goes back over 200 years (Clement, 2002). There are two steps in the energy conversion process. First, all wave energy convertors function based on the law of conservation of energy. They have some mechanisms which resist the work of a wave, or in other words the wave energy convertor causes destructive wave interference. The second step is for the mechanical energy to be converted to a more useable form (Falnes, 2007).

There are several methods used for classifying wave energy convertors. These include their location offshore, the type of technology used for energy conversion, and

4

the end use of the captured energy. Wave energy convertors can be placed in many different locations with respect to the shore such as on-shore, offshore, or near shore. They also can be placed in many different locations in the water: floating, submerged, and bottom-standing. The energy conversion technology can be mechanical, pneumatic, hydraulic or directly electrical. The end use of the wave energy can range from electricity, water pumping, desalination, refrigeration, water heating, and propulsion (Sbazehgar, 2009).

Many times, the convertors are classified by their horizontal extension in accordance to the typical wavelength. One technology is the point absorber, which is small compared to the wavelength. Another group is comparable in size to the wavelength of the wave and is classified depending on their orientation to the wave. These include "terminator devices", which lie perpendicular to the wave and are usually close to shore and attenuators which lye parallel to the wave motion (Falnes, 2007).

There are several wave energy convertors (WEC) in various stages of development being researched or produced in the following countries worldwide: United Kingdom, Portugal, Ireland, Norway, Sweden, Denmark, and the United States. Most of the current research is being completed on the point absorber type of wave energy convertor (Table 1.1).

**Table 1.1 Examples of current Wave Energy Convertors (WEC) both in development and production**

| Concepts in Development | | |
|---|---|---|
| **Research Institute** | **Type of WEC** | **Description** |
| Stevens Institute of Technology | point absorber | A bouy attached to an electrical generator which is tethered to the ocean floor. The lift force on the buoy transfers from a cable through gear boxes to a generator. (Rafftery,M. ) |
| Lysekil research site | point absorber | A bouy system with a direct drive linear generator to convert the mechanical energy to electricity.(Leijon) |
| Oregon State University | point absorber | A buoy with a direct drive system made up of 2 parts a buoy and a spar which contains an array of magnets. As the bouy and magnets move up and down relative to the spar, which is morred to the ocean floor to reduce heave, voltage is incued in the armature. (Brekken) |
| Instituto Superior de Engenharia de Coimbra | point absorber | The Archimeded Wave Swing is a off shore full submerged wave energy convertor. It consits of a floater and a siloas the pressure of the water changes from the oscillating waves the floater compressees air inside the silo which is converted to energy with a linear generator. (Valerio) |
| Uppsala University | point absorber | As the bouy heave with the wave motion the mechanical motion is converted to electricictywith a linear generator. (Bernhoff) |
| Commmercial Products | | |
| **Company** | **Type of WEC** | **Description** |
| Pelamis Wave Power Ltd. | attenuator | The Pelamis wave power system consists of semi submerged cylinders linked by hinged joints with hydrualic pumps. The motion of the cylinders at the hinges is converted into hydrualic pressure. The hydrualic pressure is converted to electricity. (Henderson) |
| Haydam Ltd | attenuator | The MCCabe Wave Power Pump consitis of semi submerged cylinders linked by hinged joints with hydrualic pumps. The motion of the cylinders at the hinges is converted into hydrualic pressure. The hydrualic pressure is converted to electricity. (McCormick) |
| Ocean Power Technology | point absorber | A buoy attached to a submeregd platform where the mechanical heaving of the buoy with respect to the platform runs a linear electrical generator. |

One technology of particular interest for the current research is the Cockerell raft. It was one of the early wave energy technologies and was developed in 1972 by Sir Christopher Cockerell. In initial development, it was modeled as a series of rafts attached by hinges. The pressure of the of the ocean waves transmitted to the rafts and the motion of the rafts relative to one another applied a torque to the hinges and absorbed the ocean energy.

Through initial testing, founded by the British Department of Energy, a 1/50 scale design was tested in a laboratory wave tank and efficiencies as high as 80% were reached. It was also discovered that the weight of the raft was not of great importance as long as contact with the water was maintained. It was found that the damping of the power take off system, marine fouling, and positioning of mooring had little effect on the efficiency of the device. They also discovered that the torque of the hinges would have to be large to account for the small movements of the raft (Sir Christopher Cockerell, 1978).

Through testing it was verified that the design could be a set of two rafts. A smaller forward raft attached to a larger raft. The larger raft had two purposes. First it was the reaction frame for the smaller raft to rotate about. Secondly, it added an anti-node to the system by preventing the wave from travelling passed the device.

Sir Cockerell and his team later abandoned this idea. They believed it was too hard to find a balance of torque and size for extreme wave conditions while maintaining high efficiencies in standard wave conditions (S.H. Salter, 1989).

**Initial Research**

It was found that most of the work in the field of wave energy conversion was on the conversion systems for point absorbers. Several researches have proposed

7

different types of conversion systems including work by Jin-Seok Oh, Jong-Do Kim, Jong Ho Lee, Han-IL Park and Toshimistu Komatsu et al 2007 on using a water column inside the point absorber. Large scale trails of a linear generator were preformed in the North Sea by researchers at Lysekil Research Site (Leijon, 2008). Others have looked at linear generators including Valerio, Beirao, and Costa et al 2007, while Luan, Onar, and Khaligh et al 2009, looked at the use of a permanent magnet linear generator. A cable integrated reel harnessing and anchoring system was developed at Stevens Institute of Technology for energy conversion (Raferty, 2007).

There was also some limited work in the field of optimizing energy absorption through the interaction of point absorbers with waves. Johannes Falnes et al 1978 one of the leaders in ocean wave energy research found that a wave absorber most be a good wave generator. He also found that by adding a reflection to the system by properly placing the point absorbers in relationship to each other or another reflector could increase the amount of energy absorbed. This was supported by work completed by Bernhoff et al 2008 in the Baltic Sea and his investigation on the potential of using sheltered seas for energy absorption. Falnes was also credited with finding that the point absorber must be in resonance with the wave frequency for optimum absorption. Researchers at the University of California presented an idea for a novel point absorber device that would add an excitation force to the system by using a square wave modulation of the masses of the wave energy convertor (Orazov, 2010).

It was proposed by Newman et al 1978 and supported by his analytical work that a raft system with two hinges was the optimum configuration for energy absorption. This was also supported by the experiments preformed on the Cockerell raft as discussed

previously. However, there was little published research found on the development of attenuator type wave energy convertors. With the research being limited to the development of the conversion systems (Henderson, R. 2006).

Since there was little research on the fundamentals of wave interaction with the attenuator type absorber, this presented a good opportunity to look into optimizing this interaction to increase energy absorption. Researchers at WMU decided to take on this task and preformed some initial research to develop a better understanding of the wave absorber interaction using some of the principals developed by Falnes for point absorbers as a starting point.
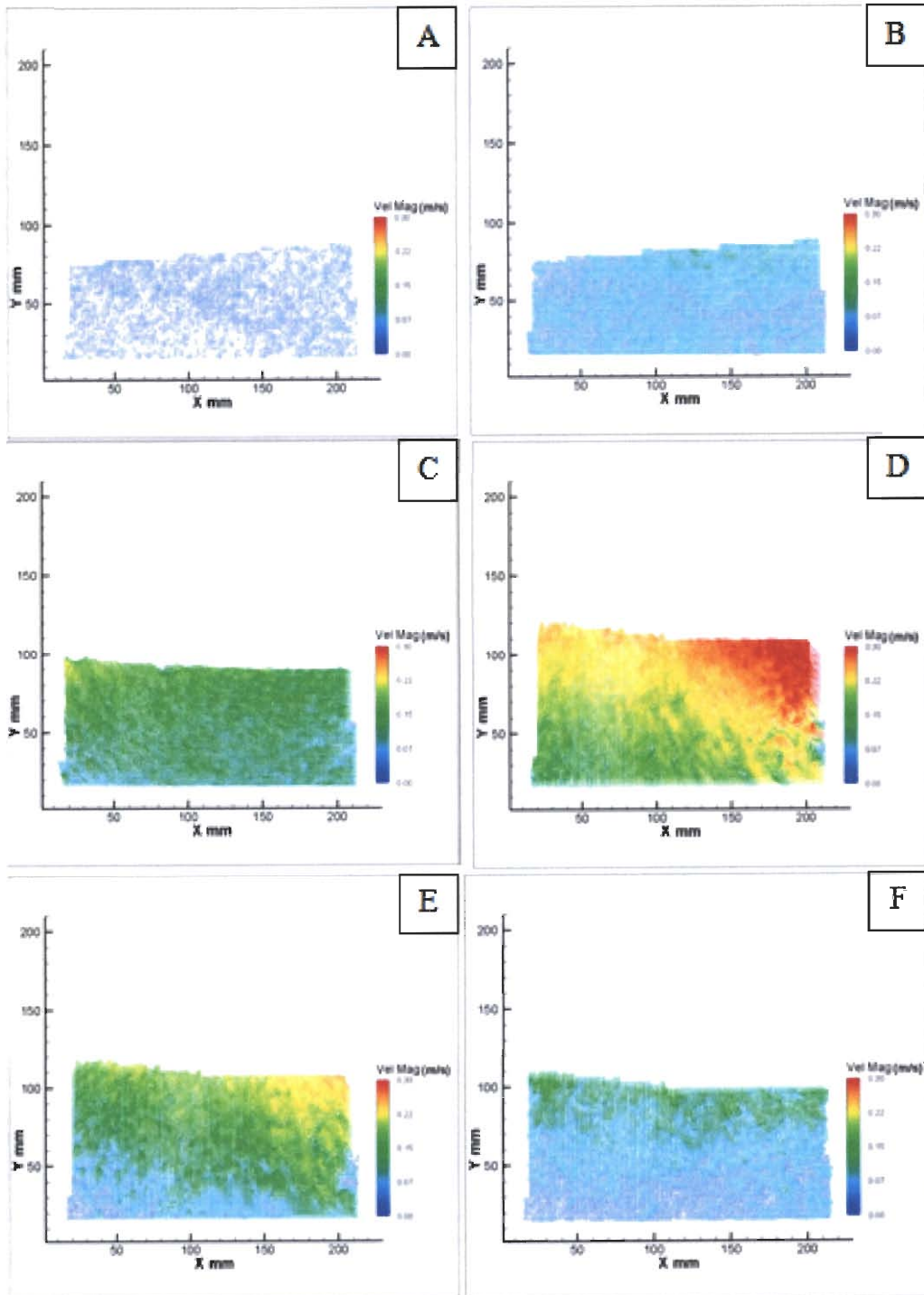
Figure 1.3 Velocity profile of an ascending wave in the wave tank at WMU
A: Calm Water, B: Wave beginning to propagate, C: Wave ascending to its crest
D: Wave at its peak, E-F: Wave descending back to calm water

In order to form a better understanding of wave motion, PIV (Particle Image Velocimetry) testing was performed in the wave tank at the WMU Fluid Dynamics Lab by a previous researcher. The velocity profile of a wave can be seen in Figure 1.3. The figure shows the instantaneous velocity profile of an ascending wave at different instances taken with PIV. It was seen that the particle motion of the wave described above holds true in the wave tank. As the depth of the water in the tank increases, the velocity of the fluid particles decreases and as the wave reaches its peak or crest it also reaches its maximum velocity and kinetic energy (D in Figure 1.4).

Computer simulations of the wave were also conducted using CFX for computational calculations. These studies concentrated on the energy extraction step of the wave energy conversion process. For these studies, a flat plate that lies on the water surface was used to absorb the wave energy. The goal was to increase the efficiency of the device by altering the geometry and wave conditions. The plate was placed in a wave take with the input of the wave being modeled as a cosine wave and the outlet placed downstream of the plate.

During the development of the computational model, it was seen that by varying the outlet boundary condition (BC) between a wall and an opening the torque produced about the leading edge of the plate would vary. By analyzing the velocity vectors of the wave for the different outlet BC, it was discovered that, depending on the outlet condition the wave would either be reflected or exit the tank. When the outlet was modeled as a wall, the wave was reflected back toward the plate creating a reflection. However, when the outlet was modeled as an opening the water freely exited the tank eliminating the reflection.
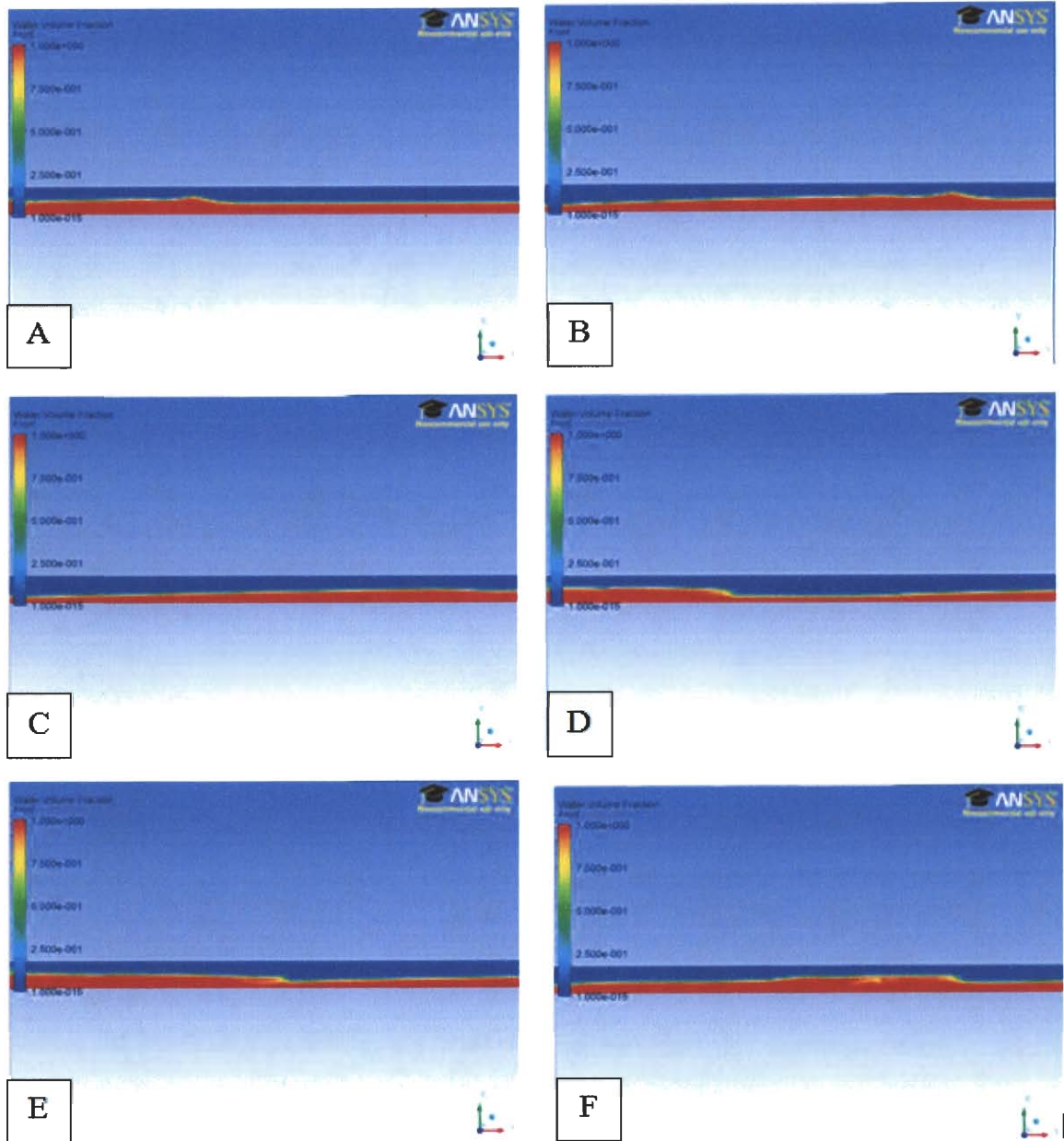
**Figure 1.4 Water volume fraction of a reflected wave in the CFX model**
**A: Wave propagating down tank from inlet, B: Wave approaching outlet**
**C: Wave reaching tank outlet, D: New wave from outlet (left) and reflection (right)**
**E. Reflection and wave approaching each other, F: Reflection and wave meeting at tank center increasing**
**amplitude**

Figure 1.4 shows the water volume fraction of a wave with a reflection. It is seen

in photo F that as the wave from the inlet (left) and the outlet (right) meet in the center of

the tank the amplitude of the wave increases. The increased wave amplitude corresponds

to an increase in torque on the plate (Figure 1.5). However, when the effects of the reflection were minimized, the torque on the plate decreased. By comparing the power spectral density curves for these two cases, it was confirmed that the energy absorbed by the plate increased when a reflection was applied to the system. The area under the power curve was proportional to the energy absorbed by the plate (Figure 1.6).
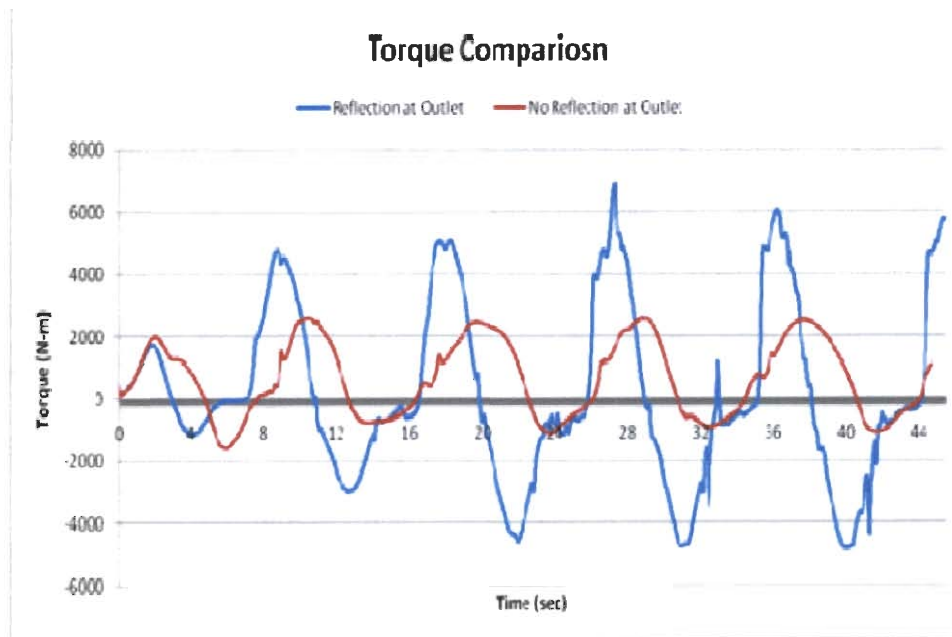


**Figure 1.5 Comparison of the torque on the wing for a reflected and non-reflected outlet in CFX**
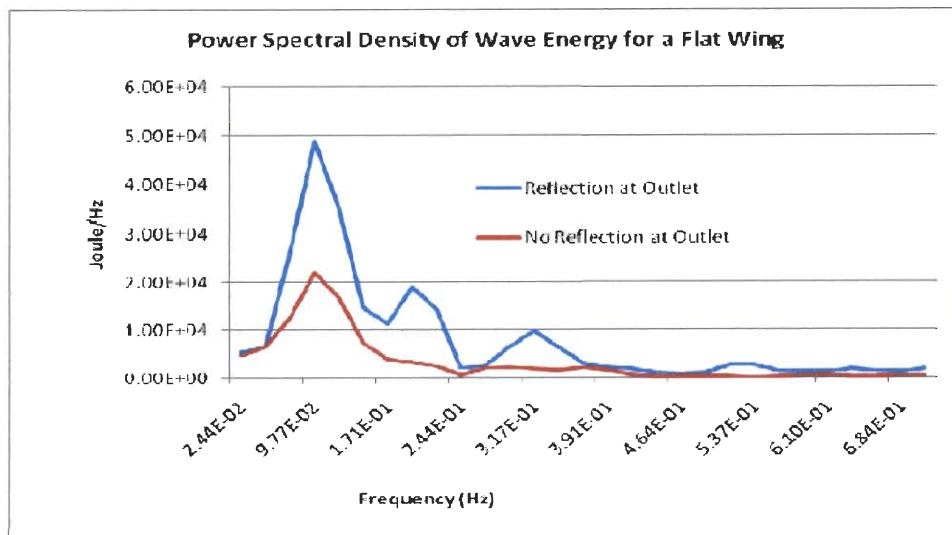


**Figure 1.6 Comparison of power spectral density for a reflected and non-reflected outlet modeled in CFX**

Using the computational model, the plate geometry was also changed to investigate the effect of its geometry on torque and energy absorption. Figure 1.7 shows that the amount of torque absorbed by the system increased when varying the geometry of the wing the reason for this increase in torque was due to the interaction of the wave and the downward bend under the surface of the water. Since energy increased with torque as seen in Figure 1.5 and 1.6, the geometry of the wing will affect energy absorption.
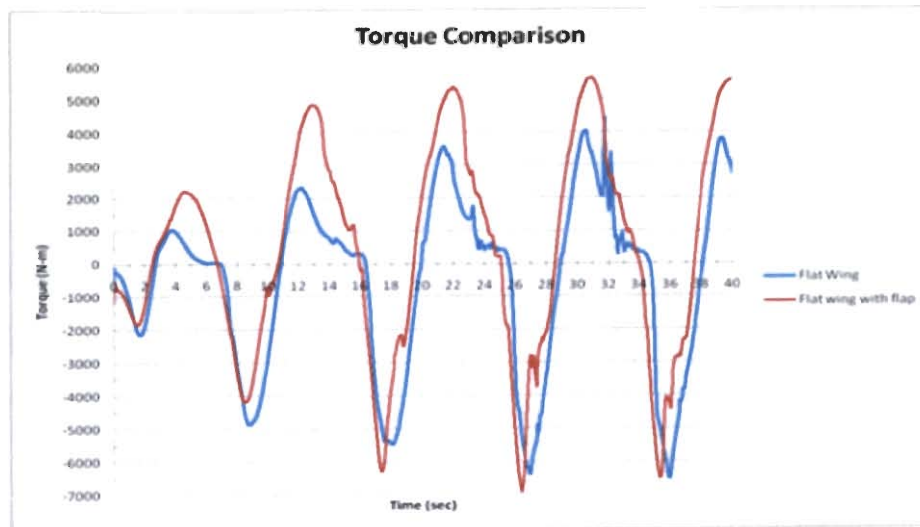


Figure 1.7 Torque comparison for varying wing geometries modeled in CFX

These initial results were used to develop the experiments to be discussed later.

**Conceptual Design**

Based on the results of the initial research a conceptual design was developed. The design of a WEC must take into account both steps of the wave energy conversion process. For the energy extraction step, the WEC must be made such that it absorbs as much of the incoming wave motion as possible. In the conceptual design of the "aqua

14

fly", this step was supported by the PIV testing completed at WMU. This design also uses some similar concepts to that of the Cockerell rafts.

For the energy conversion step, hydraulics, which are already widely used in the wave energy industry, are implemented to convert the mechanical energy to a useable form. Combining the already accepted concepts with the information on wave particle motion, the conceptual "Aqua-Fly" design was developed (Figure 1.8).
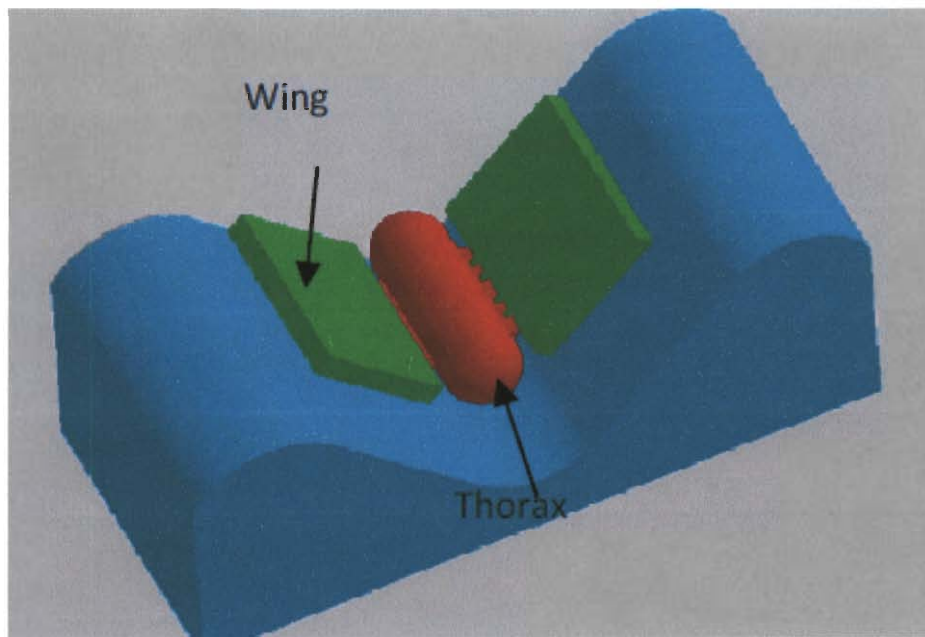


Figure 1.8. Schematic of the "Aqua-Fly" on a typical wave

The conceptual name "Aqua-Fly" comes from the resemblance of the design geometry to the anatomy of a fly. It is composed of two rafts or wings connected to a center housing or thorax by hydraulic pumps. The thorax houses accumulators that will store the hydraulic pressure to be converted to useable energy. The thorax is tethered to the ocean floor to restrict its motion relative to the wings. The method of tethering has yet to be determined and most be investigated further. The motion of the wings relative to the

15

fixed thorax will actuate the hydraulic pumps to capture the mechanical energy. This motion allows for capture of both the heaving and surging energy of the wave (Figure 1.9). Most current designs of wave energy convertors only capture the heaving motion. The electricity will be delivered to shore by cables along the ocean bottom.
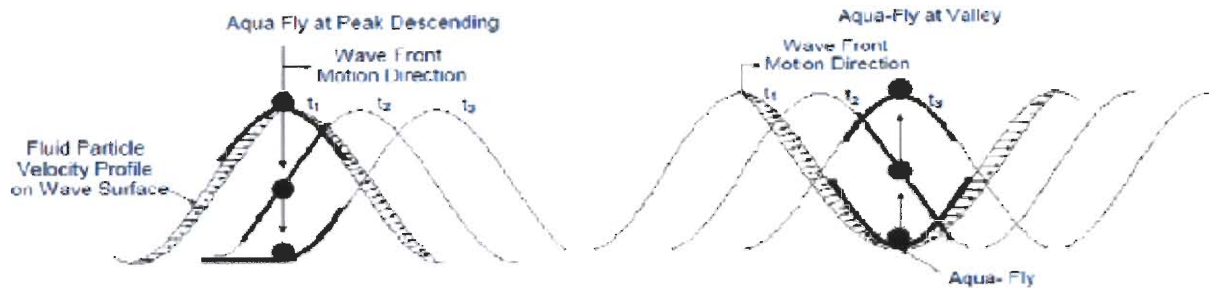


Figure 1.9. Interaction of "Aqua Fly" and wave

**Project Motivation**

The goal was to develop a more efficient wave energy convertor so that wave energy becomes a more economically viable form of alternative energy. Both steps of wave energy conversion process need to be optimized for efficiency. This thesis will concentrate on developing the energy absorption step of wave energy conversion.

It was proposed from initial findings that energy absorption efficiency can be increased by determining an optimum wing geometry and wing-wave interaction for the "Aqua Fly" concept. The criteria used for geometry and wing-wave interaction comparison were torque measured about the leading edge of the wing, energy absorption, and energy absorption efficiency when compared to a baseline case.

# CHAPTER 2

# ANALYTICAL CALCULATIONS

**Standing Waves**

A reflection added to a system of travelling waves, a wave which propagates down the tank, produces a standing wave in the tank. A standing wave is a wave that appears not to move. They form due to the interaction of two identical waves propagating in opposite directions. If it is a bounded medium, this is due to the reflection of the wave. An ideal standing wave has amplitude that is two times that of the propagating wave.
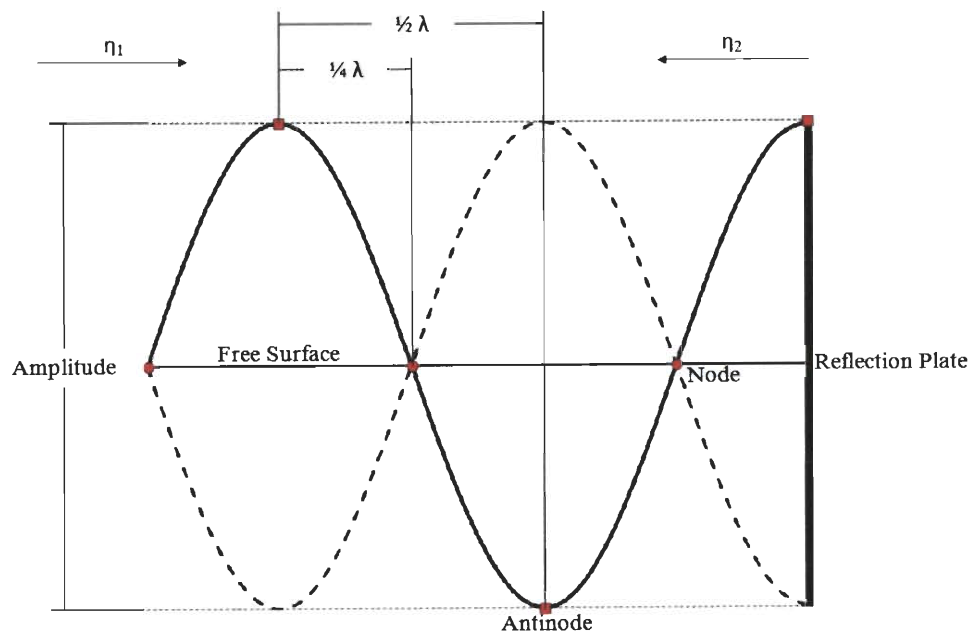


**Figure 2.1 Standing wave showing the location of nodes and antinodes**

The location where a standing wave appears to have little or no movement is called the node and the location of max amplitude is called the anti-node (Figure 2.1). The nodes and antinodes occur at quarter wavelength, $\lambda$, intervals. This means that two nodes are a half wavelength apart, with the same holding true for anti-nodes.

17

Based on linear wave theory, an equation for the amplitude, $\eta$, measured from the mean free surface of a standing, wave can be derived. As described a standing wave is the interaction of two identical waves ($\eta_1$, $\eta_2$) traveling in opposite directions Eq. (2.1).

$$\eta_1 = \frac{H}{2}\cos(\omega t - kx)$$

$$\eta_2 = \frac{H}{2}\cos(\omega t + kx)$$

(2.1)

$$\eta = \eta_1 + \eta_2 = \frac{H}{2}\cos(\omega t - kx) + \frac{H}{2}\cos(\omega t + kx) = H\cos(\omega t)\cos(kx)$$

Where $\omega$ (Eq. (2.2)) is the angular frequency and is a function of the wave period, $T$, or frequency, $f$, and $t$ is time. The wave number, $k$ Eq. (2.3), is a function of the wavelength, $\lambda$, and $x$ is the horizontal location, where the reflecting wall is considered to be at $x=0$. H/2 is the amplitude of the travelling wave (Gislason, 2009).

$$\omega = \frac{2\pi}{T} = 2\pi f$$

(2.2)

$$k = \frac{2\pi}{\lambda}$$

(2.3)

**Analytical Trends**

The energy in a wave is found via Eq. (2.4).

$$E = \frac{\rho * g * (4H_{m0})^2}{16}$$

(2.4)

Where $\rho$ is the density of the water, $g$ is the acceleration of gravity, and $H_{m0}$ is the root mean square of the wave height or amplitude Eq. (2.5).

$$H_{m0} = \sqrt{\frac{1}{N}\sum_{i=1}^{N} h_i^2}$$

(2.5)

18

Here $h_i$ is the wave height with respect to the calm water level (Figure 2.2) and $N$ is the number of data points.
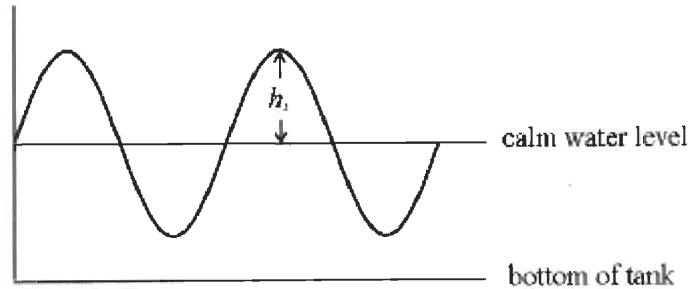


Figure 2.2 Example of wave height, *hi*

The amount of energy available in a standing wave increases when compared to the energy available from the travelling wave it was produced from. This can be shown using Eq. (2.1) and Eq. (2.4) in non-dimensional form (See APPENDIX B) with the following assumptions $g^*=1$, $H^*=1$, $t^*=2\pi$, $x^*=0$: $\pi/8$:$2\pi$. (Table 2.1)

Table 2.1 Comparison of energy absorbed by a standing wave to a travelling wave

|          | Wave      |            |
|----------|-----------|------------|
|          | Standing  | Travelling |
| E*       | 0.53      | 0.13       |
| % Change | 300%      |            |

Using the equations for a standing wave, Eq. (2.1), it can be shown that by moving the reflection plate in $0.25\lambda$ intervals the location of the nodes and anti-nodes can be controlled. This gives the freedom to allow the wing and the wave to interact in the optimum configuration to increase the amount of energy absorbed by the wing.

19

An anti-node will always form at the reflection plate which is considered the x=0 location. By substituting 0 in for x, in Eq. 2.1 it is seen that no matter what the maximum height of the wave, $H$, the frequency, $\omega$, the time $t$, or the wavelength, $k$, of the wave a maximum amplitude will occur at $x$=0. The location of maximum amplitude is the anti-node.

The quantities $\omega t$ and $kx$ are non-dimensional values. By holding the time $t$ constant and in turn the value of $\omega t$ by assuming a constant frequency, it can be shown that every quarter wavelength the wave has a either a maximum amplitude or a minimum amplitude. For calculation purposes, the following assumptions were used $cos(\omega t)=1$, $H=1$, and $x$ to from 0 to $2\lambda$ in $1/8$ $\lambda$ intervals. (Table 2.2)

**Table 2.2 Location of nodes($\eta$=0) and anti-nodes($\eta$=1) 0.25 $\lambda$ apart**

| x | η |
|---|---|
| 0 λ | 1.00 |
| 1/8 λ | 0.71 |
| 1/4 λ | 0.00 |
| 3/8 λ | -0.71 |
| 1/2 λ | -1.00 |
| 5/8 λ | -0.71 |
| 3/4 λ | 0.00 |
| 7/8 λ | 0.71 |
| 1 λ | 1.00 |
| 1 1/4 λ | 0.00 |
| 1 1/2 λ | -1.00 |
| 1 3/4 λ | 0.00 |
| 2 λ | 1.00 |

These results show that if the reflection plate is placed at an interval of ¼, ¾, 1 ¼, 1 ¾ λ, etc from the trailing edge of the wing then it will lie in a node where the amplitude

is zero. However, if the reflection plate is placed at ½, 1, 1½, 2λ, etc from the trailing edge of the wing it will be at an anti-node. (Figure 2.3)
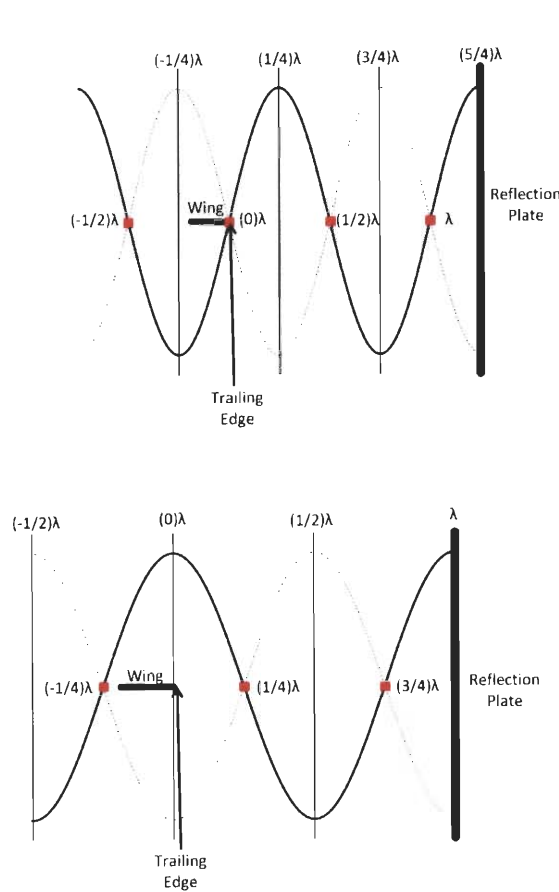


**Figure 2.3 Standing wave with the trailing edge of the wing placed at the node (top) and an anti-node (bottom)**

It can be shown that if the trailing edge of the wing is placed at an anti-node the maximum energy is absorbed and when the trailing edge is placed in node the minimum energy is absorbed when compared to the energy absorbed by the wing placed in a travelling wave. (Figure 2.4) These calculations assume that the wing absorbs all the wave energy in contact with the wing surface. (See Appendix B) They are only meant to show trends.
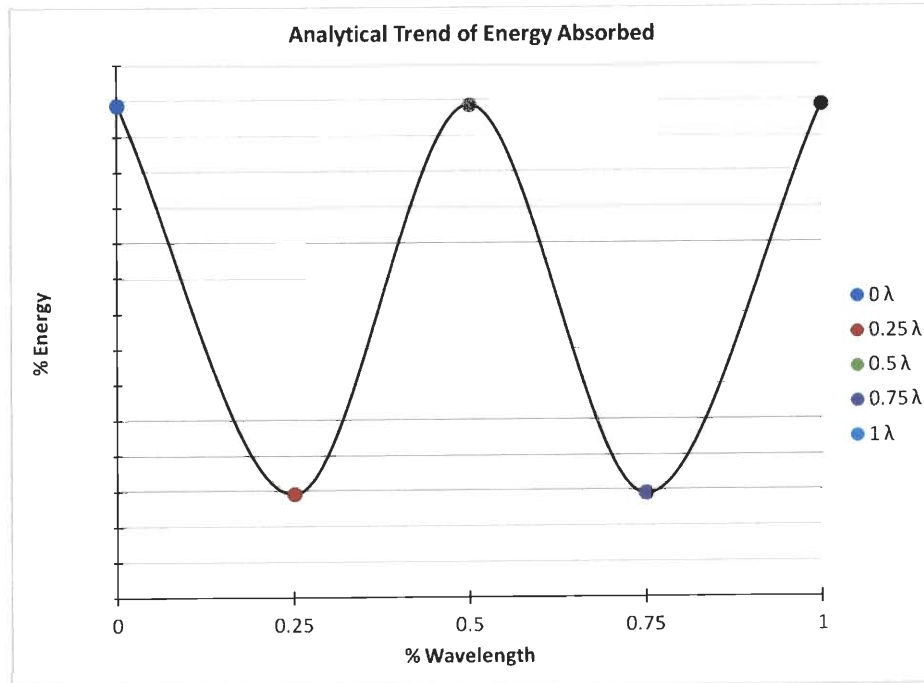
**Figure 2.4 Analytical calculations showing the trend of the energy absorbed by the wing when its trailing edge is placed in a node and anti-node**

These basic calculations are used as a starting point for placing the reflection plate at ¼ λ intervals for the experiments. They also show that the energy absorbed is fit to a cosine curve.

# CHAPTER 3

# EXPERIMENTAL SETUP

## Wave Tank Setup

In order to conduct a detailed, two-dimensional, small-scale study of wave energy absorption by a wing, a wave tank of dimensions in Figure 3.1 was used. The wave tank was located in the Fluid Dynamics Laboratory at Western Michigan University.
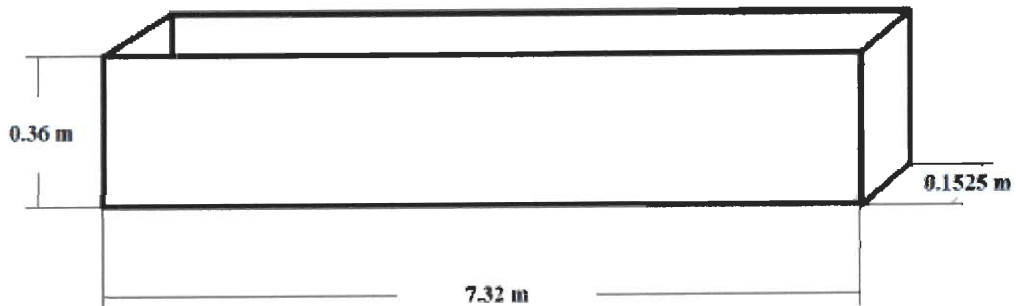


Figure 3.1 Wave tank dimensions

Wings of ten different geometries with the dimensions shown in APPENDIX G were placed in the tank. The wings were made out of aluminum to reduce the effects of rusting. The wing geometries were based on the effects of the downward bend observed from the initial computational investigations with the degrees of the bend and dimensions selected arbitrarily.

The leading edge of a wing was placed in the tank 1m downstream of the wave generator (Figure 3.2). The wave generator was composed of a ¼ HP, 1725 RPM, 115 V, 4.4A electric motor and a Plexiglas flap. The motor was attached by a disk and rod to the

flap. A length scale was applied to the back of the tank to determine wavelength and amplitude of the wave.
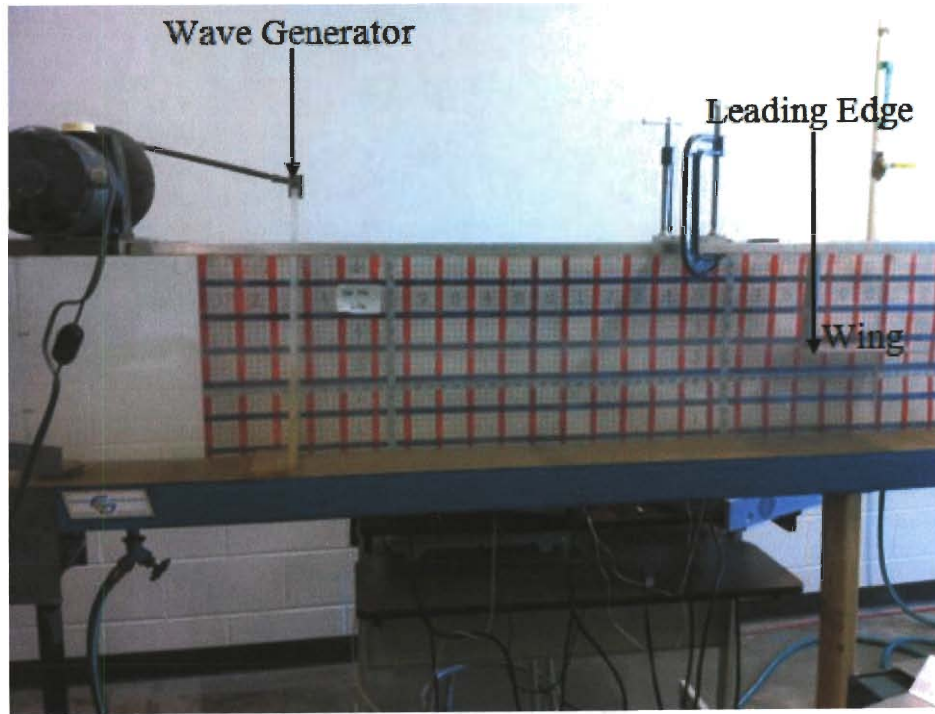


**Figure 3.2 Experimental setup: wing location**

The stroke of the flap could be adjusted from 4.5cm to 11.7cm at the top of the tank. The flap was attached to the tank by a hinge allowing it to rotate forward and backward with the rotation of the motor (Figure 3.3). By adjusting the stroke of the flap and the speed of the motor, the frequency, amplitude, and wavelength of the wave could be controlled.
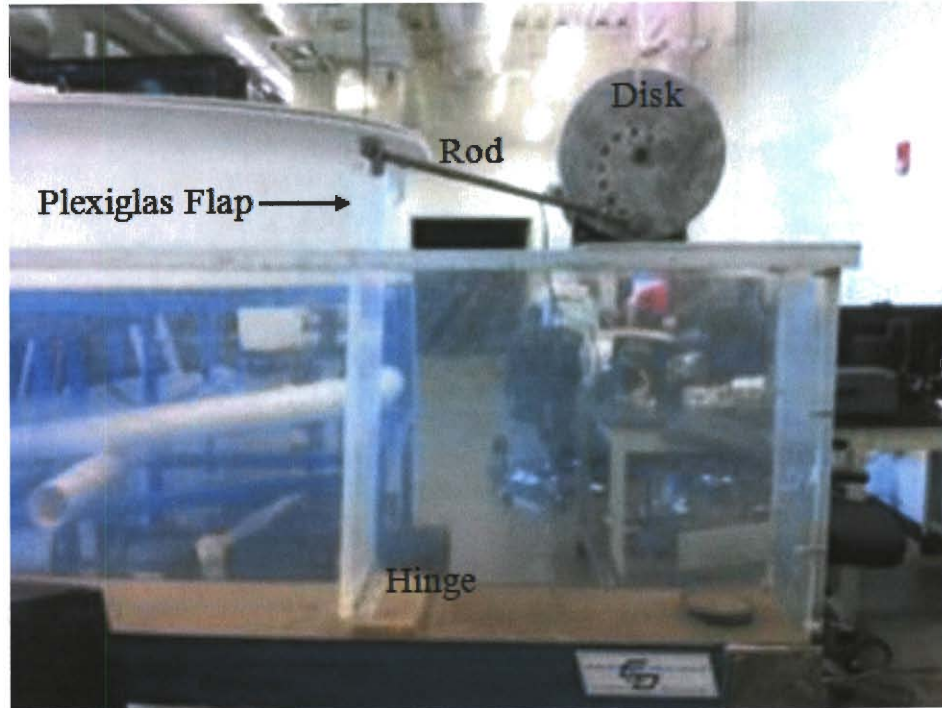
**Figure 3.3 Close up of wave generator system**

Two surveillance cameras (Color Eclipse 1/3" CCD) (Figure 3.4) attached to a DVR recorder were used to record the experiments. The cameras recorded one frame every 0.067s.
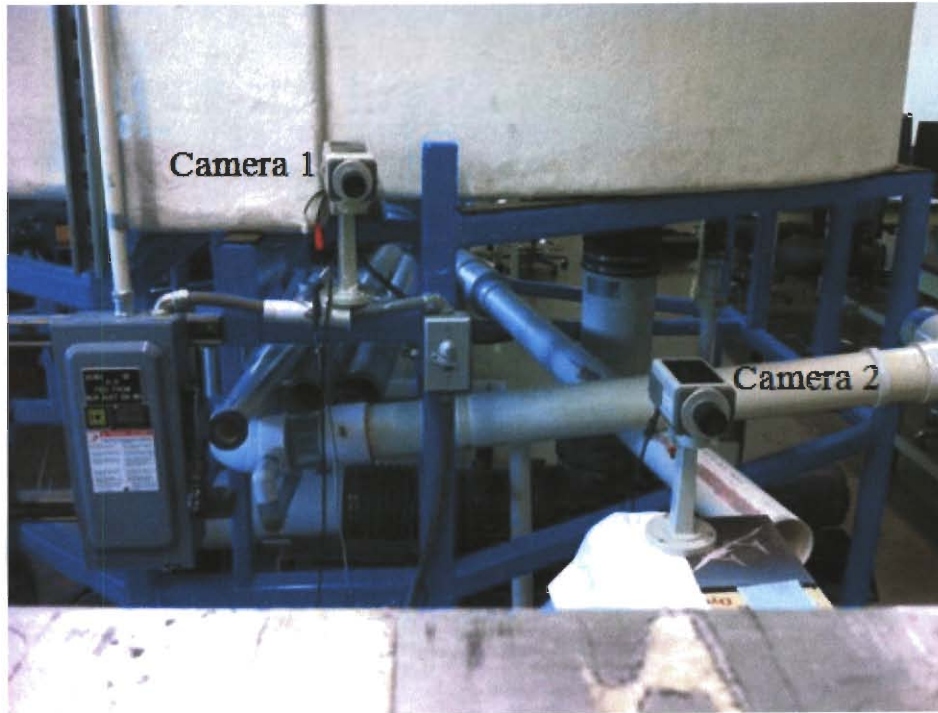
**Figure 3.4 Camera setup**

Camera 1 was setup with a wide view to allow for evaluation of the wave after interaction with the wing whereas Camera 2 provided a close up view of the wing wave interaction (Figure 3.5). SDVR Viewer software was used to step through the recorded video frame by frame.
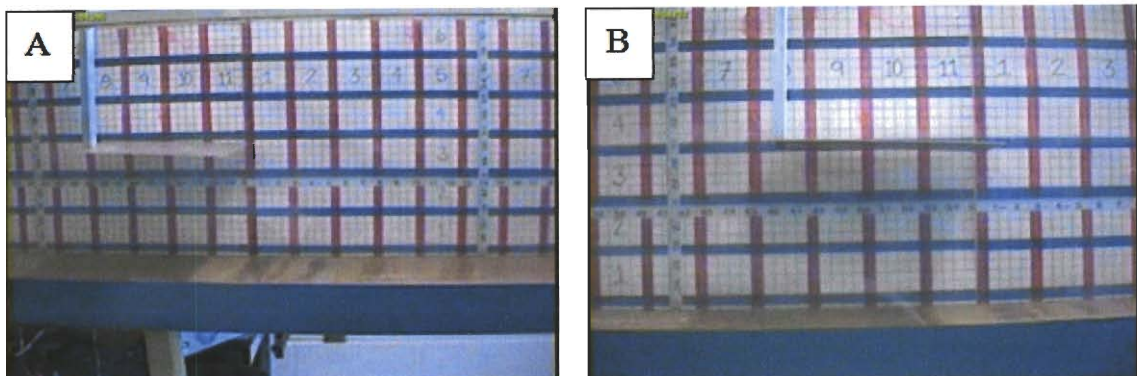


**Figure 3.5 Views from Camera 1(A) and Camera 2 (B)**

In order to measure the torque produced about the leading edge of the wing, two single-direction strain gauges were used (Figure 3.6). Two 3800 wide range stain indicators were used and the analog output was transferred to LABVIEW with a data acquisition card. The strain gauge fixture was attached to the wing by a vertical support and then attached to the tank using c-clamps.
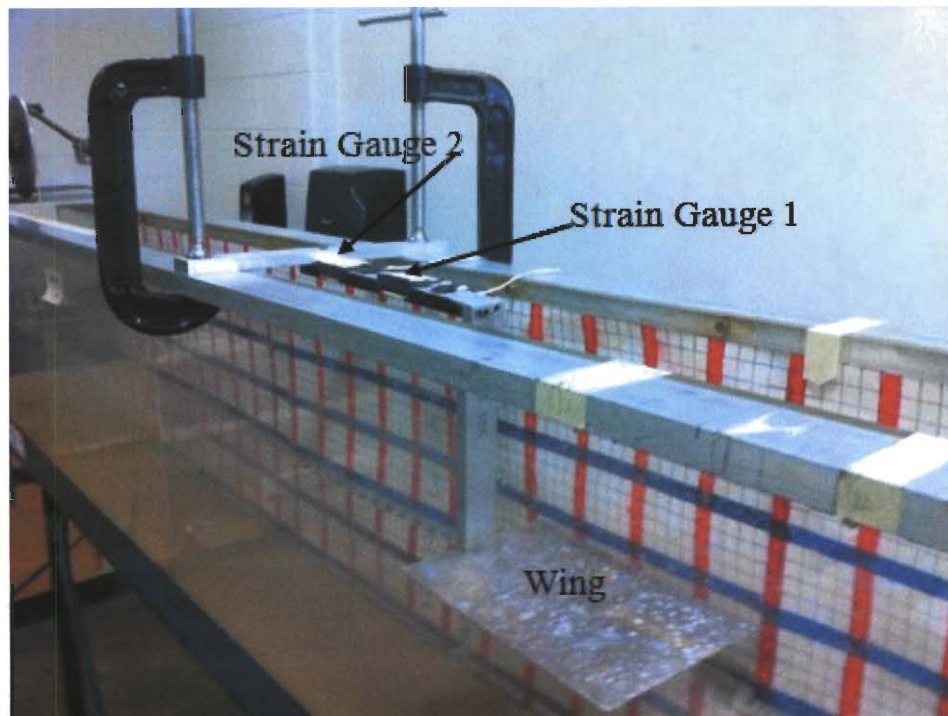


**Figure 3.6 Experimental setup in wave tank with wing and strain gauges**

To eliminate the reflection off the end wall and produce a travelling wave in the tank, a ramp with 1:4 height to length ratio was added downstream of the test structure (Figure 3.7).

**Figure 3.7 Ramp at end of the tank used to eliminate reflection off end wall**

This allowed the water to run up the ramp and the energy to dissipate, which is a similar to a beach (Huang, 2007). This set up produced a baseline case for comparison to a system with added reflection.

To add reflection to the system, a reflection plate was added to the tank at specified distances downstream of the trailing edge of the wing (Figure 3.8).
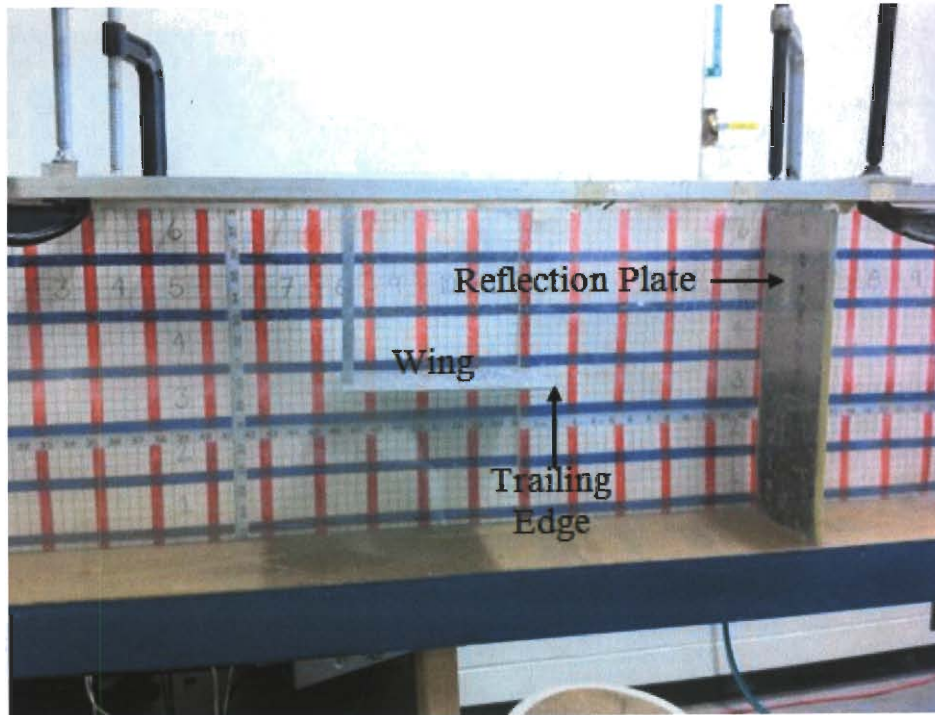
**Figure 3.8 Tank with wing and reflection plate**

## Measurement System

The torque produced about point A, leading edge of the wing, could be solved for using the strain created by the force, F, at strain gauges $S_1$ and $S_2$ even though the location of the force, $L_3$, on the surface of the wing was unknown (Figure 3.9). Table 3.1 lists the dimensions for the test structure that was used, where V is the length of the vertical support.
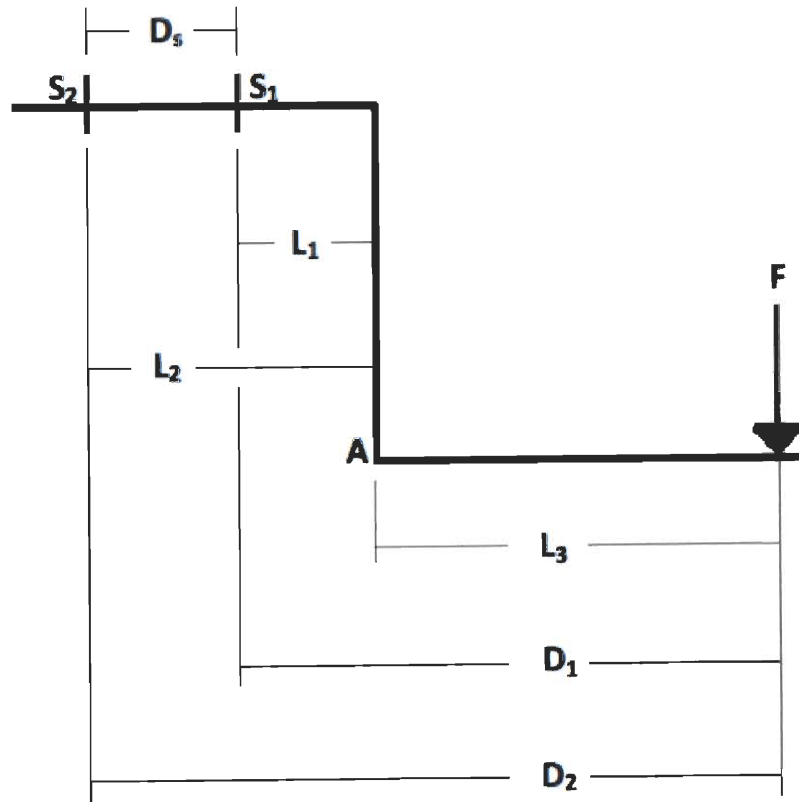
**Figure 3.9 Schematic of test fixture used for measuring torque on the wing**

**Table 3.1 Dimensions of fixture**

| Knowns | |
|---|---|
| $L_1$ | 0.1 m |
| $L_2$ | 0.211 m |
| $D_s$ | 0.111 m |
| V | 0.205 m |

The moments $M_1$ and $M_2$ were the moments of Force, $F$, at stain gauges $S_1$ and $S_2$ and could be solved for using Eq. (3.1)

$$M_1 = FD_1 = F(L_3 + L_1)$$

$$M_2 = FD_2 = F(L_3 + L_2)$$

(3.1)

To calibrate the strain gauges and find the desired torque a series of weights from $F= 0-450g$ in 50g increments were placed on the wing at a known value $L_3$. The moment

30

that each weight produced at strain gauges $S_1$ and $S_2$ were found using Eq. (3.1). The measured strain for each case at $S_1$ and $S_2$ were then set equal to the calculated moments $M_1$ and $M_2$ respectively. Using, these measured and calculated values calibration curves where made to correlate the measured strain to the moment produced. Calibration constant were found from these curves. (See APPENDIX E)

Now, the measured moments and known distances could be used to calculate the moment, $M$, of force, $F$, at point A, Eq. (3.2),

$$M = FL_3 \qquad (3.2)$$

Using $M_1$ and $M_2$, the distance $L_3$ could be found Eq. (3.3)

$$L_3 = \frac{M_1}{F} - L_1$$
$$L_3 = \frac{M_2}{F} - L_2 \qquad (3.3)$$

These two equations were then set equal to each other Eq. (3.4)

$$L_3 = \frac{M_1}{F} - L_1 = \frac{M_2}{F} - L_2 \qquad (3.4)$$

and multiplied by $F$ Eq. (3.5)

$$FL_3 = M_1 - FL_1 = M_2 - FL_2 \qquad (3.5)$$

The force, $F$, acting on the wing could then be found by eliminating the $FL_3$ term and setting the two right side terms equal to each other. Eq. (3.6)

$$M_1 - FL_1 = M_2 - FL_2 \qquad (3.6)$$

The terms of Eq. (3.6) were rearranged to find F Eq. (3.7), where $D_s$ was the distance between the strain gauges.

$$M_1 - M_2 = F(L_1 - L_2)$$

$$L_1 - L_2 = D_s \qquad\qquad (3.7)$$

$$F = \frac{M_1 - M_2}{D_s}$$

The moment about the leading edge of the wing could then be found by rearranging Eq. (3.5) in another fashion Eq. (3.8).

$$M = FL_3 = \frac{(M_2 - FL_2) + (M_1 - FL_1)}{2} \qquad\qquad (3.8)$$

**Experimental Procedure**

First the frequency, wavelength and amplitude of the wave were measured and confirmed. The frequency of the wave was found by timing how long it took for the flap to complete ten strokes. This frequency was also confirmed with the Fast Fourier Transform (FFT) of the measured data. The wavelength and amplitude were found using the cameras and applied scale. By running the tank without a wing, the amplitude and wavelength of the wave could be read off the scale from the recorded video. This was completed every time the frequency of the motor was changed.

Using the measured wavelength, the location of the reflection plate was found and marked off along the edge of the tank. To control the location of the nodes and antinodes with respect to the trailing edge of the wing the reflection plate was placed at quarter wavelength intervals from the trailing edge (Figure 3.10). Dimension X represents the

location of the reflection plate, as a function of the wavelength, λ, from 0λ to1λ in 0.25λ steps.
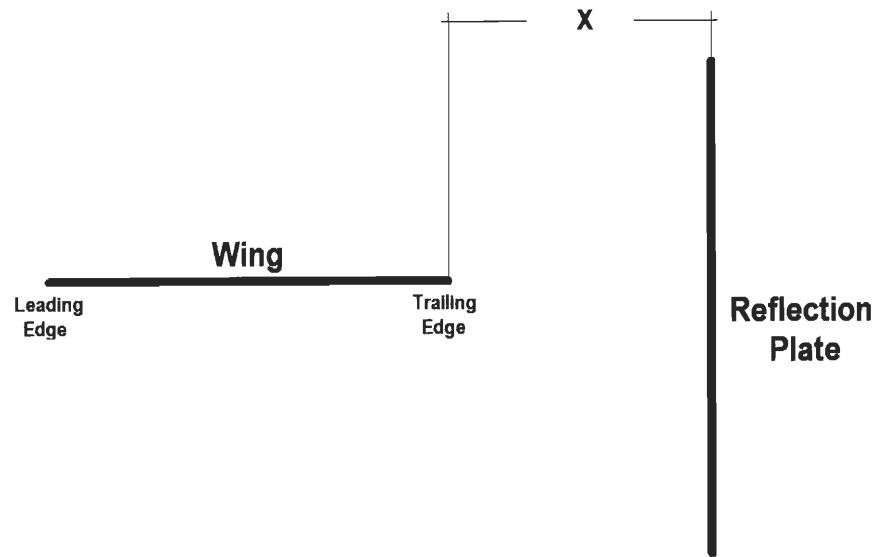


Figure 3.10. Diagram of the relationship of the reflection plate to the trailing edge of the wing

The wing was then placed in the tank and the square and level were verified. This procedure was completed every time the wing geometry was changed. The tank was filled to a water depth of 19.5 cm. This was enough water for the bottom of wing to be sitting on the free surface. The water depth was checked prior to each test and adjusted if necessary. Water depth was adjusted every time the test configuration was changed.

For each wing geometry, six separate test configurations were run (Table 3.2). This included a test with the ramp for the baseline measurement of the travelling wave and tests with the reflection plate placed from 0-1λ in 0.25λ increments as prescribed above. Every time the reflection plate was moved it was checked for square and level.

33

Table 3.2 Test matrix

| Test Matrix | |
|---|---|
| Test # | Reflection plate Location |
| 1 | Travelling Wave |
| 2 | $0\lambda$ |
| 3 | $0.25\lambda$ |
| 4 | $0.5\lambda$ |
| 5 | $0.75\lambda$ |
| 6 | $1\lambda$ |

Prior to each test the start time of the test was recorded so that the video data could be reviewed and saved after each test. The data acquisition system was started in LABVIEW (See APPENDIX F). The motor was then started and the test was run for five minutes to allow enough time for the wave to fully develop. At the end of each test, the data acquisition system was stopped, the motor was turned off and the end time was recorded. Each test configuration was run three times to confirm repeatability of the measured data (See APPENDIX A).

**Data Processing**

Finally, the torque and video data were processed. Using MATLAB (APPENDIX D), the torque about the leading edge of the wing and the energy absorbed were calculated from the measured strains and calculated calibration constants.

The absorbed energy was found by taking a FFT of the torque data, which provided the power spectral density. Spectral power was then converted to spectral energy and the area under this curve was the total energy absorbed.

The torque, spectral energy curve, and total energy of each of the three runs were compared to verify consistency of measurements. The total energy of all three runs was then averaged to produce the total energy absorbed for each wing geometry and configuration.

The percent energy increase from the baseline or travelling wave was calculated with Eq. (3.9), where the baseline energy was the amount of energy absorbed by the flat wing when no reflection plate was added to the system and the ramp was used. The total energy calculations from the FFT curves were used in this equation.

$$\%\Delta Energy\ Absorbed = \left(\frac{Energy\ Absorbed}{Baseline\ Energy\ Absorbed} - 1\right) * 100\% \qquad (3.9)$$

The video data was then processed using the SDVR software that came with the surveillance system. From the video data amplitude and wavelength of the wave were recorded. The interaction of the wing and the wave was observed. These observations included the location of the nodes and anti-nodes with respect to the wing. The amplitude of the wave off the reflection plate was also observed along with the movement of the trailing edge of the wing. The observation of the video data along with the torque measurements and energy calculations were combined to understand the trends and optimize the wing geometry and reflection plate location.

# CHAPTER 4

# EXPERIMENTAL RESULTS

## Development of Wave in Tank

In order to investigate the effects of a standing wave on energy absorption, two different types of waves needed to be developed in the wave tank. The first was a travelling wave, a wave that propagates down the wave tank; this was used as the baseline case for comparison. It was meant to imitate a wave in the ocean and was accomplished by adding a ramp to the end of the tank. The ramp dissipated the energy of the wave and eliminated reflection off the end wall. It was developed to replicate a beach in the ocean.

Figure 4.1 shows a travelling wave in the wave tank. Starting from photo A and moving to E, one cycle of the travelling wave can be observed. A wave peak can be seen entering the screen in photo A and progressing or traveling down the tank and exiting the screen in photo E. The progression of the wave peak down the tank supports that a travelling wave was developed.
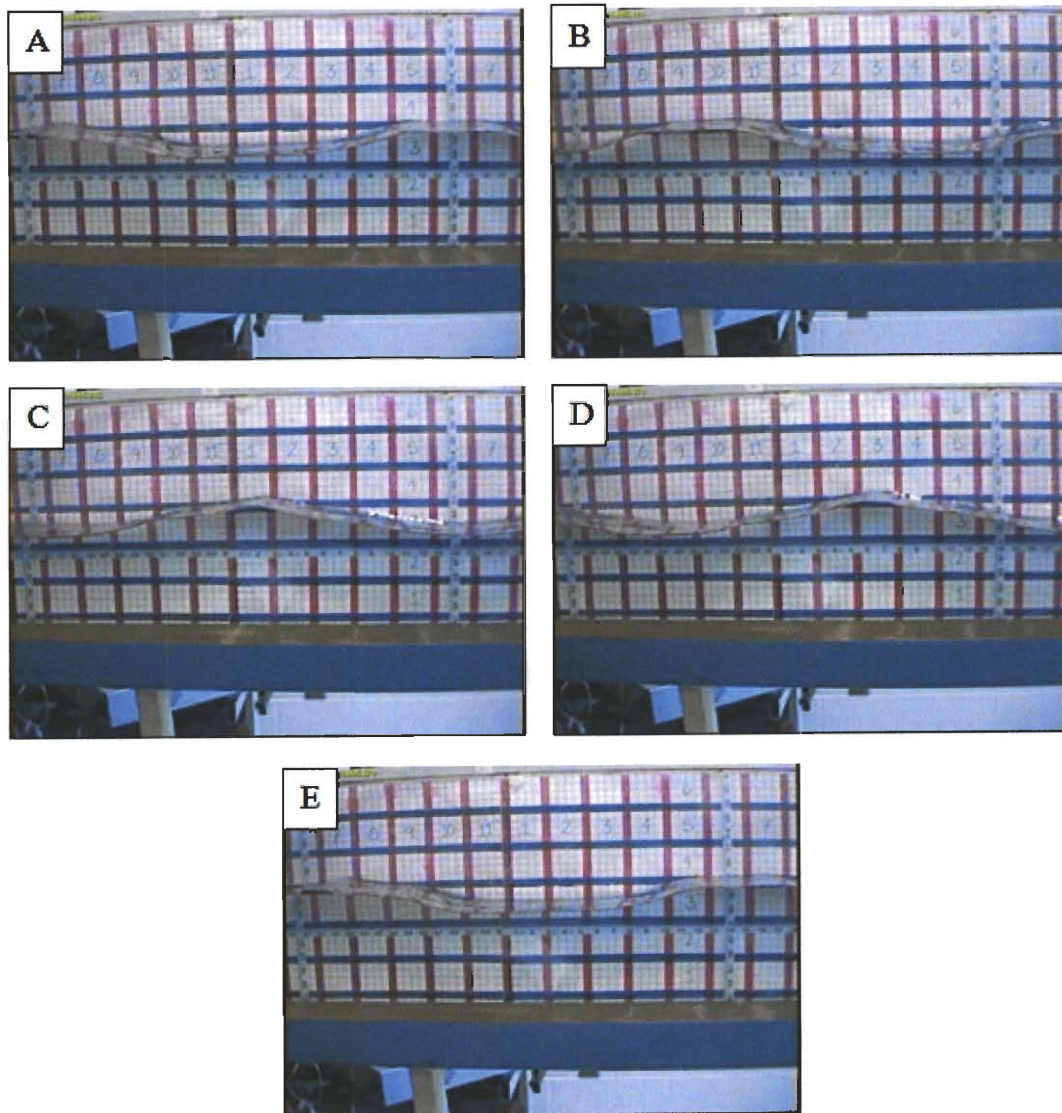
**Figure 4.1 Progression of one cycle of a travelling wave down the wave tank**
**A: Wave peak entering view from the left and another exiting on the right,**
**B-D: Wave peak progressing down tank,**
**E: Wave peak exiting on right and new one entering on left**

The second type of wave was a standing wave. It was hypothesized from the initial research and analytical calculations that adding a standing wave to the system would increase that amount of energy absorbed by the wing by increasing the amount of energy available in the wave. A standing wave was created in the tank by adding a reflection plate to the system.

Figure 4.2 shows one wave cycle of a standing wave in the wave tank. Photo A shows the standing wave at the calm free surface. In photo B, the wave has ascended to its peak. The wave then descended back through the calm free surface (C) to its trough seen in photo D. It then ascends back to the calm free surface in photo E.
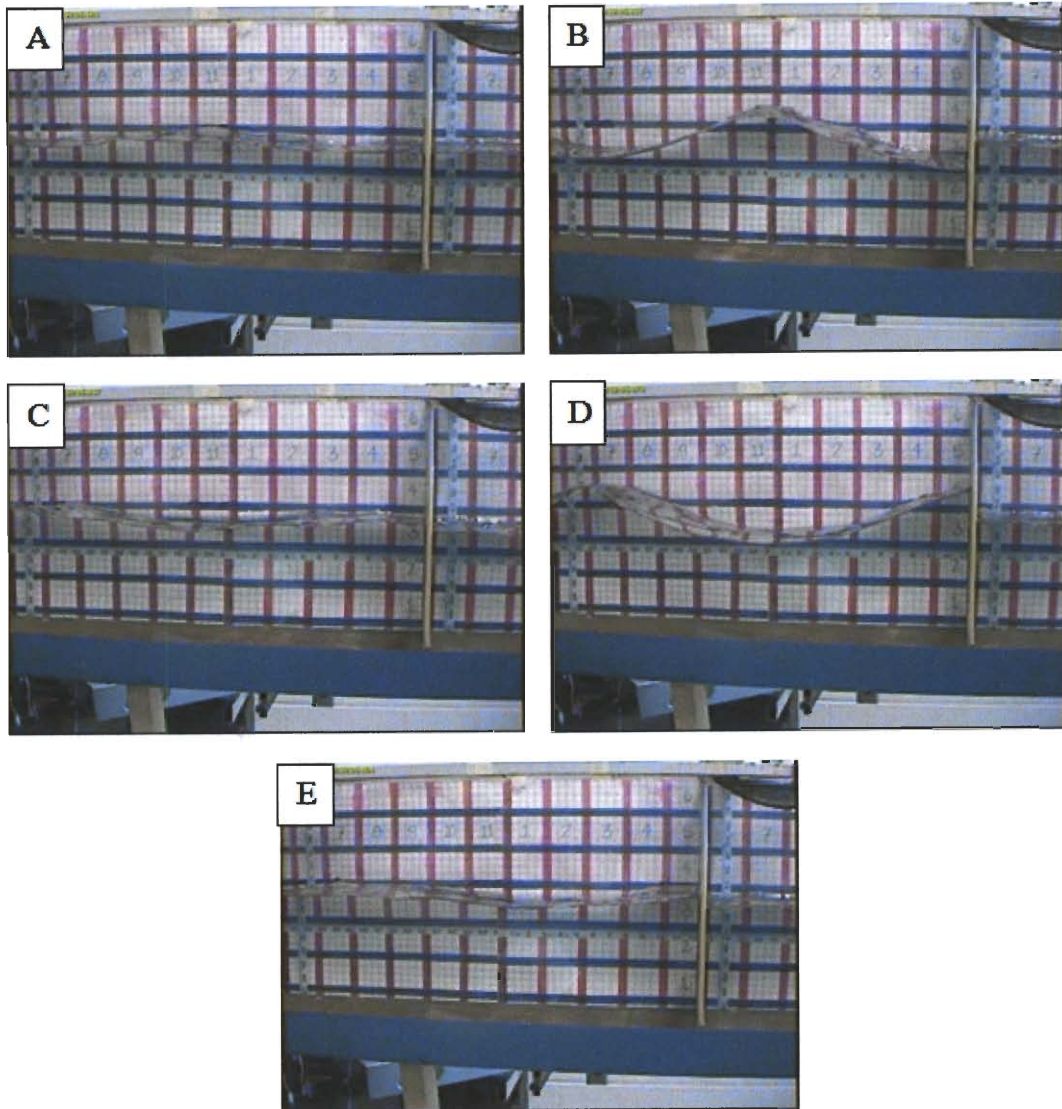


**Figure 4.2 One wave cycle of a standing wave**
**A: Calm free surface, B: Wave at peak location**
**C: Calm free surface, D: Wave at trough**
**E: Calm free surface**

It was observed that the location of the peak (B) and trough (D) are in the same location. This location is called the anti-node. The location where the wave appears not to move is called a node (Figure 4.3). The nodes and anti-nodes occur at quarter wavelength intervals.
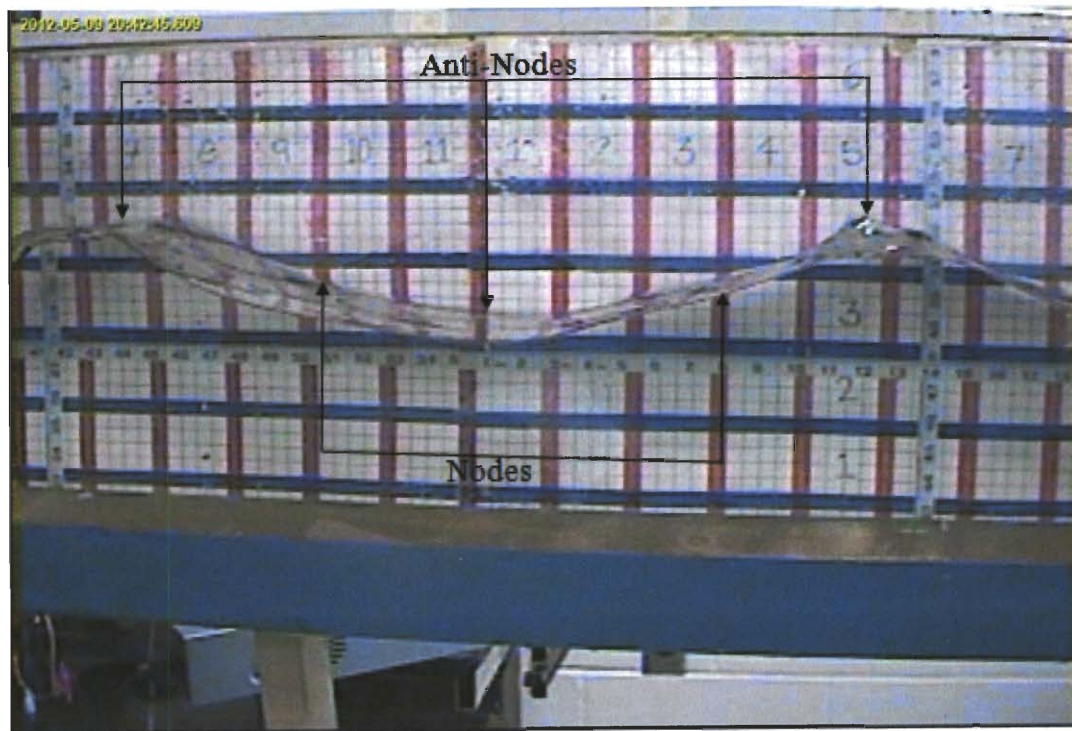


**Figure 4.3 Nodes and anti-nodes of a standing wave in the wave tank**

By varying the location of the reflection plate in the tank the location of nodes and anti-nodes of the standing wave could be controlled. This allowed for the wing to be placed in the optimum location of the standing wave to absorb the maximum amount of energy (Figure 4.4).
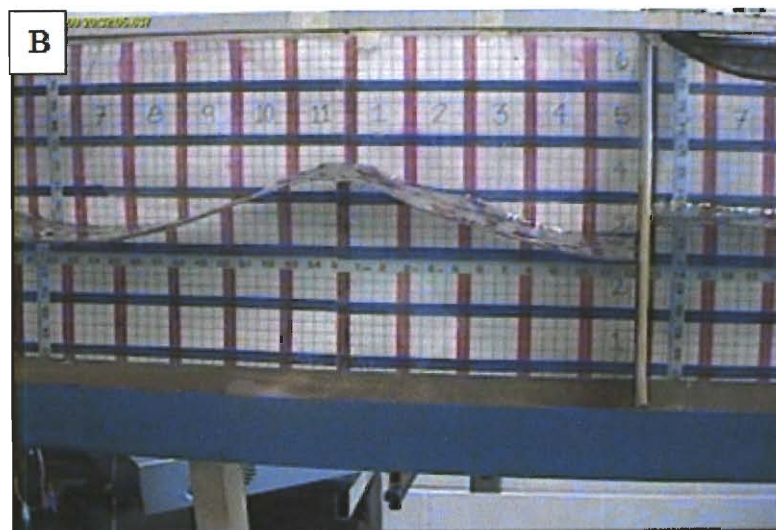
**Figure 4.4 Movement of anti-node with respect to reflection plate location**
**A: Reflection plate at 0.25λ, B: Reflection plate at 0.5λ**

Photo A and B show the reflection plate placed a quarter wavelength apart. It could be seen that the change in the reflection plate location shifts the location of the anti-node. The shift of the standing wave occurred because an anti-node was always created at the reflection plate as seen above.

## Torque and Energy Measurements

In order to develop a physical understanding of the torque curves, a comparison of the torque about the leading edge of the wing to the wing-wave interaction was made. Comparing the torque curves to the interaction showed that the torque measurements were consistent and had physical meaning.

A positive torque corresponded to the wave pushing downward on the surface of the wing. This occurred as the wave was descending from its peak location to its trough. A negative torque about the leading edge of the wing occurred as a wave ascended from its trough location to its peak or pushed upward on the wing.

Figure 4.5 shows the torque produced on the leading edge of the wing when the trailing edge of the wing was place in a node.
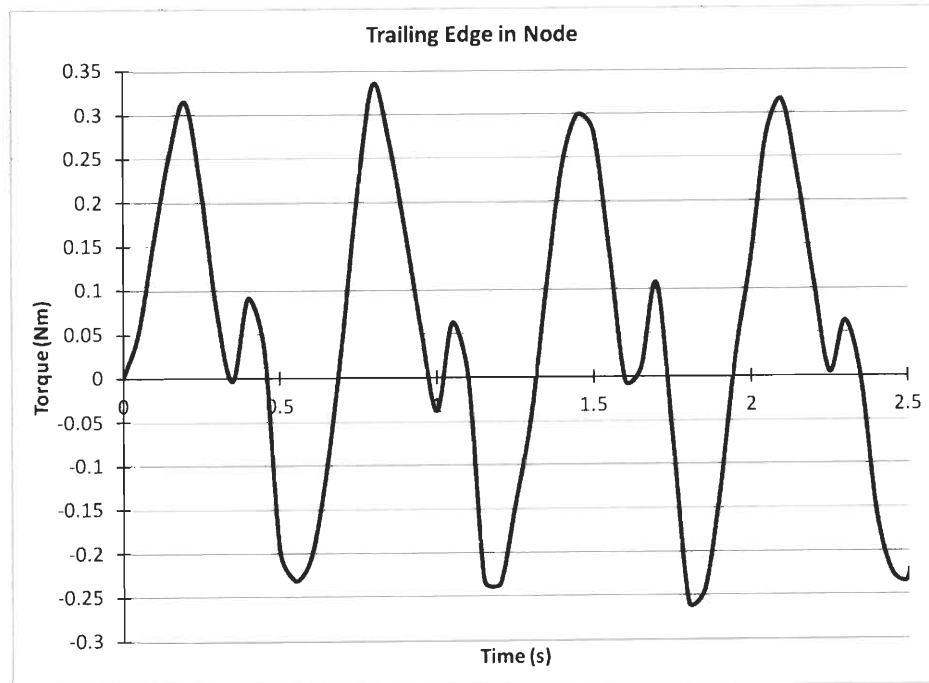


**Figure 4.5 Torque about the leading edge with the trailing edge was placed in a node**

There is a secondary reaction observed in the torque curves as the wave pushed downward on the wing. This interaction can be seen in Figure 4.6 in photos C-E. As the wave was reaching its trough (C), a reflection from the trailing edge of the wing created one more downward force on the wing (D) before it began to ascend back to its peak position (E).
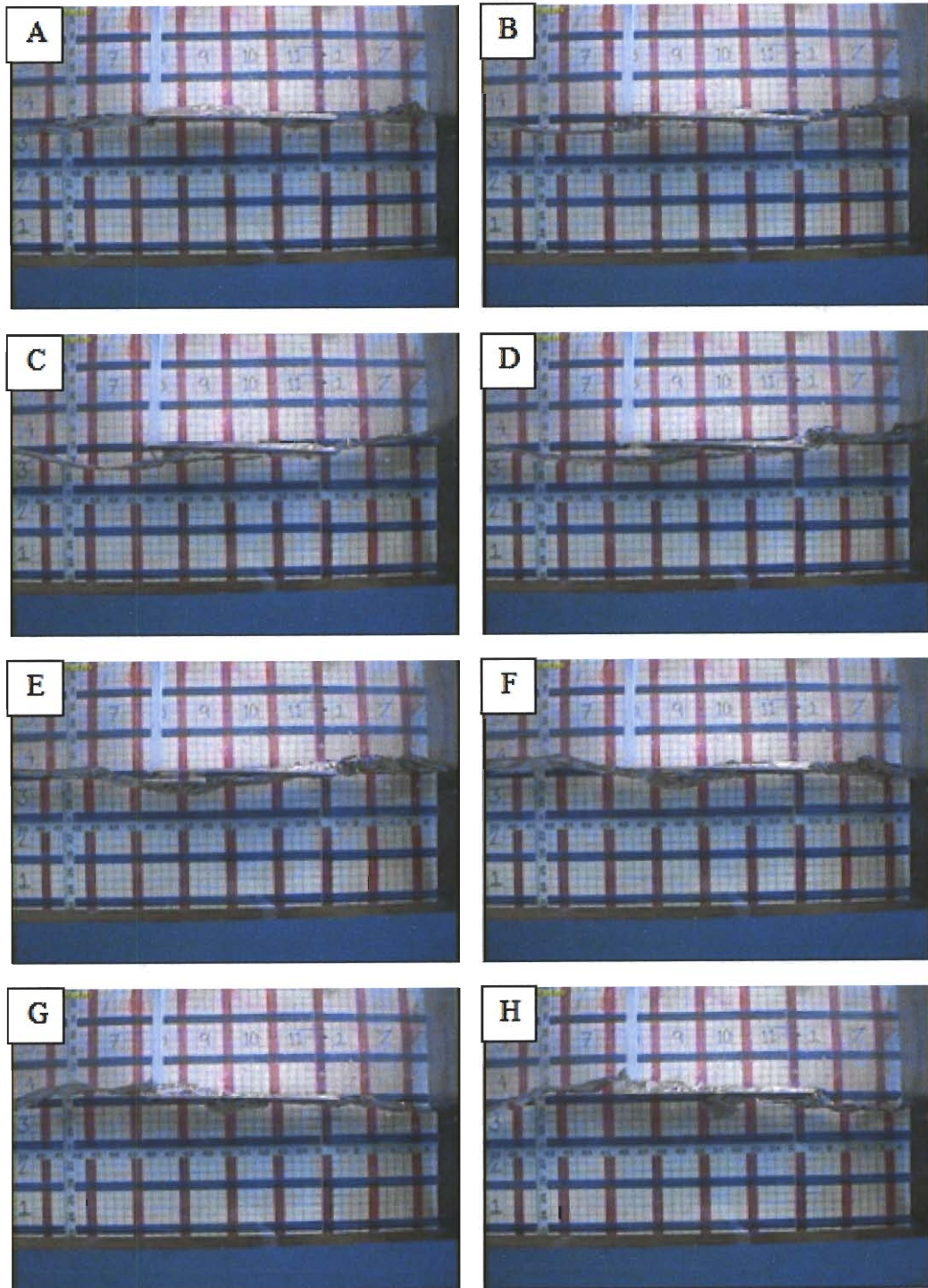
**Figure 4.6 One cycle of a wave with the trailing edge of the wing placed in a node for comparison with the torque curves**

A: Neutral wing location, B: Wave descending to trough location, C: Wave at its trough, D: Reflection off the trailing edge of the wing, E: Wave ascending to its peak position, F: Wave ascending to its peak through the neutral wing location, G: Wave ascending to its peak, H: Wave at its peak

A similar comparison could be made when the trailing edge of the wing was placed in an anti-node. (Figure 4.7) It was again observed that there was a secondary reaction created. This reaction was also as the wave was descending from its peak location to its trough.
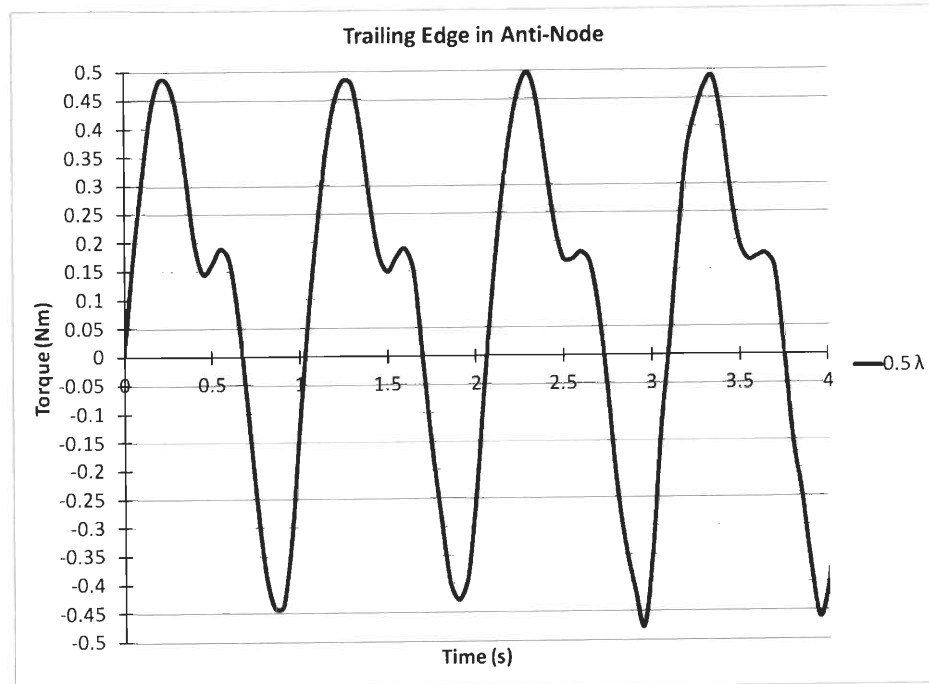


**Figure 4.7 Torque measured about the leading edge of the wing when the trailing edge was placed in an anti-node**

Comparing the torque curves to the wave wing interaction (Figure 4.8), D-F, showed that this reaction was due to a reflection off the trailing edge of the wing as the wave reached its peak location (D). As the wave began to descend this reflection broke back over the surface of the wing (F,E).
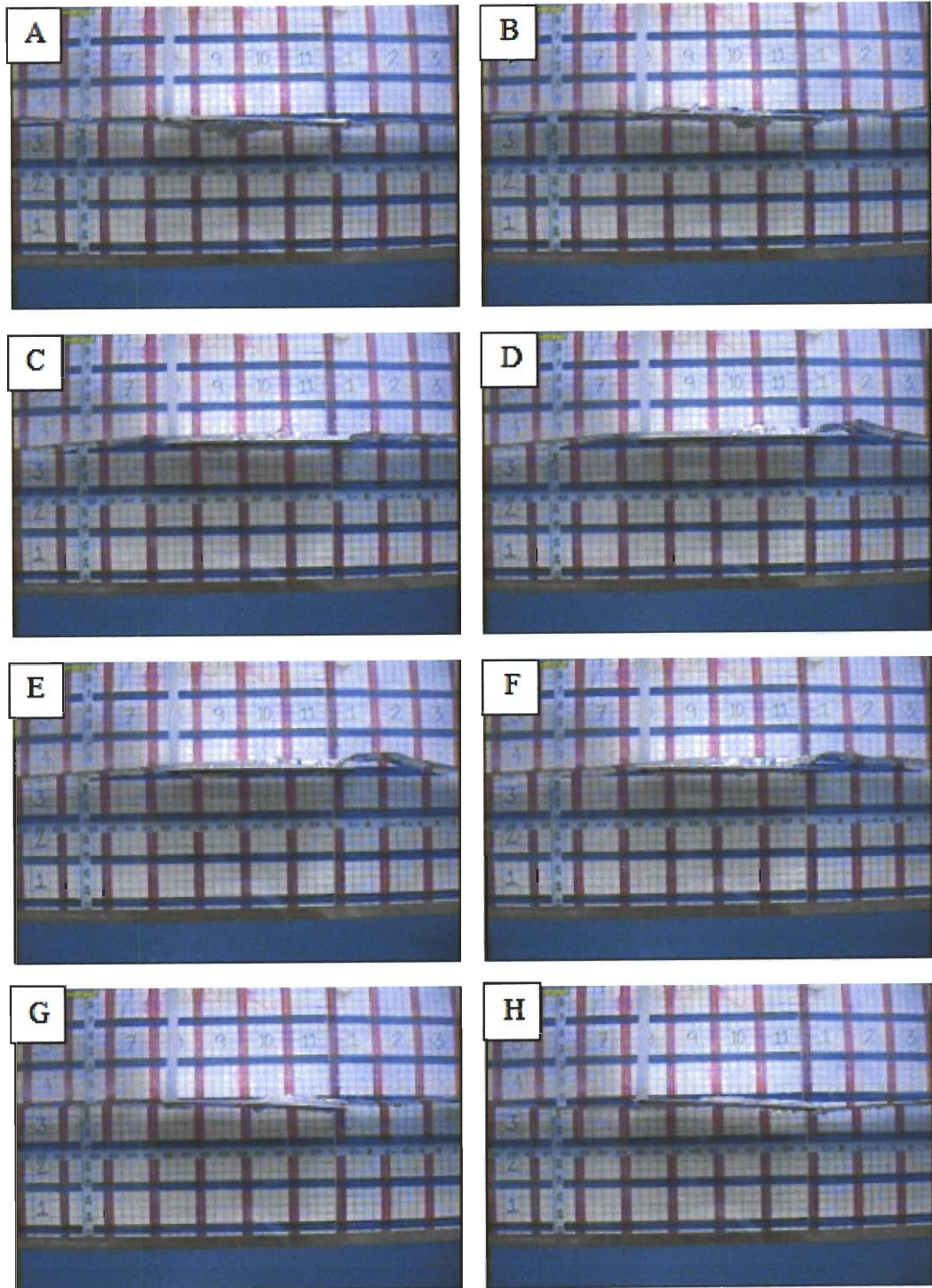
**Figure 4.8 One cycle of a wave with the trailing edge of the wing placed in an anti-node for comparison with the torque curves**

A: Neutral wing location, B-C: Wave ascending to peak location, D: Peak location with reflection off trailing edge, E-F: reflection off trailing edge breaking over wing as it descends to its trough, G: Wave descending to its trough position though the neutral wing location, H: Wave at its trough

The spectral energy density curves also showed an interesting trend. By observing the spectral energy curves, it was seen that the dominant frequency had the most energy, where the dominant frequency was that of the wave being produced. All other spikes in the curve corresponded to a harmonic frequency of the wave and the amount of energy of each subsequent harmonic decreased. There were two different wave frequencies used for comparison purposes Figure 4.9 shows the 0.97 Hz wave and Figure 4.10 shows the 1.56 Hz wave. These two frequencies were chosen arbitrarily.
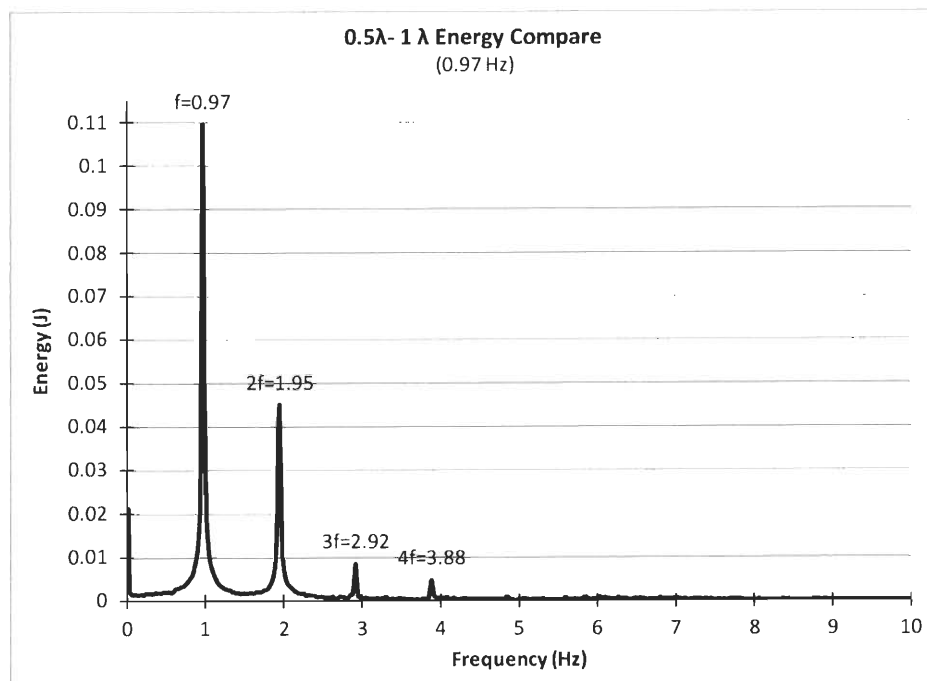


**Figure 4.9 Spectral energy for the 0.97Hz wave (dominant frequency and its harmonics)**
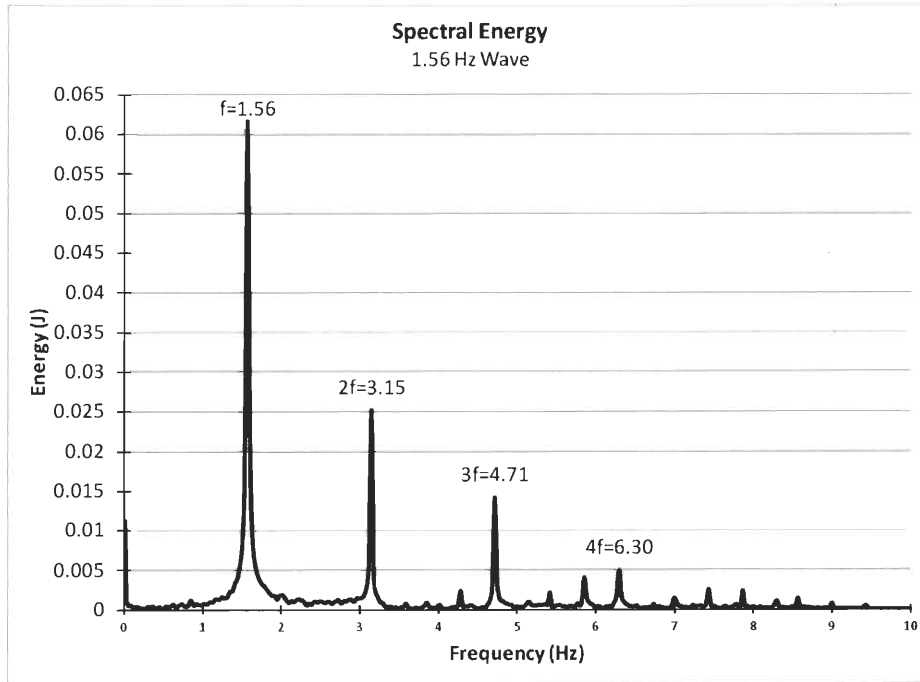
**Figure 4.10 Spectral energy for the 1.56Hz wave (dominant frequency and its harmonics)**

## Error Analysis

### *Measurement System*

In order to determine the error of the strain gauge measurement system, weights from 0-450 g in 50g increments where place along the surface of the wing at three different locations. The moment created by each weight was measured using the strain gauges in a process similar to the calibration procedure. The torque produced by each weight at each location was also solved analytically using Eq. (4.1), where $M$ is the moment, $F$ is the force of the weight, and $d$ is the distance of the weight to the leading edge of the wing.

$$M = Fd \qquad\qquad (4.1)$$

The measured and calculated values where then compared and the error of the measurements where determined using Eq. (4.2).

$$\% \ Error = \frac{calculated - measured}{calculated} * 100\% \tag{4.2}$$

Table 4.1 shows a comparison of the measured and calculated values. It was seen that the error ranged between one and three percent for the measurement system over the range of calibration.

Table 4.1 Error analysis comparison of the strain gage measurement system check error m2

| Error | | | |
|---|---|---|---|
| F | $M_1$ | $M_2$ | $M_3$ |
| 0 | 0% | 0% | 0% |
| 50 | 1.79% | 2.04% | 3.07% |
| 100 | 1.66% | 0.41% | 0.01% |
| 150 | 0.85% | 0.62% | 0.13% |
| 200 | 0.13% | 2.15% | 1.48% |
| 250 | 0.54% | 2.37% | 1.58% |
| 300 | 0.04% | 2.03% | 0.62% |
| 350 | 1.16% | 1.49% | 2.54% |
| 400 | 1.57% | 1.53% | 1.74% |
| 450 | 0.92% | 1.68% | 0.33% |

*Water Depth Sensitivity*

Experiments were conducted in order to understand the sensitivity of the torque created about the leading edge of the wing to the water depth. This was accomplished by using the flat wing and altering the water depth by 5mm above and also below the standard water depth of 19.5 cm. The measurements were taken for a travelling wave and with the reflection plate placed at 0.25 and 0.5λ respectively. They were then

compared to the results when the water depth was at its standard location, using Eq. (2.9) (Table 4.2). The results shown here are for a 1.56 Hz wave because the sensitivity was highest for this frequency.

Table 4.2. Percent energy absorption increase (+) or decrease (-) depending on water depth

| | water depth | |
|---|---|---|
| wave | +5mm | -5mm |
| travelling | 12% | -10% |
| 0.25 λ | 2% | -1% |
| 0.5 λ | 25% | -29% |

It was seen that the deeper water caused an increase in the energy absorbed by the plate and the magnitude of the sensitivity was dependent on the wave being produced. The water depth had a direct effect on the amplitude of the wave (Figure 4.11). Comparing the amplitude of the wave for the +5mm, standard and -5mm cases showed that as the water depth decreased the amplitude of the wave decreased. This was why the amount of energy absorbed by the plate decreased with a decrease in depth and vice versa.
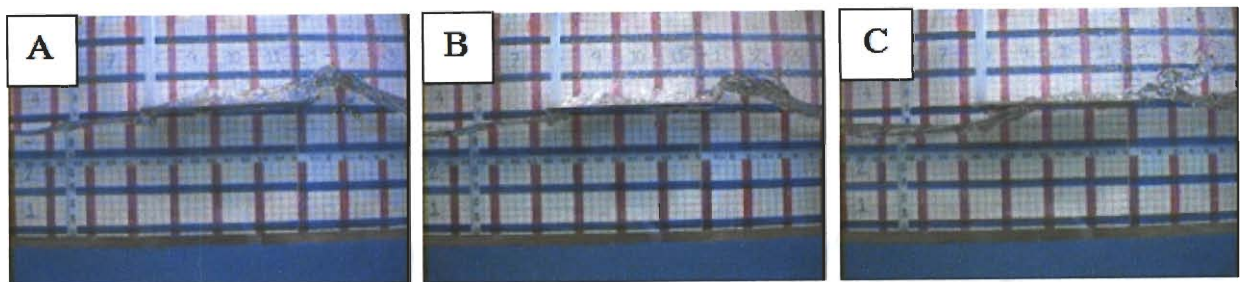


Figure 4.11 Variations in water depth changes the amplitude of the wave. Waves shown are at their peak amplitude for the following three cases with the reflection plate at ½ λ
A: standard +5mm B: standard, C: standard -5mm

49

The type of wave was also a factor in the effect of the water depth. For the 0.25 λ case, the trailing edge of the wing was in a node, the amount of energy absorbed was not greatly affected because the amplitude of the wave at the trailing edge was zero. The effect was much more prominent when the trailing edge of the wing was placed in an anti-node, 0.5 λ; at this location the amplitude of the wave was very important because the maximum wave amplitude interacted with the trailing edge of the wing.

*Reflection Plate Location Sensitivity*

Similar testing was completed to determine the sensitivity to reflection plate location. The reflection plate was moved 5mm upstream and downstream of it standard position. This testing was completed on a flat wing, 45° up, and 45° down geometries at the 0.75 and 1 λ locations(Table 4.3). Results shown here are for the flat plate with a 1.56 Hz wave because this case had the greatest sensitivity.

Table 4.3 Effect of moving the reflection plate a small amount

| % Change of Energy Absorbed with movement of reflection plate | | |
|---|---|---|
| | 5 mm Upstream | 5mm Downstream |
| 0.75 λ | 3.04% | 2.83% |
| 1 λ | -12.04% | -12.07% |

Since the amplitude of the wave is insignificant at the node location, the small shift up or downstream of the 0.75λ location was not expected to have a large effect on

50

the energy absorbed. A small increase was seen because the amplitude of the wave increased upstream and downstream of the node as the anti-node is approached. The increased amplitude at the trailing edge of the wing caused an increase in the force acting on the wing, which accounted for the increase in energy.



**Figure 4.12** Node and anti- node locations for steepness comparison. It is seen the wave is steeper on either side of the anti-node than at the node.

The amount of energy absorbed was more sensitive to the translation of the reflection plate at the $1\lambda$ location. This was because at the peak of the wave the steepness was greater than near the mean free surface at the node location (Figure 4.12). Therefore, when the trailing edge of the wing interacted with an anti-node, a small shift in reflection plate location had a greater effect on the amount of energy absorbed because the amplitude of the wave in contact with the trailing edge of the wing decreased.

*Conclusion*

Based on the results above, it was seen that there was about a 3% error in the results of the measurement system. The location of the reflection plate and the depth of the water also had an effect on the amount of energy absorbed if not placed in the exact location. To account for any error in the measurements and any accuracy error in the test setup an overall error of 5% is assumed when comparing results.

**Effect of Reflection Plate on Energy Absorption**

Two waves with varying frequencies, wavelengths, and amplitudes were used to examine the effects of adding a reflection plate to the system on the amount of energy absorbed (Table 4.4). The waves will be referenced by their frequencies from this point forward.

Table 4.4 Wave descriptions

| Waves Examined | | | |
|---|---|---|---|
| | Frequency (Hz) | Wavelength (cm) | Amplitude (cm) |
| Wave 1 | 0.97 | 122.3 | 2.5 |
| Wave 2 | 1.56 | 61.2 | 4.4 |

The interaction of the wave and wing can be seen in Figures 4.13-4.16 for the following cases respectively: 0.97 Hz and 1.56 Hz with reflection plate a $0.5\lambda$ and 0.97 Hz and 1.56 Hz with reflection plate at 0.25 $\lambda$.
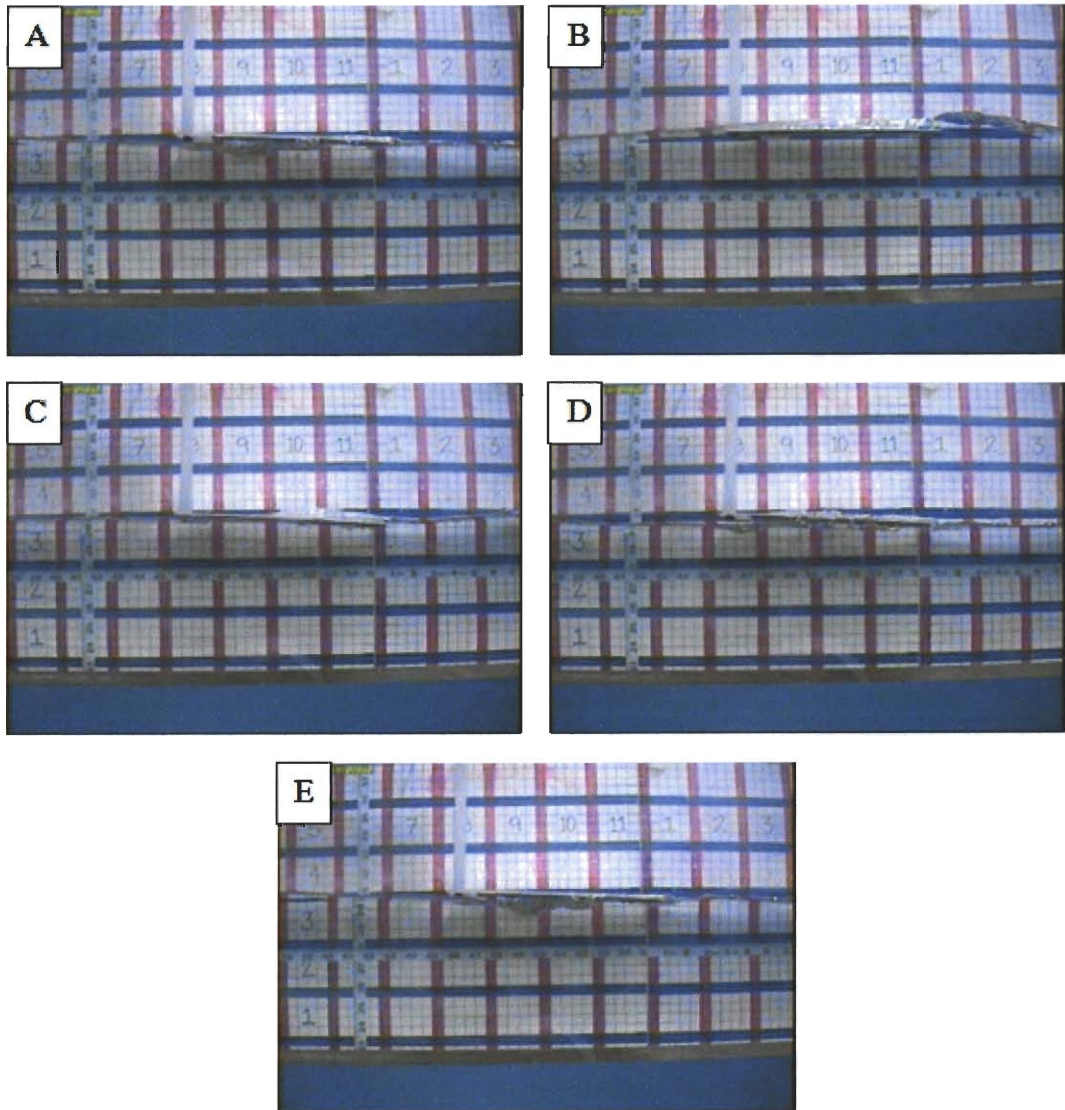
**Figure 4.13 One wave cycle for a 0.97Hz wave with the reflection plate at 0.5λ**
**A: Calm free surface, B: Wave at Peak, C: Calm free surface**
**D: Wave at trough, E: Calm free surface**
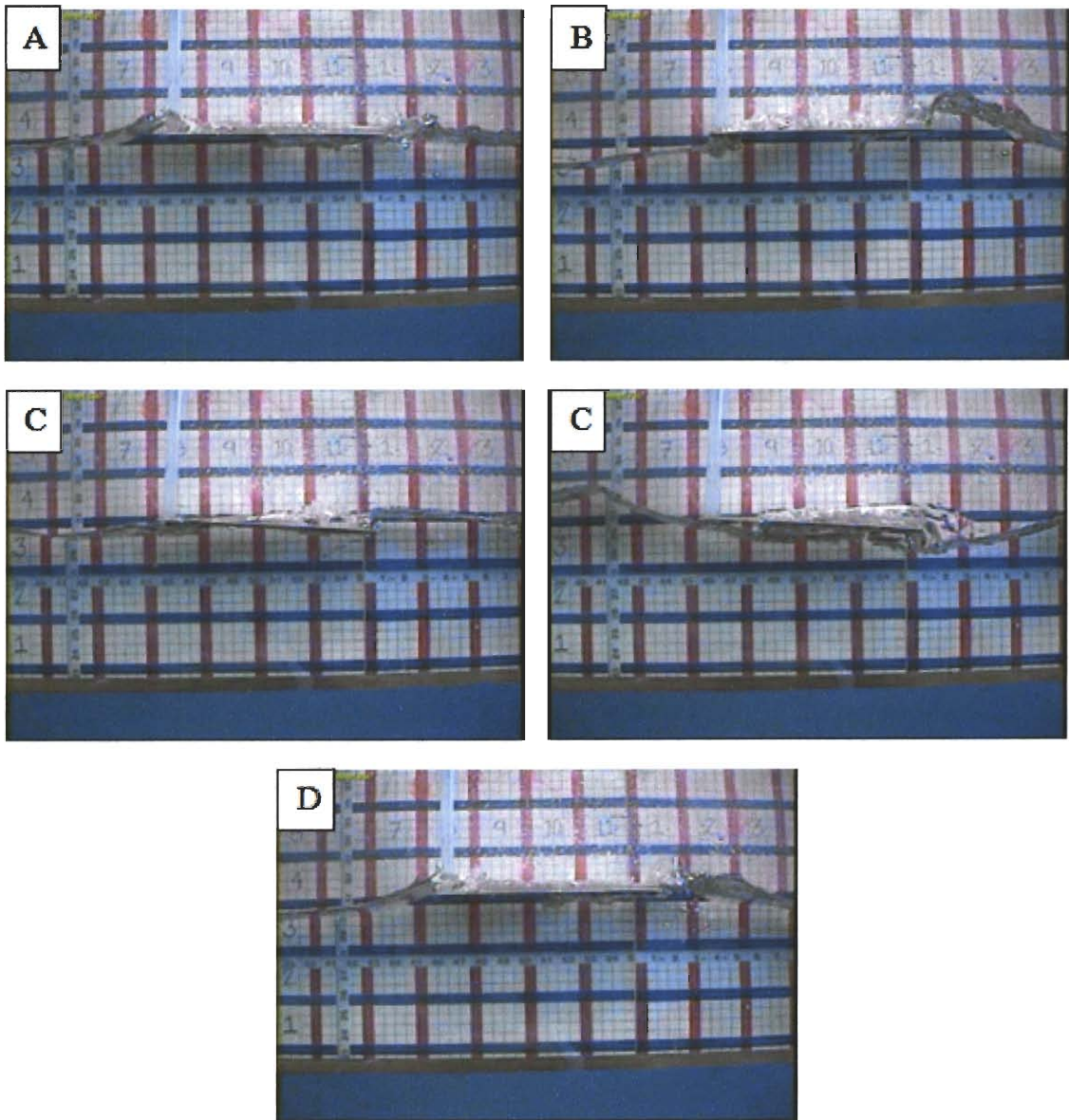
**Figure 4.14 One wave cycle for a 1.56Hz wave with the reflection plate at 0.5λ**
A: Calm free surface, B: Wave at Peak, C: Calm free surface
D: Wave at trough, E: Calm free surface

A similar reaction was seen for both waves when the reflection plate was placed at 0.5λ. In both cases, the trailing edge of the wing lies in an anti-node. When the reflection plate was placed at 0.25λ, an anti-node was located at the trailing edge of the wing for both cases.
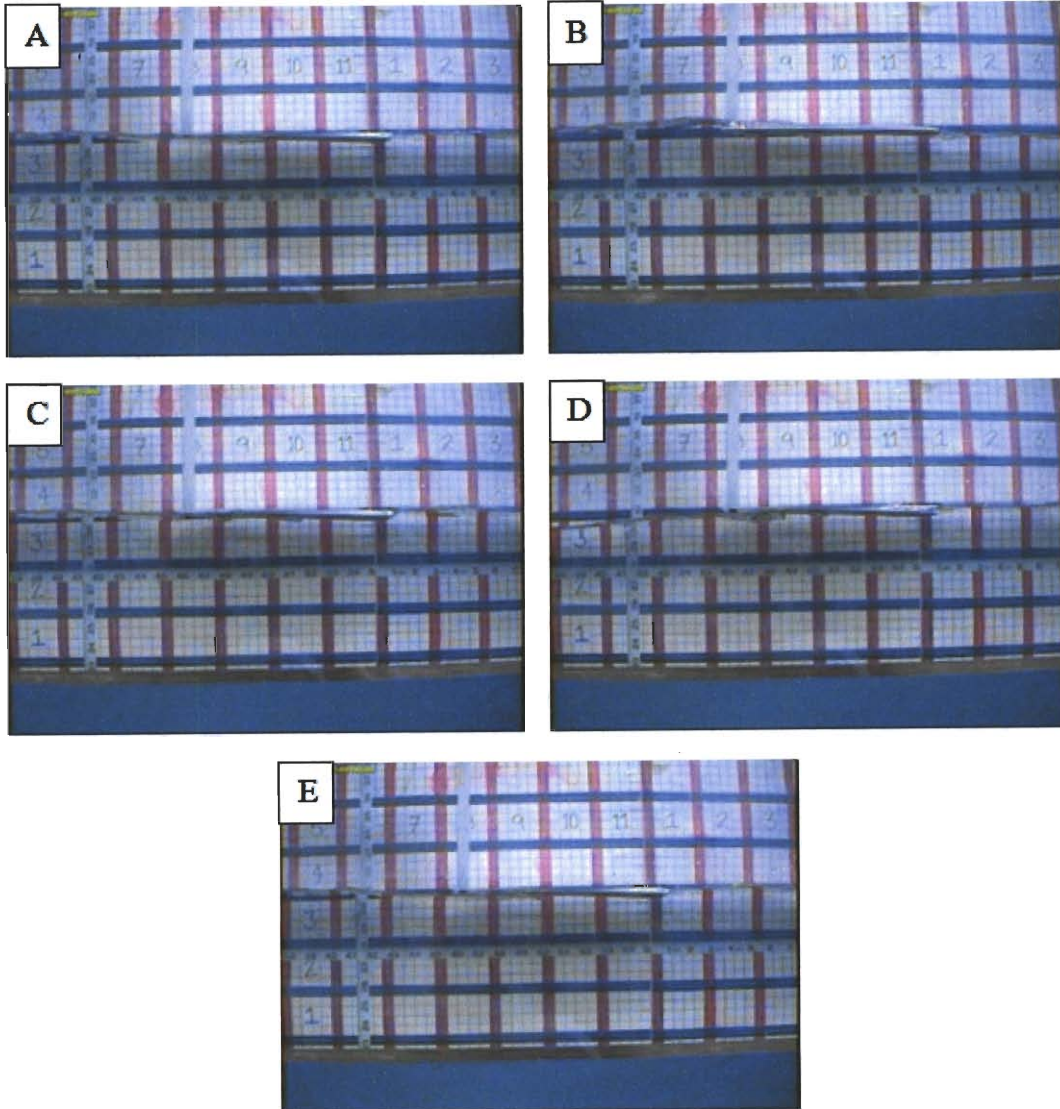
**Figure 4.15 One wave cycle for a 0.97Hz wave with the reflection plate at 0.25λ**
A: Calm free surface, B: Wave at Peak, C: Calm free surface
D: Wave at trough, E: Calm free surface
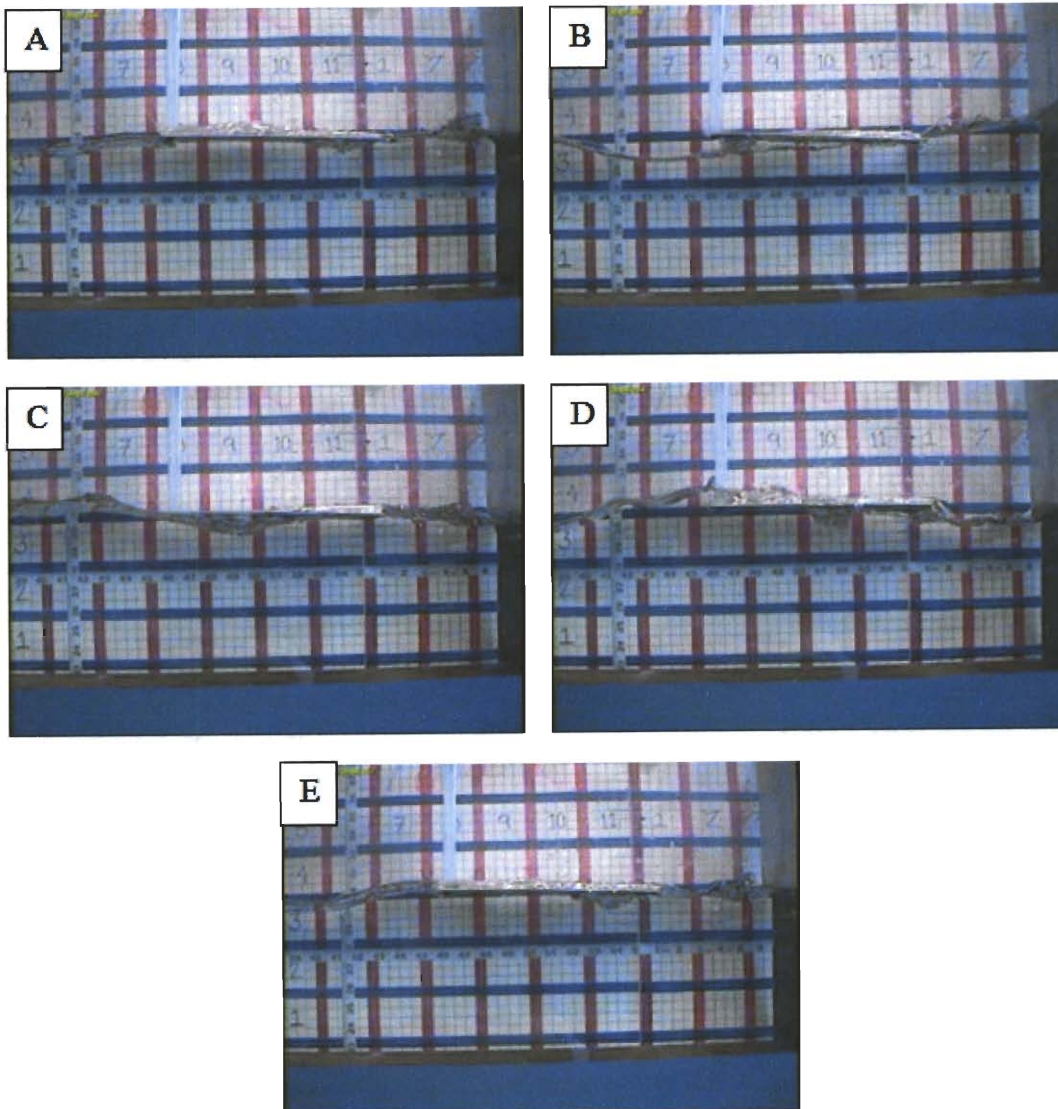
**Figure 4.16 One wave cycle for a 1.56Hz wave with the reflection plate at 0.25λ**
**A: Calm free surface, B: Wave at Peak, C: Calm free surface**
**D: Wave at trough, E: Calm free surface**

The difference in wavelength was however apartment when comparing the two frequencies. It was seen for the 1.56 Hz wave both a node and anti-node interact with the wing since the quarter wavelength of the wave was shorter than the length of the wing. For example in B of Figure 4.14, an anti-node is acting at the trailing edge and a node is acting near the leading edge of the wing.

56

By moving the location of the reflection plate, the interaction of the wing and wave could be controlled as seen above. When the reflection plate was placed at 0, 0.5, or 1λ, the energy absorbed by the wing was maximized. However, when the reflection plate is placed at 0.25 or 0.75λ, the amount of energy absorbed was minimized. Finally, when the reflection plate is placed at an interval between 0.25 and 0.5λ the energy absorbed falls in between the maximum and minimum.

The energy comparisons in Figure 4.17 are for the two different wave frequencies. The graphs compare the percentage of energy absorbed by the wing with the reflection plate at a given location to the baseline energy absorbed for the travelling wave case Eq. (2.9).
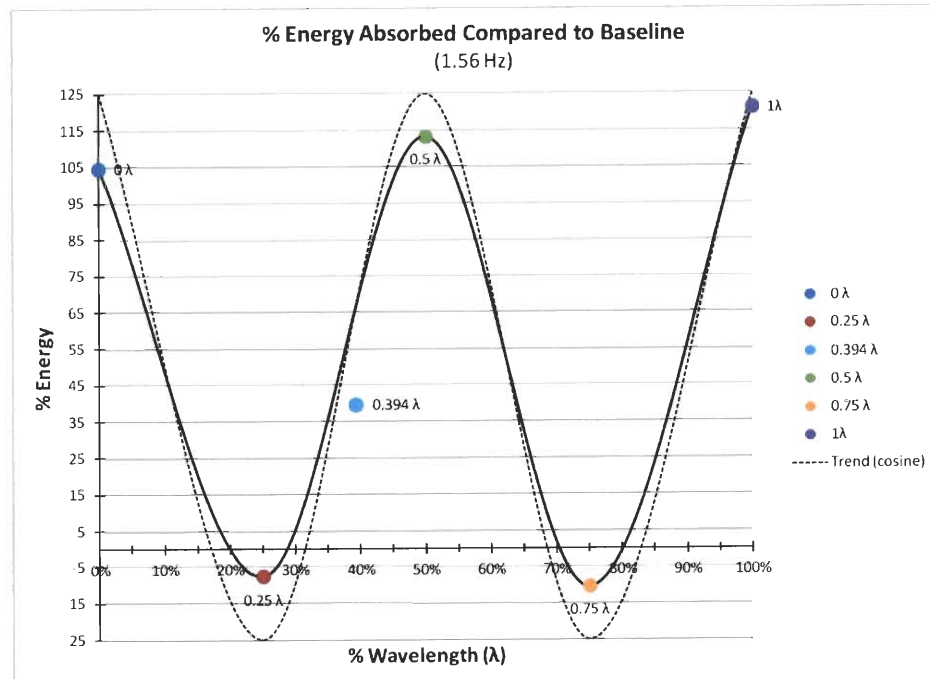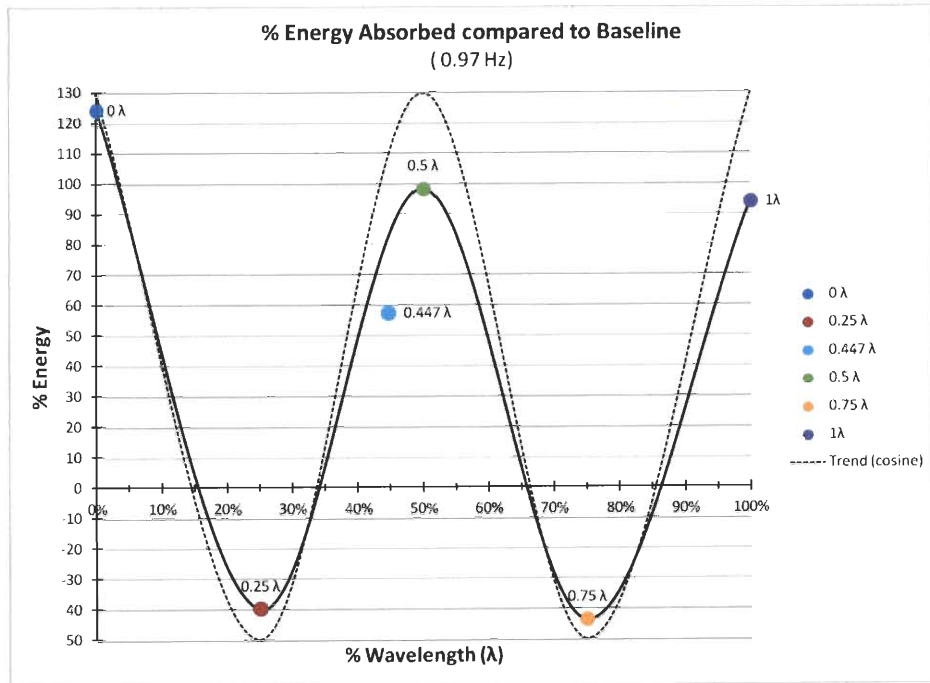
Figure 4.17 Effect on energy absorbed compared to baseline wave with the reflection plate placed at several different locations

58

The trend that the energy absorbed was maximized when the plate was placed at 0, 0.5, or 1λ holds true for both wavelengths. It also holds true that the energy absorbed was minimized for the 0.25 and 0.75λ locations. It was seen in both cases that this relationship follows the trend of a cosine curves. These results were supported by the analytical results in Chapter 3.

The reasoning for this minimum and maximum relationship had to do with how the wing and the wave interacted when the reflection plate was placed at a given location. When the reflection plate is at 0, 0.5, or 1λ, an anti-node was located at the trailing edge of the wing (Figure 4.18). The maximum amplitude or the peak of the wave could be seen acting at the trailing edge of the wing.
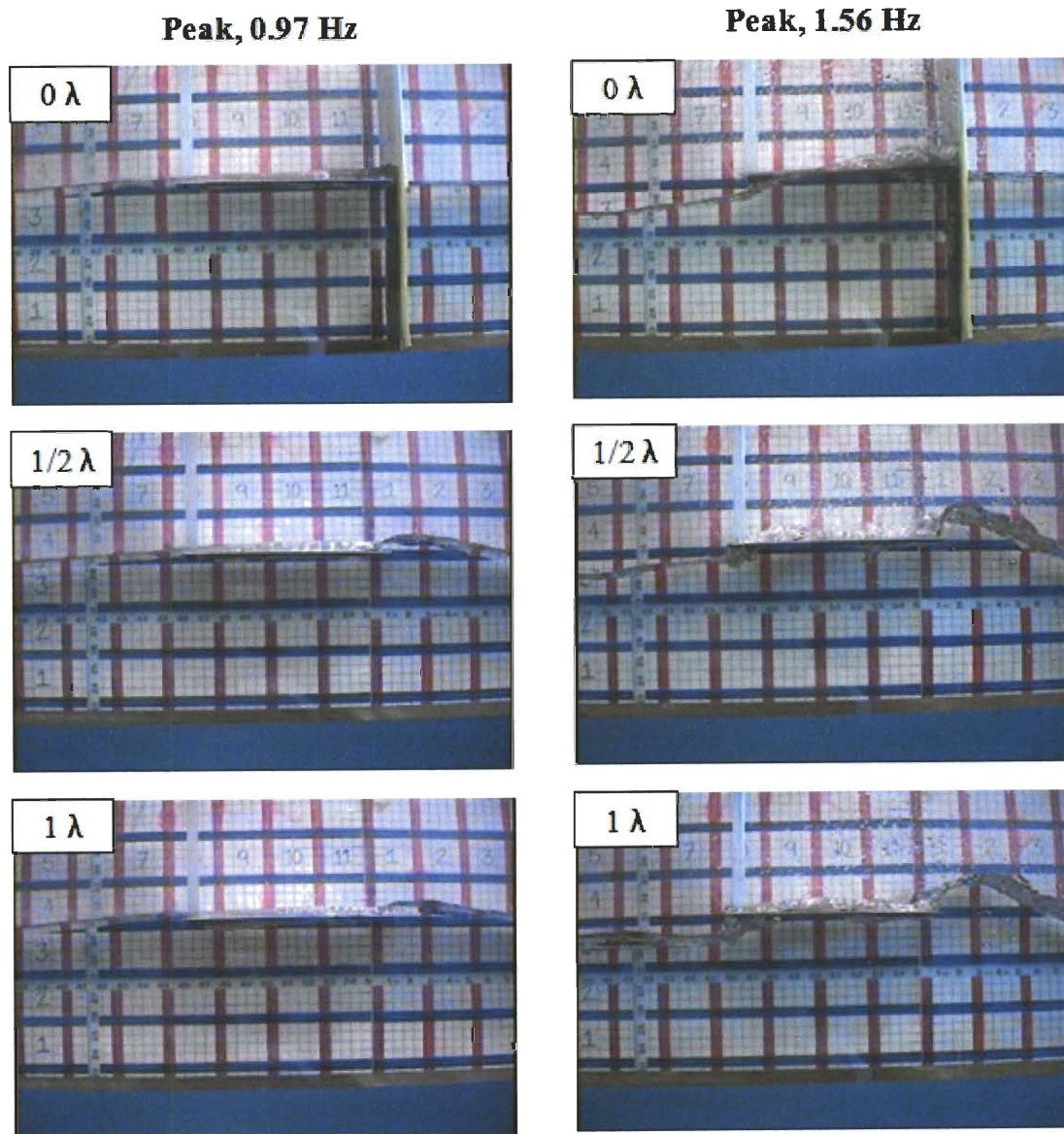
**Figure 4.18 Anti-node at the trailing edge of the wing**

Since the torque was measured about the leading edge of the wing, this created the longest moment arm possible between the maximum amplitude of the wave and the leading edge resulting in the maximum energy being absorbed. The amplitude of the wave was directly related to the available energy of the wave. In general, the larger the amplitude of the wave the more energy there was available to be absorbed Eq. (3.4).

However, when the reflection plate was placed at 0.25 or 0.75λ the trailing edge of the wing was placed in a node. So the maximum amplitude of the wave in contact with the plate was at the leading edge, which minimized the moment arm and in turn the amount of energy absorbed by the wing (Figure 4.19).
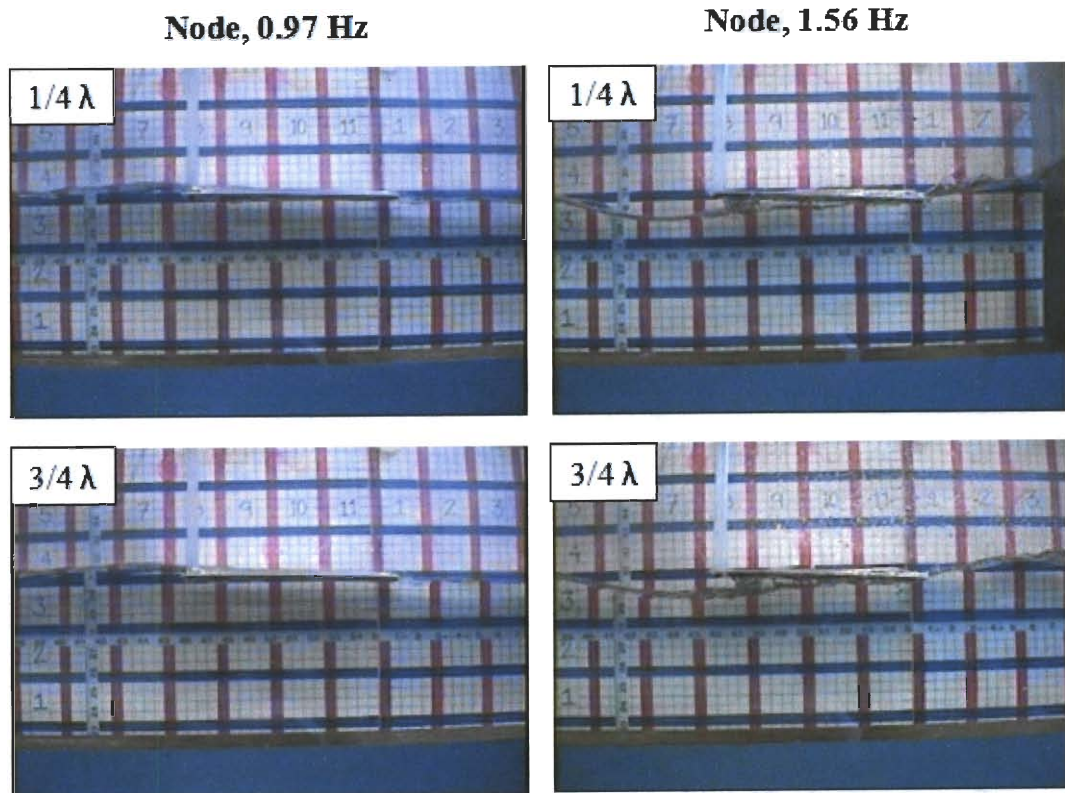


Figure 4.19 Node at the trailing edge of the wing

As the location of the of the reflection plate was moved between 0.25 and 0.5λ, the amount of energy absorbed by the wing increased from its minimum at 0.25λ to its maximum at 0.5λ and vise versa as the reflection plate was moved from 0.5 to 0.75λ. This was because the moment arm of the anti-node interacting along the profile of the wing increased from its minimum to its maximum and vise versa respectively (Figure 4.20).

**0.97 Hz**  **1.56 Hz**

.45 λ   .39 λ
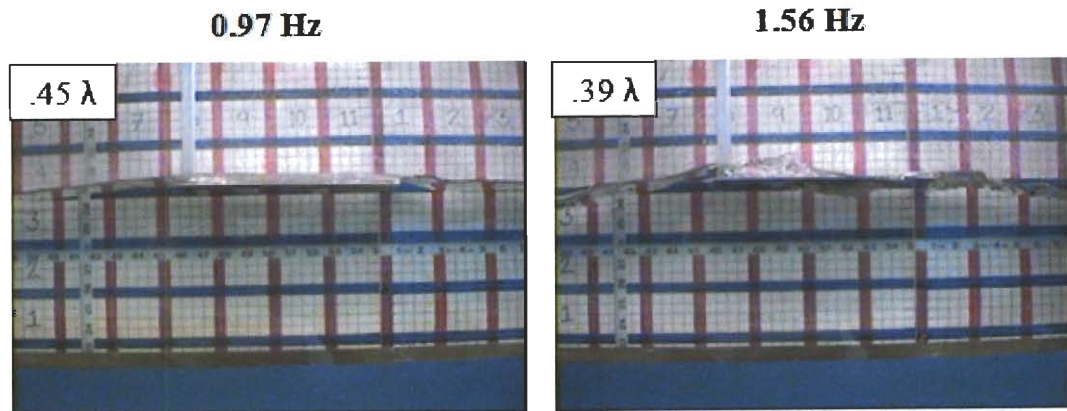
Figure 4.20 Anti-node shifted along plate profile when reflection plate was placed between 0.25 and 0.5λ

This is supported by comparing the moment or torque measured around the leading edge of the wing for the travelling wave and standing wave cases with the reflection plate placed at 0.25, 0.5 and an in intermediate wavelength (Figure 4.21).

For both frequencies, it was seen that the torque and the spectral energy density curves support the energy absorption trends observed. The 0.5λ locations had the highest torque measurements and in turn the most energy. While the 0.25λ, had the lowest torque measurement and the least energy absorbed. The travelling wave and intermediate location cases fell between the two extremes as was expected.
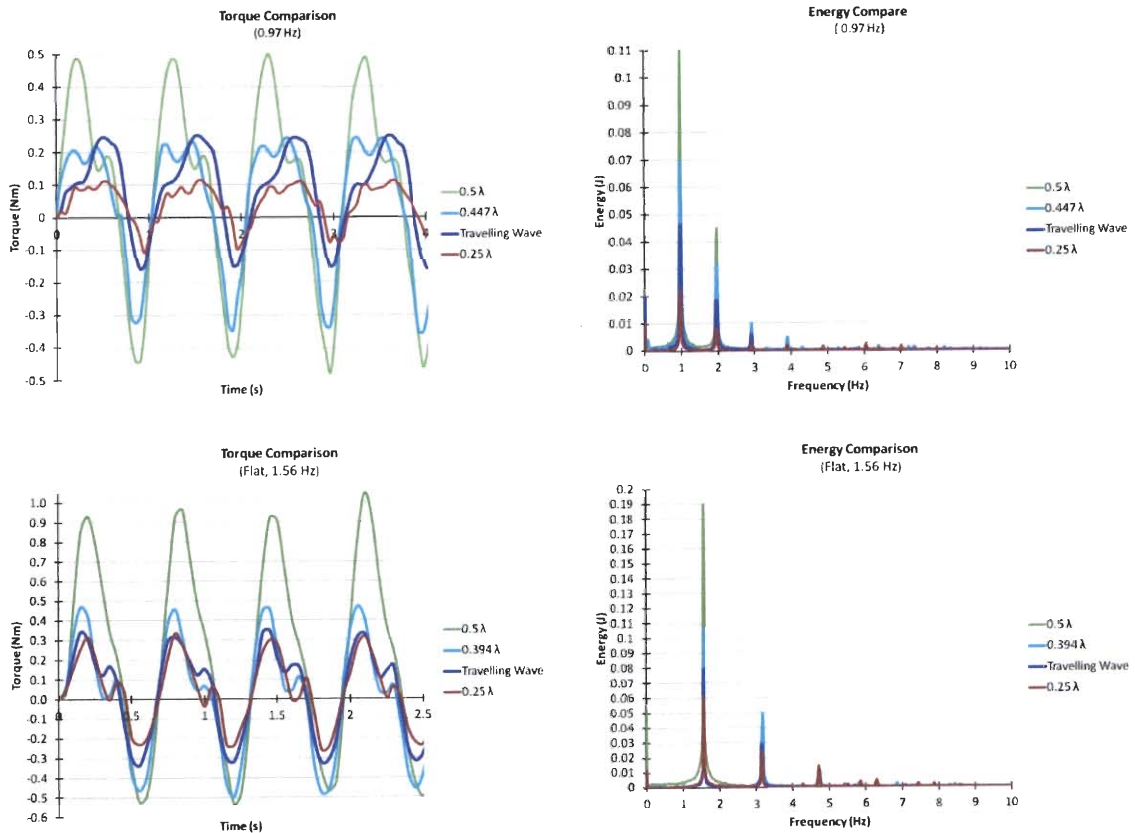
**Figure 4.21 Torque and energy comparison of different reflection plate locations and frequencies**

Another trend that was observed was that the percentage of energy absorbed by the wing was within the 5% tolerance for 0.5 and 1λ cases and the 0.25 and 0.75λ cases. This was confirmed by comparing the torque and spectral energy curves, which were very similar (Figure 4.22 and 4.23). This was the expected result due to the nature of a standing wave having an anti-node every ½ wavelength and the analytical calculations discussed in Chapter 3.
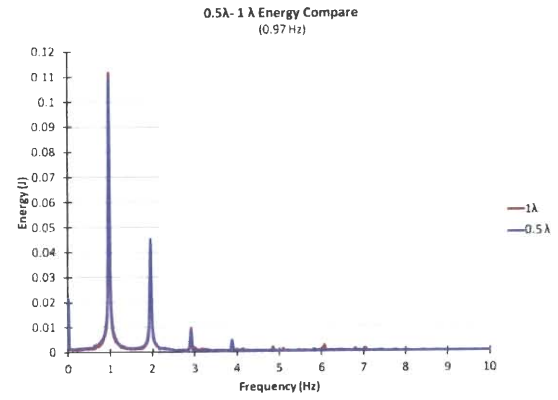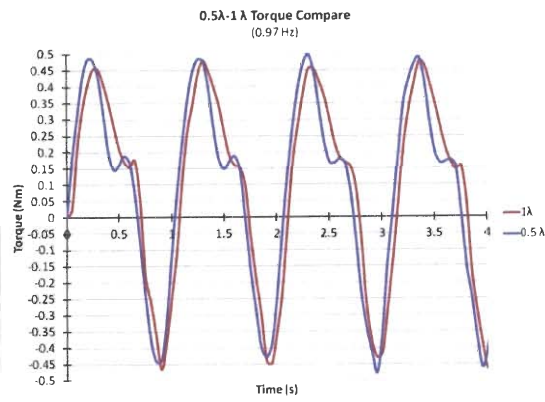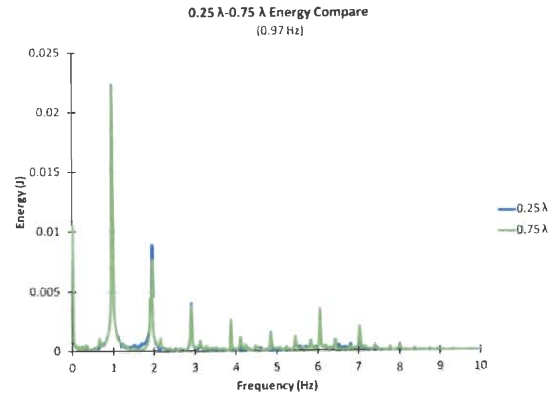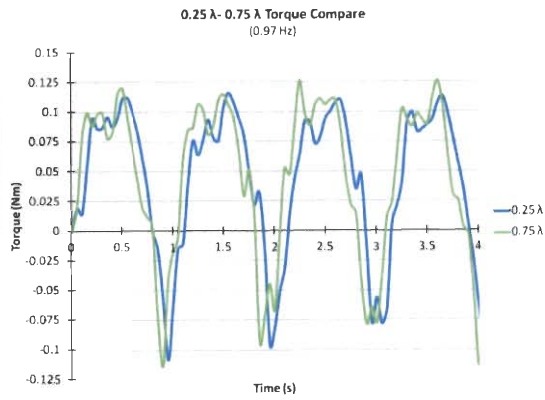
Figure 4.22 Torque and energy comparison for 0.25-0.75λ and 0.5-1λ at 0.97Hz
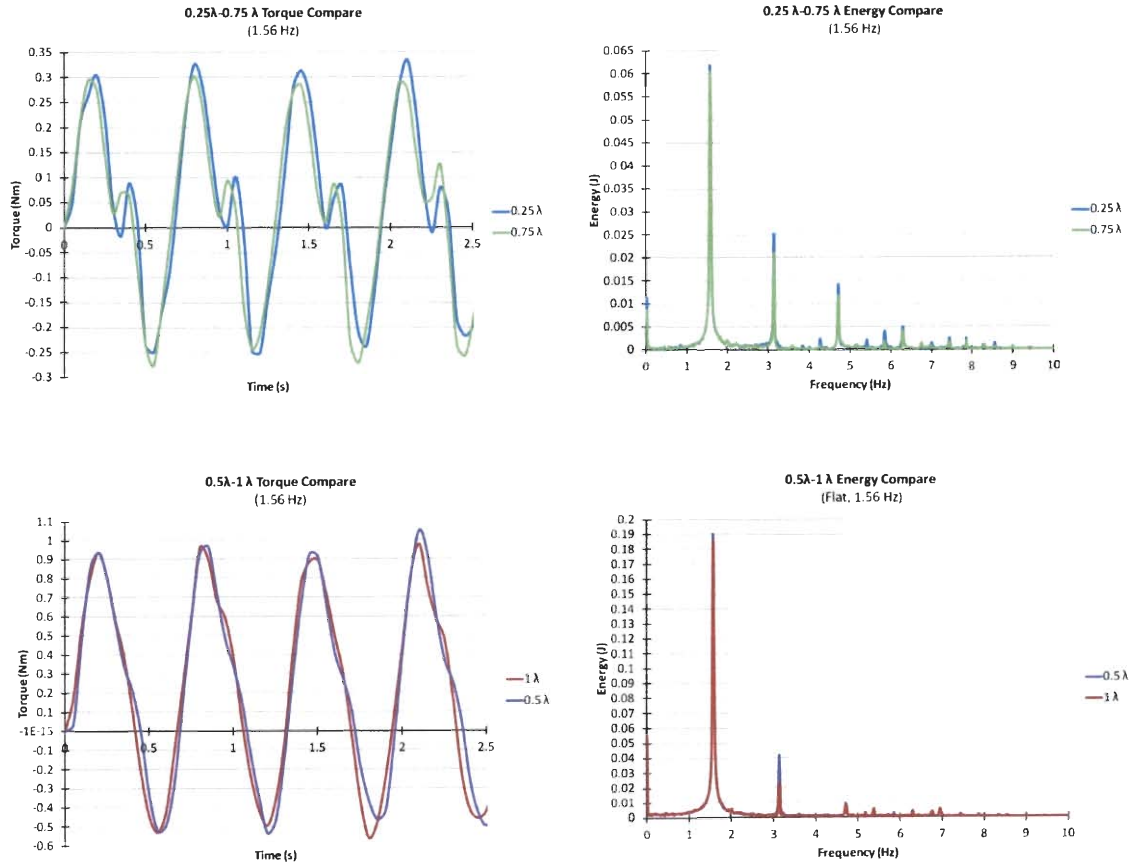
**Figure 4.23 Torque and energy comparison for 0.25-0.75λ and 0.5-1λ at 1.56Hz**

## Effect of Wing Geometry on Energy Absorption

Once it was understood that energy absorbed by the wing was maximized when the reflection plate was placed at 0, 0.5, 1λ downstream of the trailing edge of the wing, the geometry of the wing was varied to find the optimum configuration. Several geometries where used (Table 4.5) with the results all compared to the flat plate with a travelling wave which was considered the baseline case.

**Table 4.5 Wing geometries investigated for optimization of energy absorption**

| Wing Geometries | | |
|---|---|---|
| Flat | | |
| 90 ° up and down | | |
| | Down | Up |
| 15° | | |
| 30° | | |
| 45° | | |
| 90° | | |

The wings tested included 15, 30, 45, and 90° bends the bend was first placed upward, out the water, and then downward, into the water. The final geometry tested was a wing with a 90° up and down plate attached at the trailing edge. For each case, the moment arm of the wing was held consistent to keep the anti-node or node acting at the trailing edge of the wing as previously discussed.

### *Effect of upward bend from 15-45°*

Figure 4.24 shows the comparison of the energy absorbed by the wing with an upward bend in relation to the flat plate case. The amount of energy absorbed when the wing was bent out of the water decreased. The decrease in absorbed energy increased with an increase in angle from 0 to 45° for the 0.5 and 1$\lambda$ cases. When the trailing edge of the wing was placed at a node, the dependence on the degree of the bend was minimal.
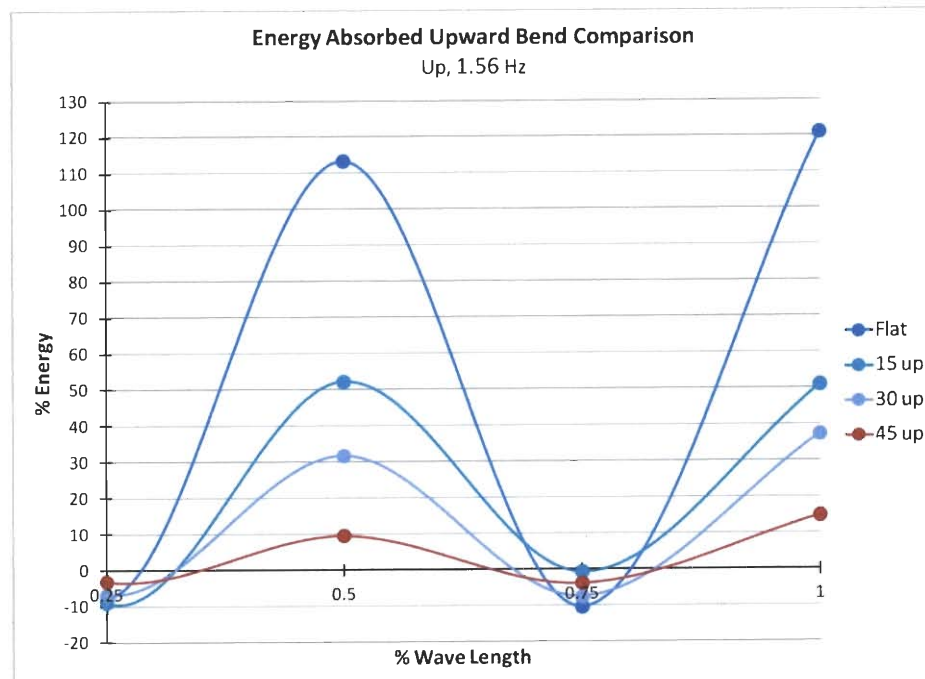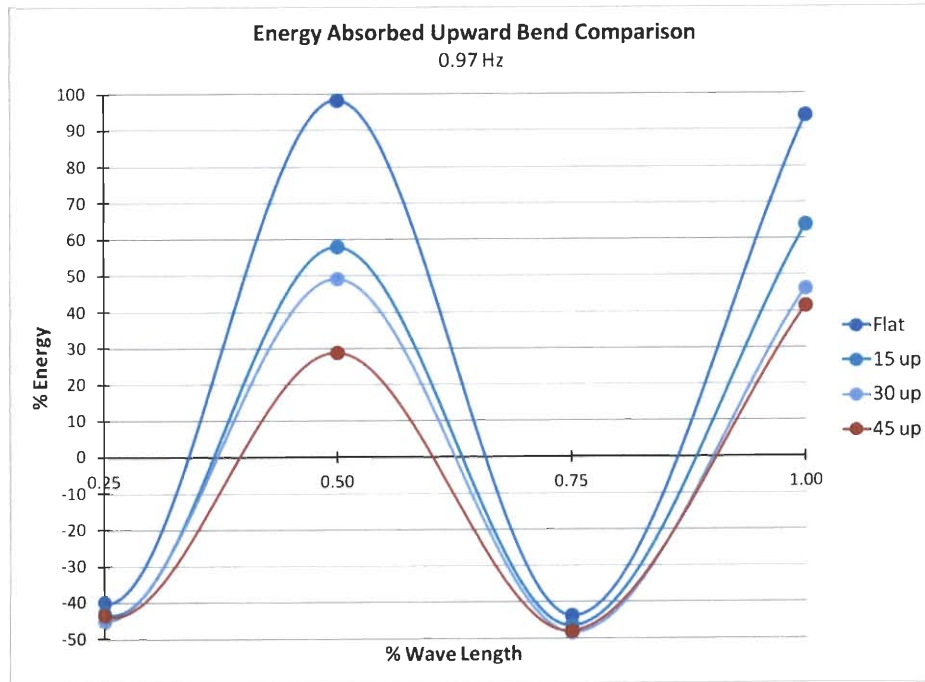
**Figure 4.24 Comparison of energy absorbed by a wing bent out of the water for several reflection plate locations**

By observing the interaction of the wing and the wave, a better understanding of the energy decrease could be had. The decrease in energy absorbed was a direct result of the amount of torque created around the leading edge of the wing (Figure 4.25). The

1.56Hz case was used for comparison since the interaction of the wing and the wave are more pronounced due to the larger wave amplitude.



**0.5 λ Torque Comparison**
**(1.56 Hz)**
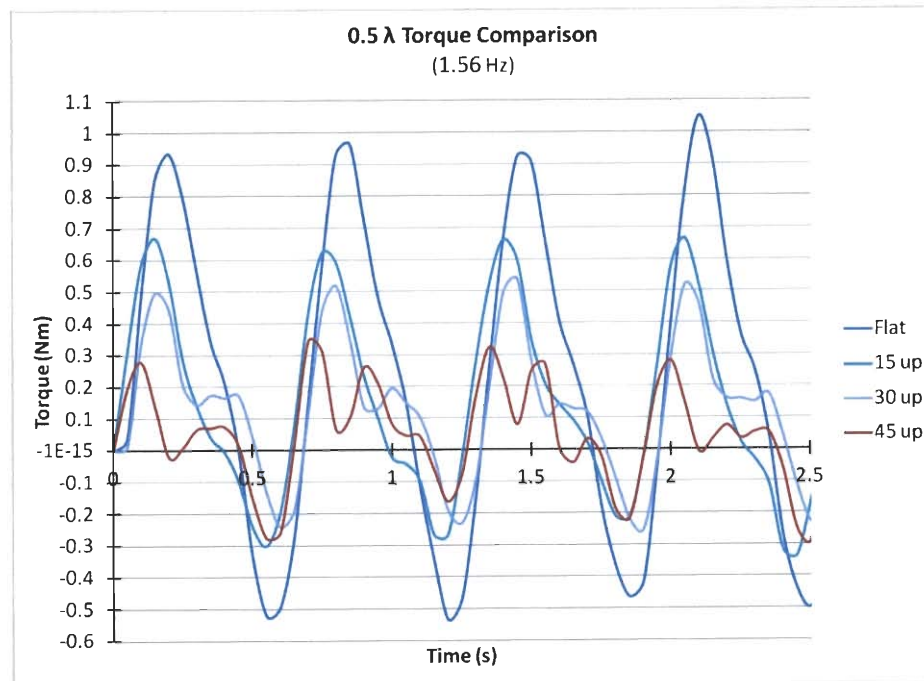
Figure 4.25 Comparison of the torque about the leading edge of the wing for a wing bent out of the water

The torque curves show that there was a decrease in torque about the leading edge of the wing as the degree of the bend increased from 0 to 45°. The amount of negative torque on the wing was fairly consistent for all three bent wing cases. Negative torque corresponds with the wave ascending to its peak or pushing up on the wing.

The reason for the consistent negative torque, which had decreased from the flat plate geometry, was the surface area of wing in contact with the water was decreased when the wing was bent out of the water (Figure 4.26). The surface area of the wing in contact with the water was held consistent between the 15°, 30°, and 45° wings. The shorter surface area reduced the moment arm and the amplitude of the wave in contact with the plate, which accounts for the decrease in negative torque.

69
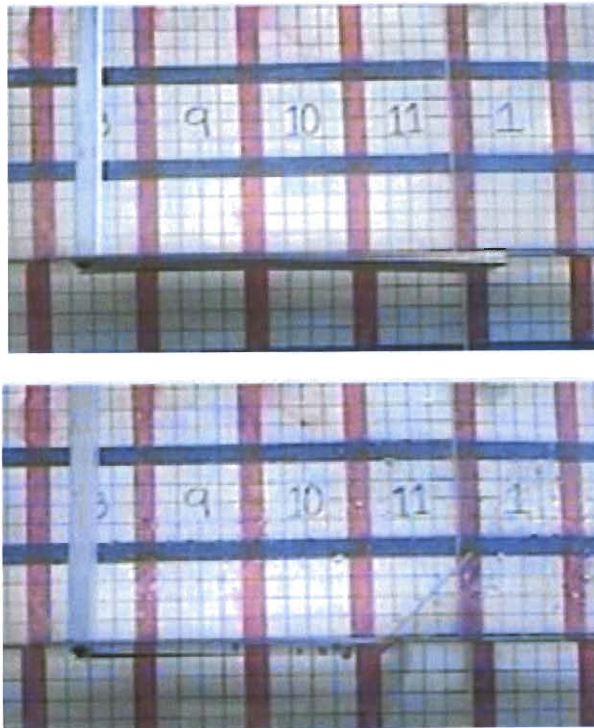
**Figure 4.26 Comparison of the surface area of wing in contact with the water between the flat wing and a bent wing**

It was also observed that the positive torque decreased as the angle of the wing increased. This corresponded to the torque created by the wave descending from its peak or the wave pushing down on the wing. Figure 4.27 shows an interaction comparison of the flat and 45° up wing geometries.
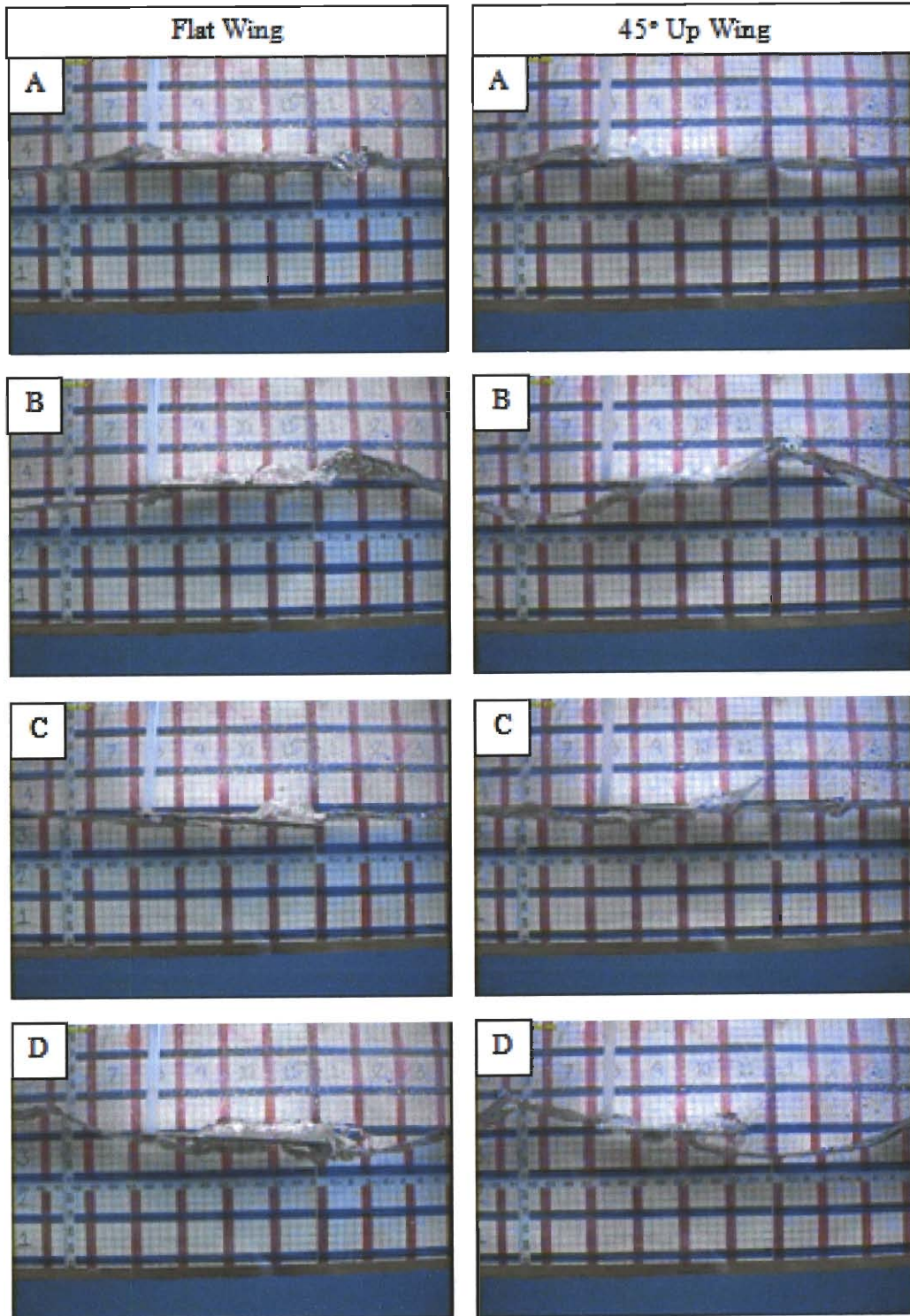
**Figure 4.27 Comparison of the interaction between the wing and the wave for the flat and 45° bent up wing, with a wave frequency of 1.56 Hz.**

A: Calm water level, B: Wave peak acting at trailing edge,
C: Wave ascending onto trailing edge, D: Wave at trough

Comparing the interaction of the wing and wave in photos B through D for the flat and 45° up cases showed that the upward bend prohibited the wave from breaking over the trailing edge of the wing. The breaking of the wave over the wing was what created the increased downward force on the trailing edge and the increased torque and energy.

As the angle of the bend in the wing increased, the percentage of the wave that broke over the wing decreased (Figure 4.28). This was why the torque and energy absorbed decreased as the angle of the wing increased.
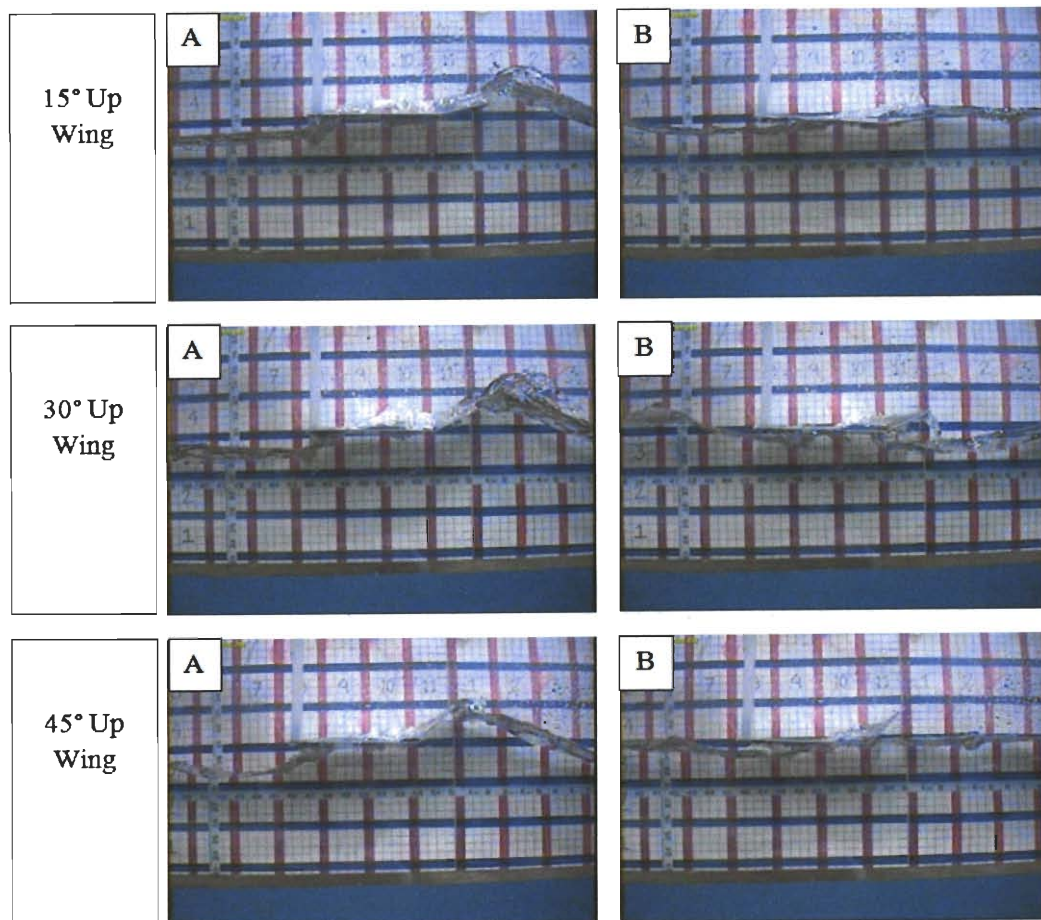


**Figure 4.28 Comparison of the parentage of the wave peak that breaks over the wing surface creating the positive torque about the leading edge of the wing**
**A: Wave at peak, B: Wave descending over trailing edge**

To better understand the contribution of the bent portion of the wing to the energy absorption two different comparisons were made. First, the energy absorbed by a wing with the same surface area as the flat portion of the bent wings was compared to the bent wing geometries(Figure 4.29). For the shorter wing case, the reflection plate was shifted to allow the anti-node or node to act at the trailing edge of the wing. Figure 4.30 shows the energy comparison of the shorter wing to the upward bend.
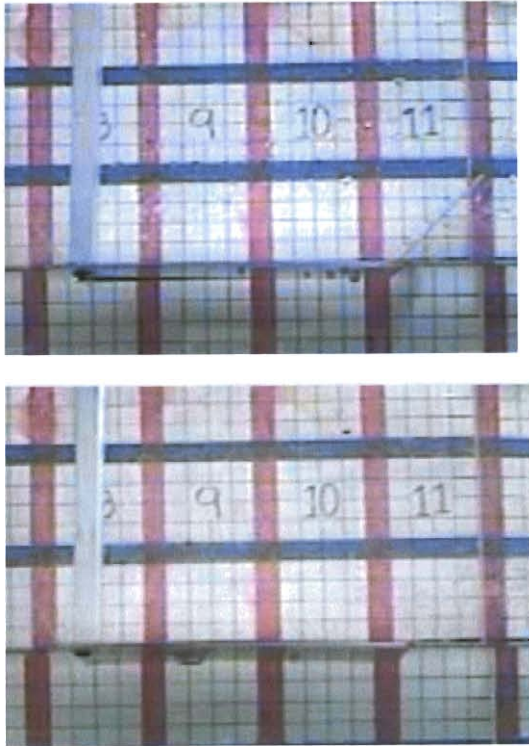


Figure 4.29 Length comparison of the shorter wing

The -0.25% wavelength on the charts in Figure 4.30 corresponds to the travelling wave case. Based on the energy comparison, the amount of energy absorbed by the bent portion of the wing was dependent on reflection plate location, wave amplitude, and wavelength. The locations of greatest interest were when the shorter wing absorbed more

or the same amount of energy as the bent wing. This means that the bend was detrimental to the absorption of energy.
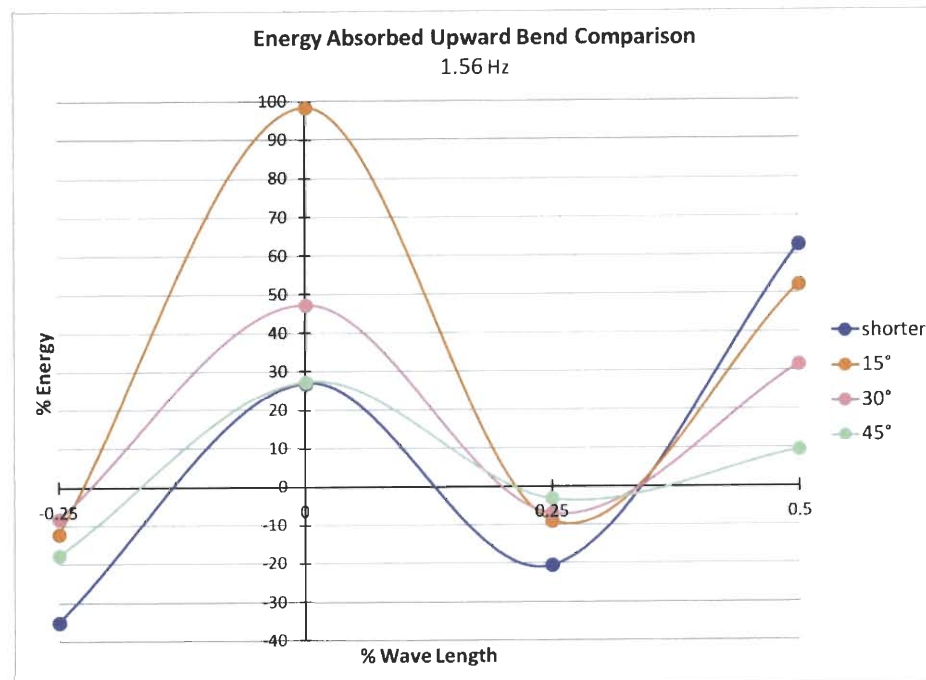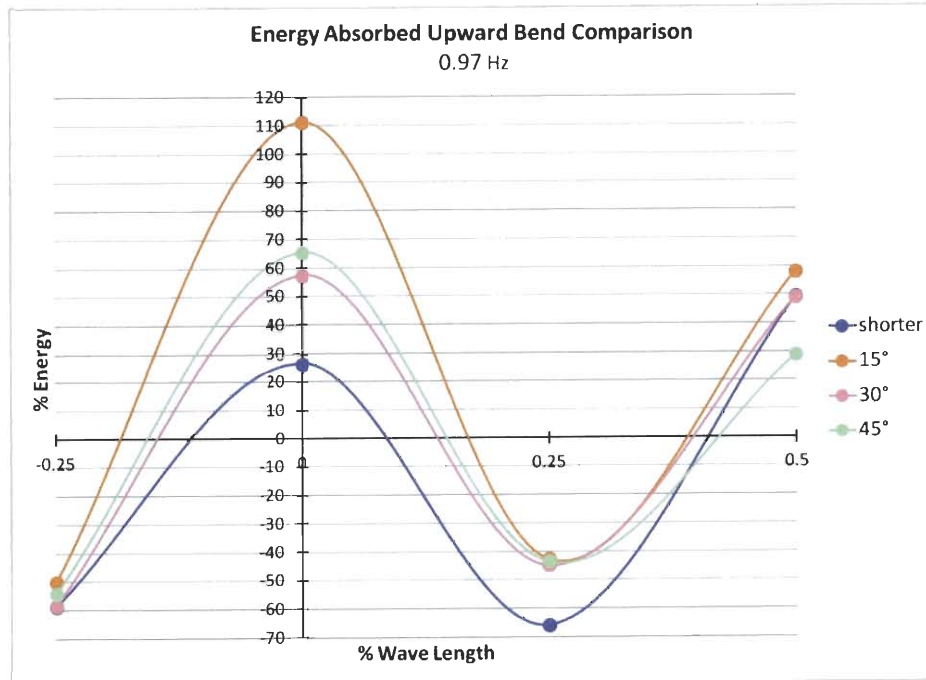


**Figure 4.30 Energy comparison with shorter wing**

This occurred several times. For the 0.97Hz wave that included: the travelling wave with all degrees of bent wing and the 0.5 λ reflection plate location with both the 30° and 45° geometries. For the 1.56 Hz wave this included: the 0λ reflection plate location with the 45° bend and 0.5 λ location with all bent geometries.

When the trailing edge of the wing was placed in an anti-node, the bent portion of the wing has a negative effect on energy absorption. This was clear because five of the six bent cases at the 0.5 λ reflection plate location absorbed less energy than the shorter plate. This means that the volume of water breaking over the surface of the wing was more significant than the length of the moment arm. Since the bend in the wing, prevented the wave from breaking over the surface of the wing the volume of water was decreased as previously shown.

Secondly, the anti-node was shifted to the location where the upward bend began (Table 4.6). The effect of moving the location of the anti-node also depended on the amplitude and wavelength of the wave.

Table 4.6 Energy comparison with anti-node shifted to the location of bend

| Precent Energy Absorbed 45° Upward Bend | | |
|---|---|---|
| | Location of Anti-node | |
| Frequency | bend | trailing edge |
| 0.97 Hz | 26% | 29% |
| 1.56 Hz | 40% | 10% |

For the 0.97 Hz case, the energy absorbed decreased slightly when the anti-node was moved to the location of the bend. However, the decrease was within the 5% tolerance. So statistically the amount of energy absorbed was the same. The energy

absorbed by the wing was increased when the anti-node was shifted to the location of the bend for the 1.56 Hz case. This shows that the 0.97Hz case was less sensitive to the location of the anti-node.

These results support the conclusion that the volume of water that breaks over the surface of the plate has a larger effect on the energy absorbed than the length of the moment arm. Since the wavelength of the 0.97Hz wave was longer than that of the 1.56 Hz wave, the volume of water on the surface of the plate was less sensitive to the location of the anti-node (Figure 4.31).
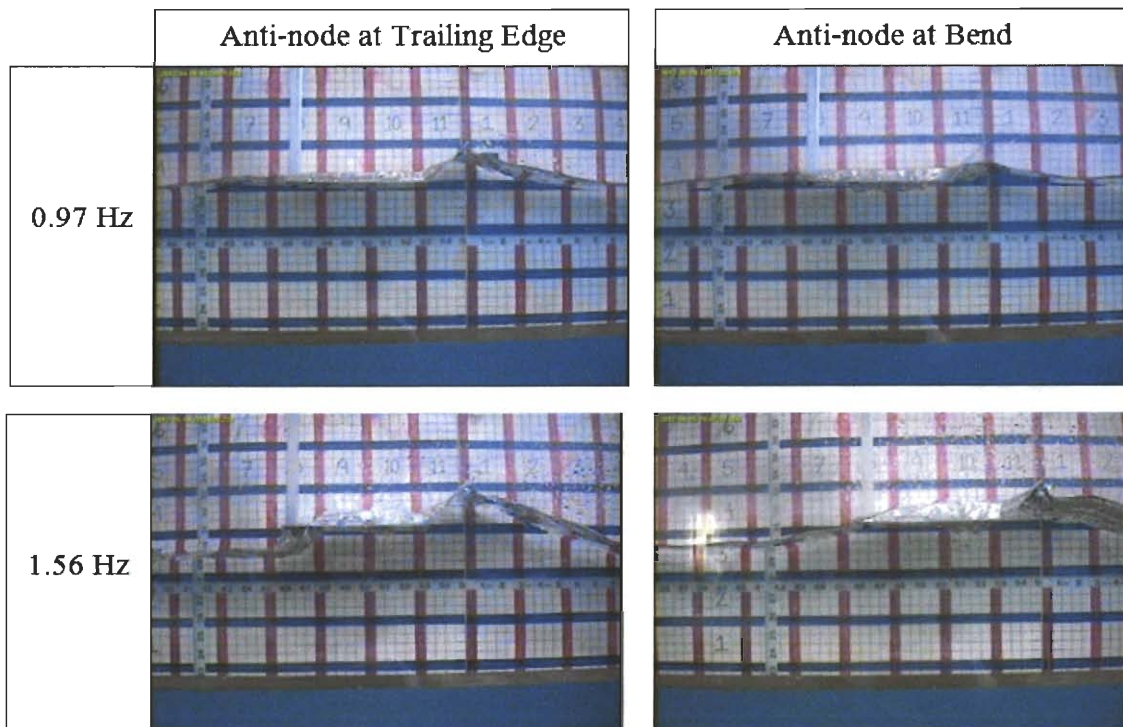


**Figure 4.31 Comparison of the volume of water over the surface of the plate when the anti-node is located at the trailing edge or the bend of the wing for the 0.97Hz and 1.56 Hz cases**

76

A downward bend of the wing had the opposite effect as the upward bend. The amount of energy absorbed increased. The greater the bend the more the energy absorbed increased from 0 to 45° (Figure 4.32). Unlike the upward bend, the energy absorption at the 0.25 and 0.75 $\lambda$ locations was also affected by the degree of the bend. As the degree of the bend in the wing increased, the effect of location of the reflection plate became less significant. The effect of the degree of the bend also depended on the wave's amplitude and wavelength but both waves followed a similar trend.

By analyzing the wave and wing interaction and understanding the particle motion of a wave, the reason for the increased energy absorption can be explained. The same phenomenon created the increase in both the negative and positive torque on the wing. A wave particle remains in the same transverse location and rotates in a circular motion as described in Chapter 1. The downward bend of the wing interacts with this wave motion to create the increased torque.

An increase in positive torque, force pushing down on the wing, was created by the wave particles acting on the upper surface of the wing as it descended from its peak to its trough. While, an increase in negative torque, upward force on the wing, was created by the wave particles interacting with the underside of the wing as the wave ascended from its trough to peak. Observe that, the breaking of the wave over the surface of the wing does not contribute to the energy absorption, unlike with the upward bend. The important reaction was under the surface of the water.
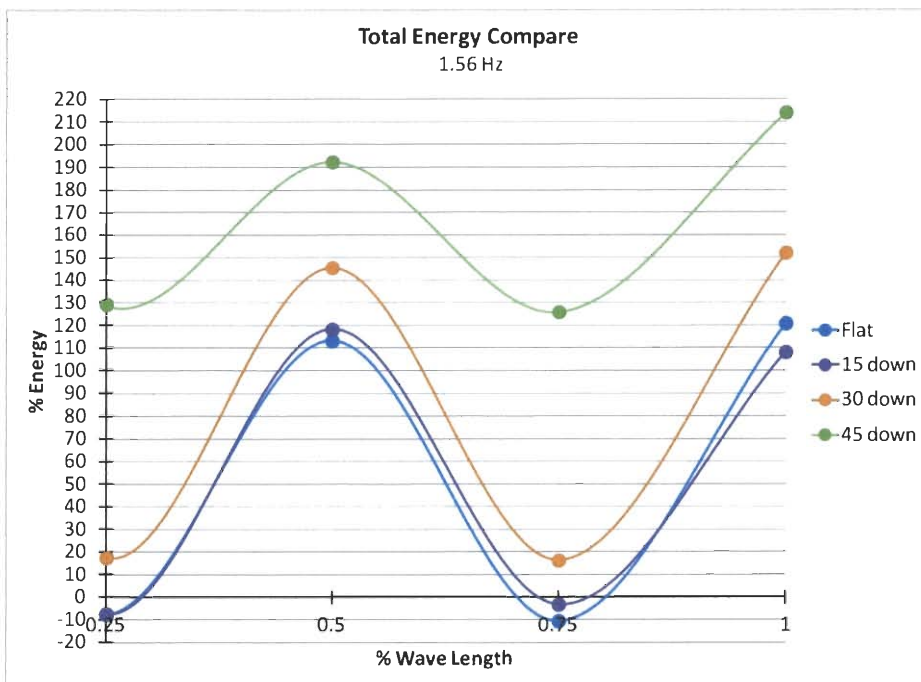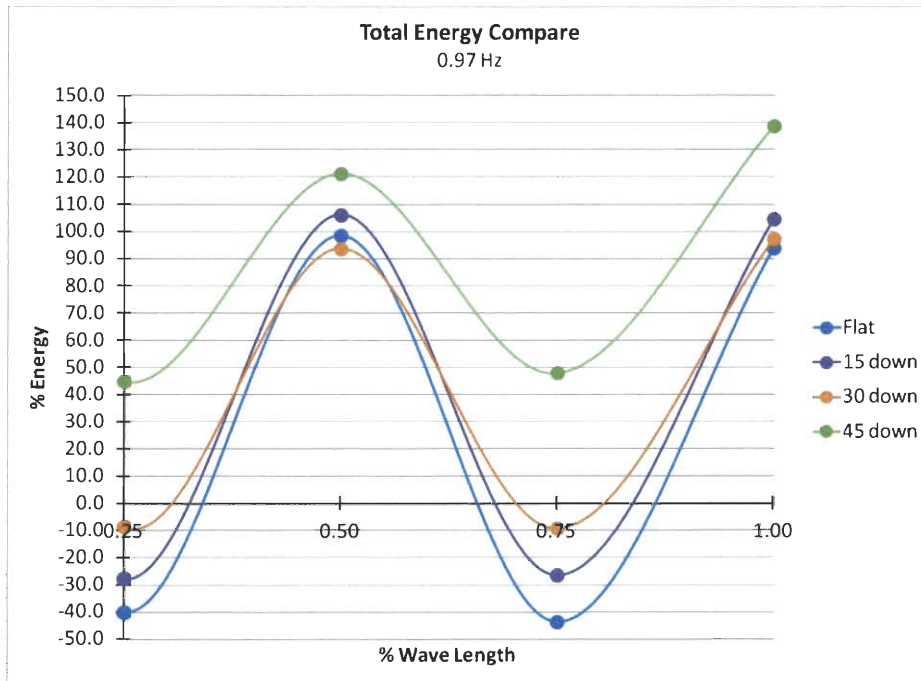
**Figure 4.32 Energy comparison for a wing with a downward bend from 15-45° to the flat wing**

Beginning with the trailing edge of the wing in the node of the wave, the effects

of the downward bend will be analyzed. Comparing the torque created about the leading

edge of the wing for the 0.97Hz case (Figure 4.33) showed a large increase in torque at

78

the 45° downward case. For the 30° downward case, the effect of the bend was much less significant. The effect decreased even more for the 15° wing. A similar trend was seen for the 1.56 Hz case. In fact for the 1.56Hz wave, the 15° wing essentially became a flat wing when comparing the amount of energy absorbed in both cases. This was because the amplitude of the wave made the bend insignificant (Figure 4.34). Comparing the flat and 15° wing showed a similar interaction with the wave.
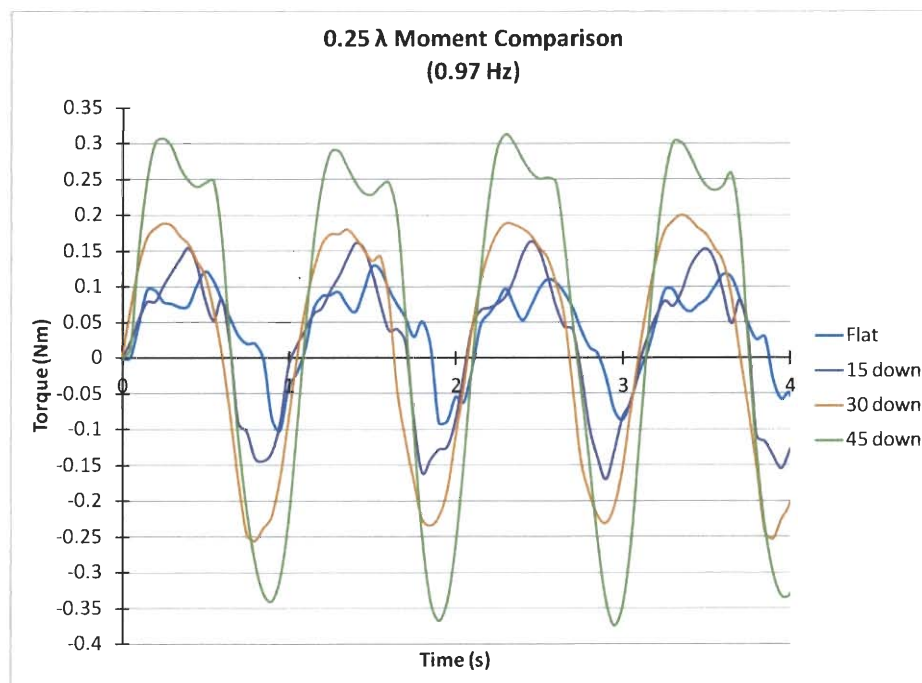


**Figure 4.33 Torque created about the leading edge of the wing when the trailing edge was placed in a node**

Comparing the wave and wing interaction showed that the portion of the wing under the surface of the wave increased as the angle of the wing increased (Figure 4.34). This increase corresponded to an increase in torque. When the wave was at its peak, the portion of the wave over the bent portion of wing was what created the positive torque due to the downward force of the water particles on the wings surface. The larger the surface area of the wing under the surface of the water the more water particles acted on the surface the greater the downward force.

When the wing was at its trough, the portion of the wave under the wing was what produced the negative torque. The deeper the bend in the wing the more energy from the water particles that was contained under the wing and absorbed as the wave ascended to its peak (Figure 4.35).

The amount of negative torque was directly influenced by the amount of positive torque on the wing. The more positive torque about the leading edge of the wing the further the trailing edge would go from the node location as the wing rotated downward. Comparing the locations of the trailing edge at the trough in Figure 4.34 shows that as the angle of the wing increased the distance of the trailing edge from the node location increased. This was especially true for the 45° case as was expected from the torque curves. As the distance from the node location increased, the amplitude of the wave increased and in turn the energy of the water particles. As the available wave energy increased, the amount of energy absorbed by the wing increased. These reactions were the reason why as the bend angle increased the location of the reflection plate was less significant to energy absorption even when the trailing edge was placed in a node.

|  | Trough | Peak |
|---|---|---|
| Flat Wing | | |
| 15° Down Wing | | |
| 30° Down Wing | | |
| 45° Down Wing | | |
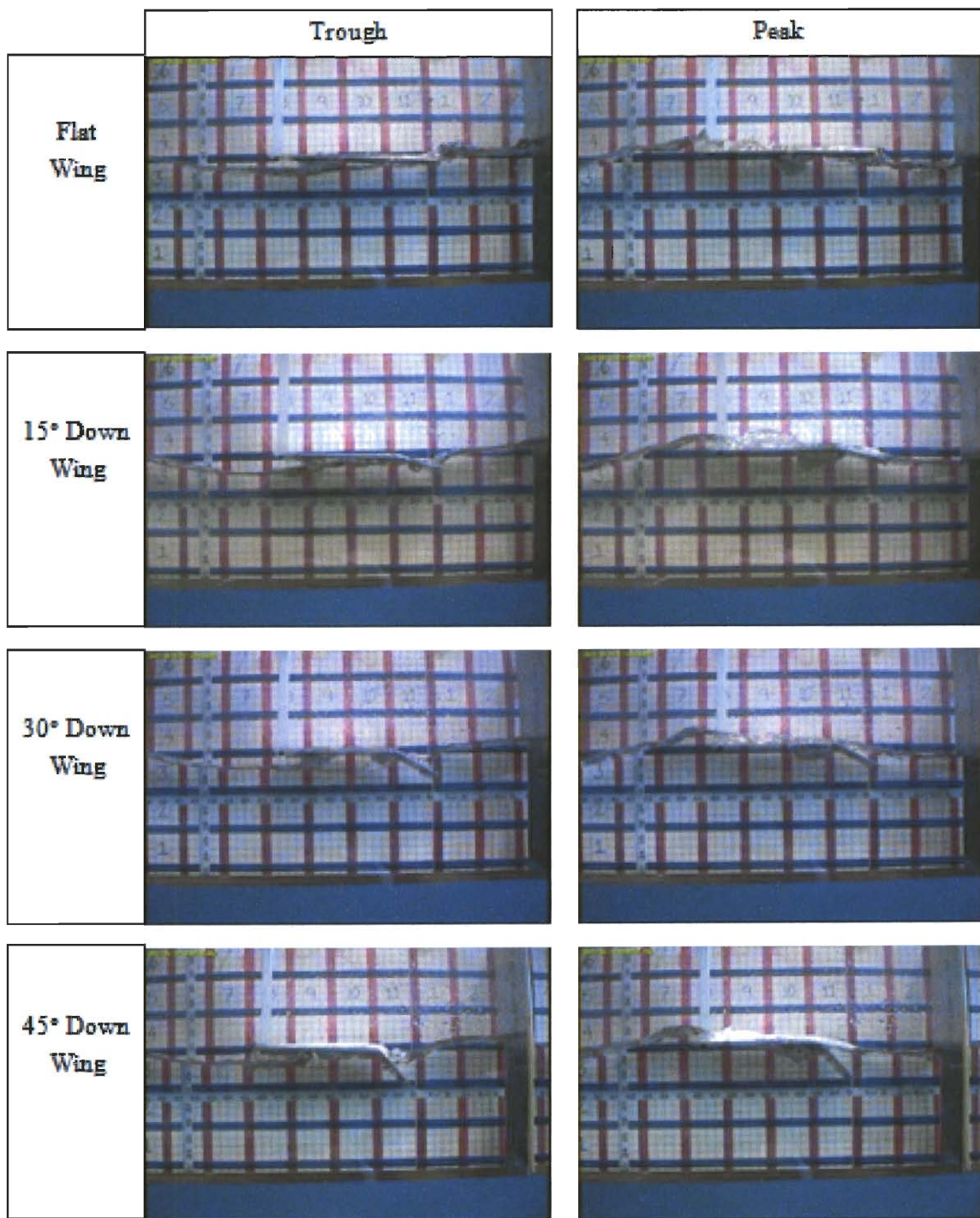
Figure 4.34 Comparison of wing and wave interaction when the trailing edge of the wing is placed in a node
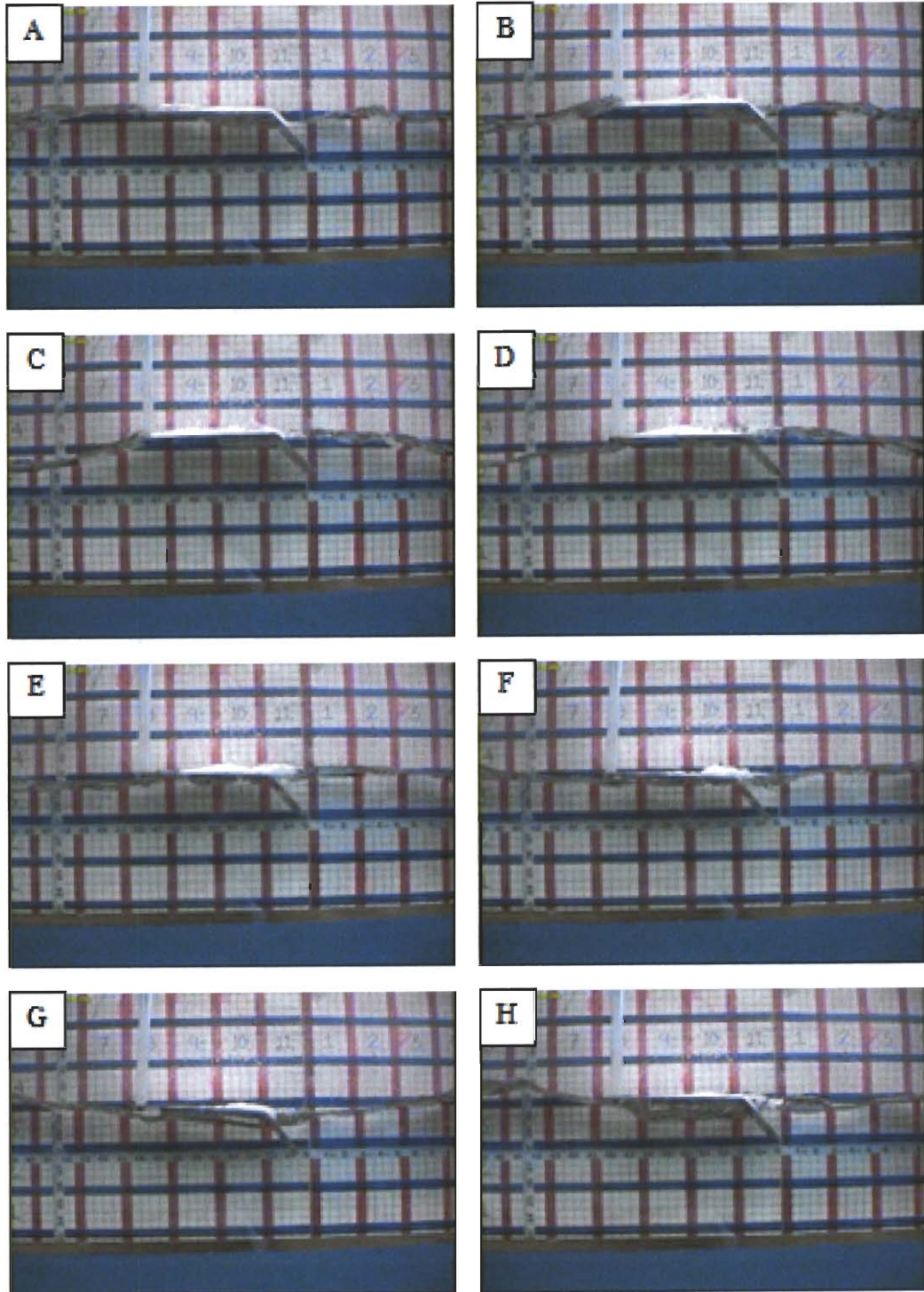
**Figure 4.35 One cycle of the wave and (45°) downward bent wing interaction**

A: Wing is neutral, B: Wave ascending to peak, C: Wave at its peak,
D: Wave descending to trough, E: Descending through the neutral wing location,
F: Continuing Descent, G: Wave at its trough, H: Being Ascent

Next, the interaction of the wave and the bent wing with the trailing edge in an anti-node will be discussed to further support the theory for the increased energy absorption. Figure 4.36 shows a comparison of the torque absorbed about the leading edge of wing for the 1.56Hz case. It was seen that there was a large effect on the negative torque as the angle of the wing increased.
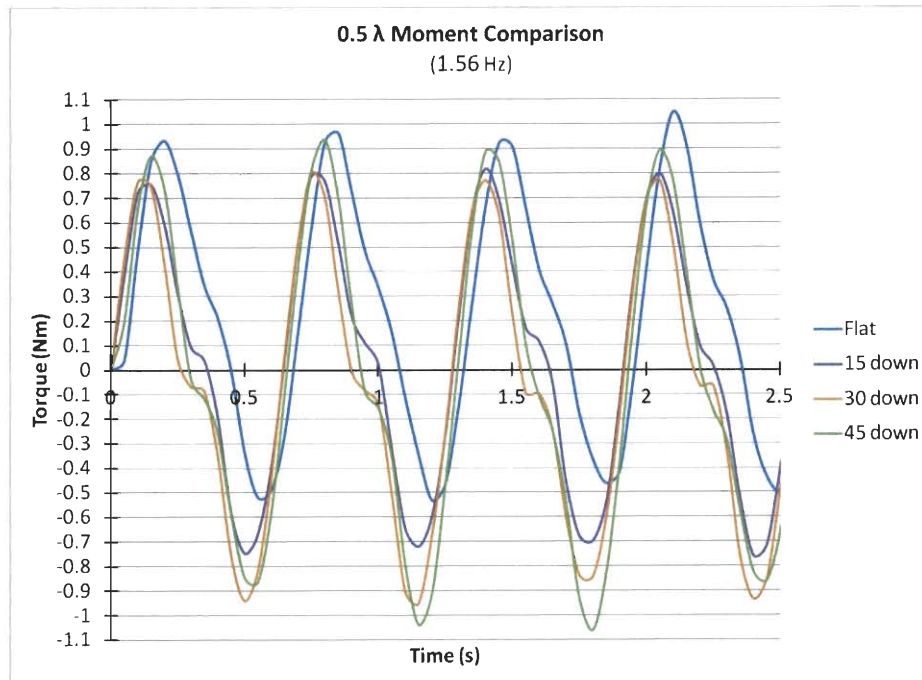


Figure 4.36 Torque comparison for a bent wing with its trailing edge in an anti-node

The interaction that creates the increase in negative torque was the same for these cases as when the trailing edge of the wing was placed in the node. The portion of the wing in contact with the water when the wave is at its trough allows the circular rotation of the water particle to push the wing upward as the wave ascends (Figure 4.37). Observe that much of the flat portion of the wings was not in contact with the water. So as the wave ascends, the interaction with the bent portion created the torque until the remainder on the wave came in contact with the wing. Hence why, the greater the

83

surface area of the bent portion under the free surface of the wave the more torque created.
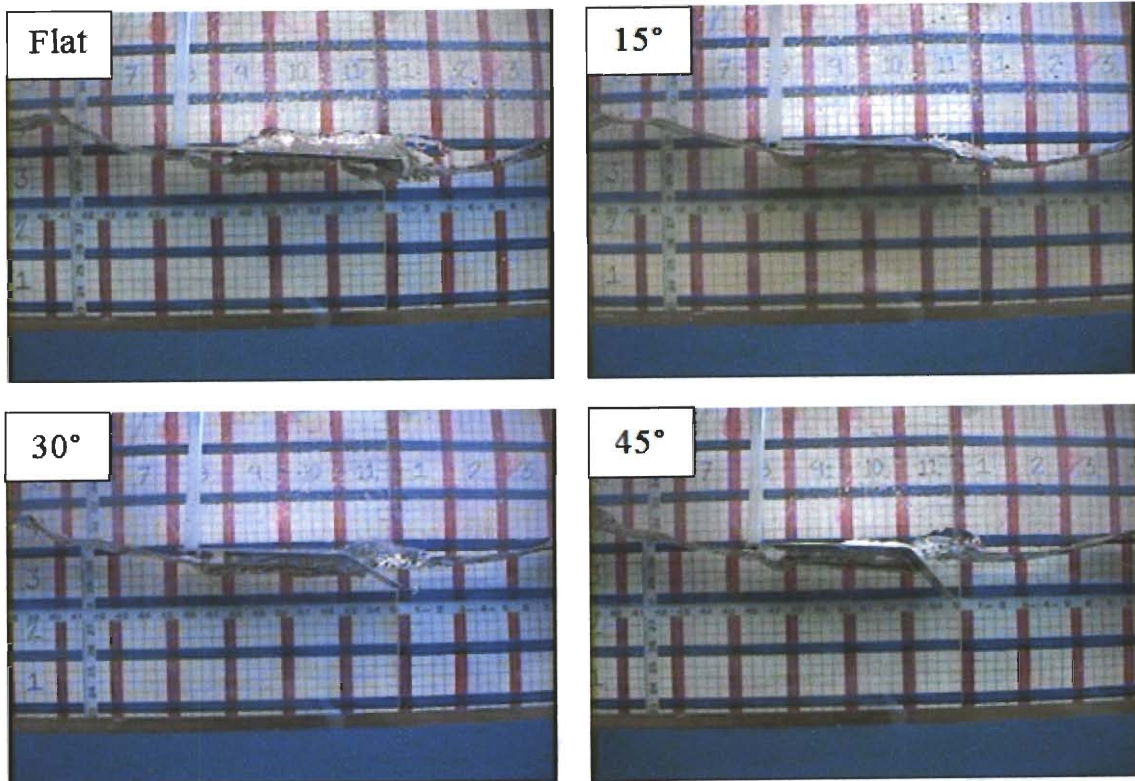


**Figure 4.37 Wave wing interactions when the trailing edge of the wing was placed in an anti-node and the wave was at its trough**

Comparing the amplitude of the standing wave downstream of the wing showed a decrease in wave amplitude as the angle of the wing increased, which supports the results that more energy was absorbed by the large degree bends (Figure 4.38). It also supports the theory that the bent portion of the wing under the wave surface was interacting with the circular path of the water particles. The reason a wave appears to be propagating even though the water particles are stationary is because the particles transfer their energy to their neighbors. The wing was absorbing this energy instead of the neighboring water particle reducing the wave amplitude.

84
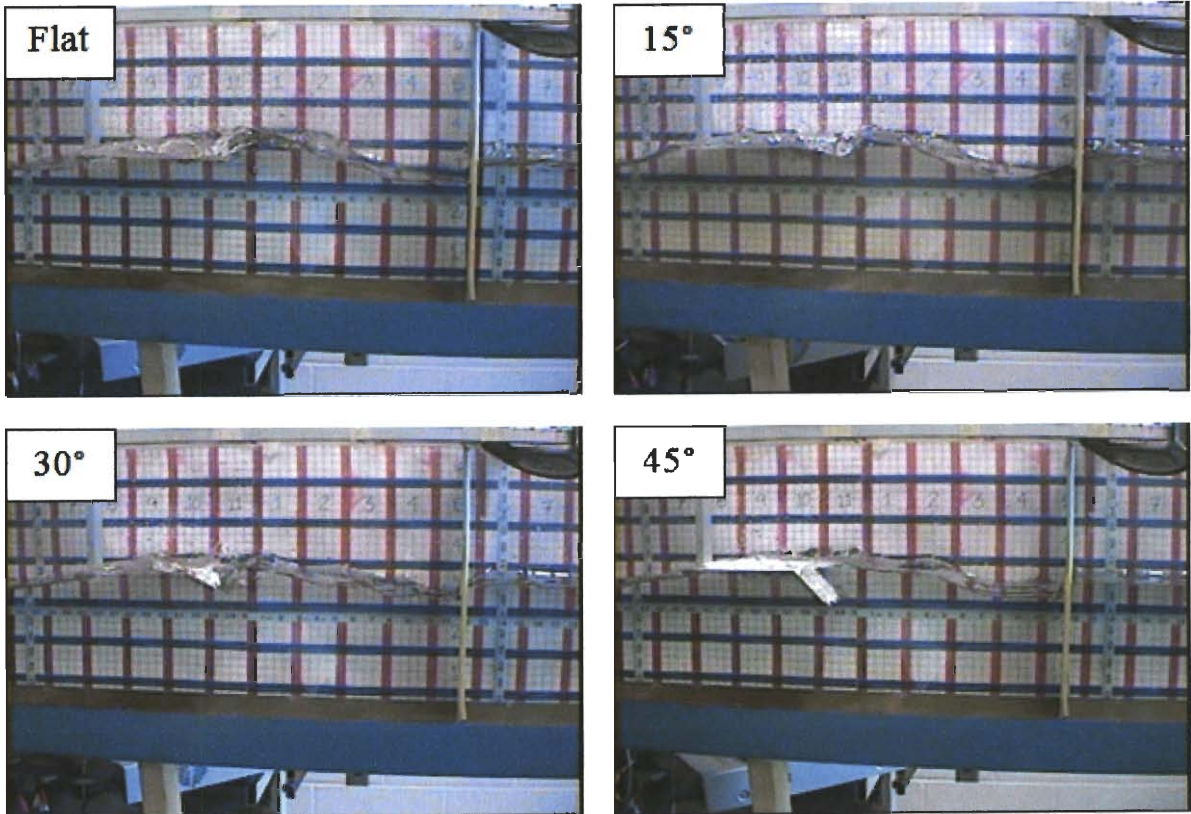
**Figure 4.38 Example of the reduced amplitude of the standing wave downstream of the wing as the degree of downward bend increases**

When comparing the energy absorbed for the 0.97Hz case it was observed that the 30°case deviates from the trend that the energy absorption increased with increasing degree bends. This deviation was because there was a secondary reaction off the trailing

edge of the 15° and flat wings that increased the torque in these cases (Figures 4.39).

This reaction was not present in the 30° case because the trailing edge of the wing remained under the surface of the water.



**0.5 λ Moment Comparison**
(0.97 Hz)
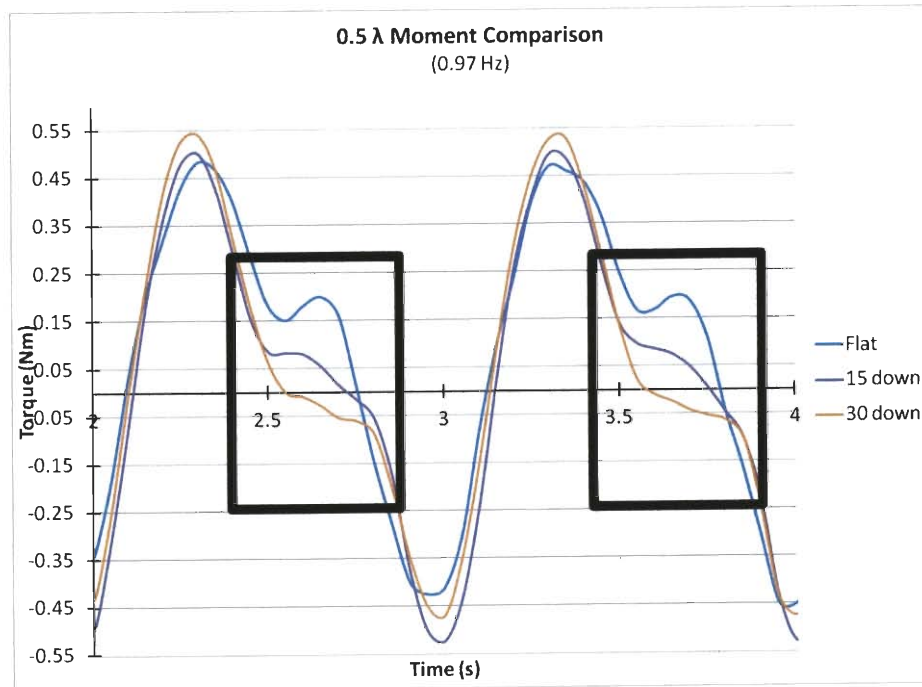
Figure 4.39 Secondary reaction (highlighted in black boxes) of 15° and flat wing which increased energy

## Effect of 90° Bends

The effect of the 90° up and down and the 90° down wing geometries continued the trend seen with the other downward geometries (Figure 4.40). These two wings absorbed more energy than the lesser degree bends and reduced the effect of the reflection plate location.

86

## Total Energy Compare
### 0.97 Hz



## Total Energy Compare
### Down, 1.56 Hz
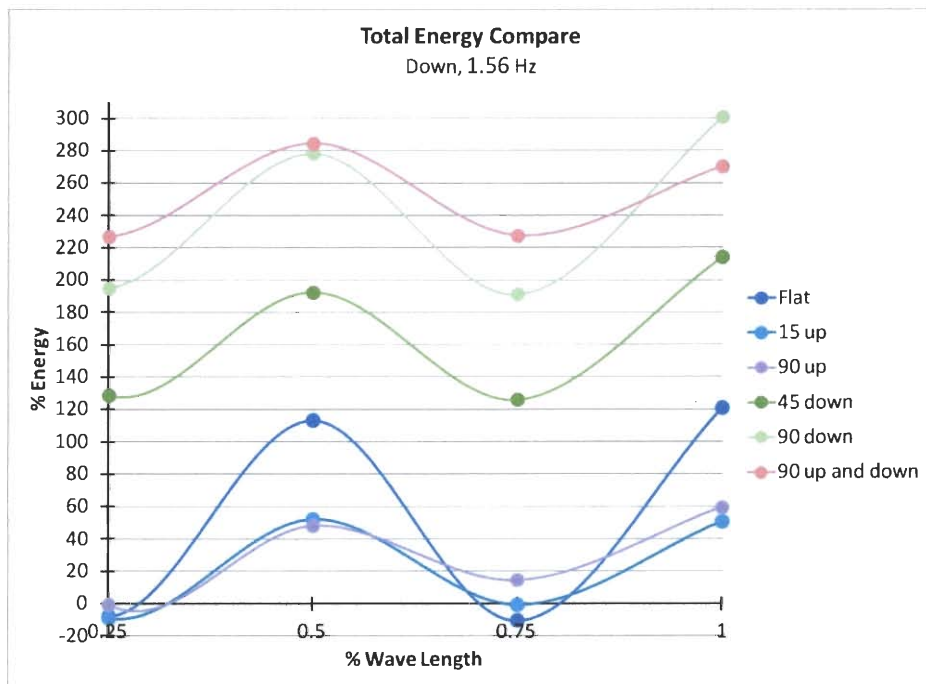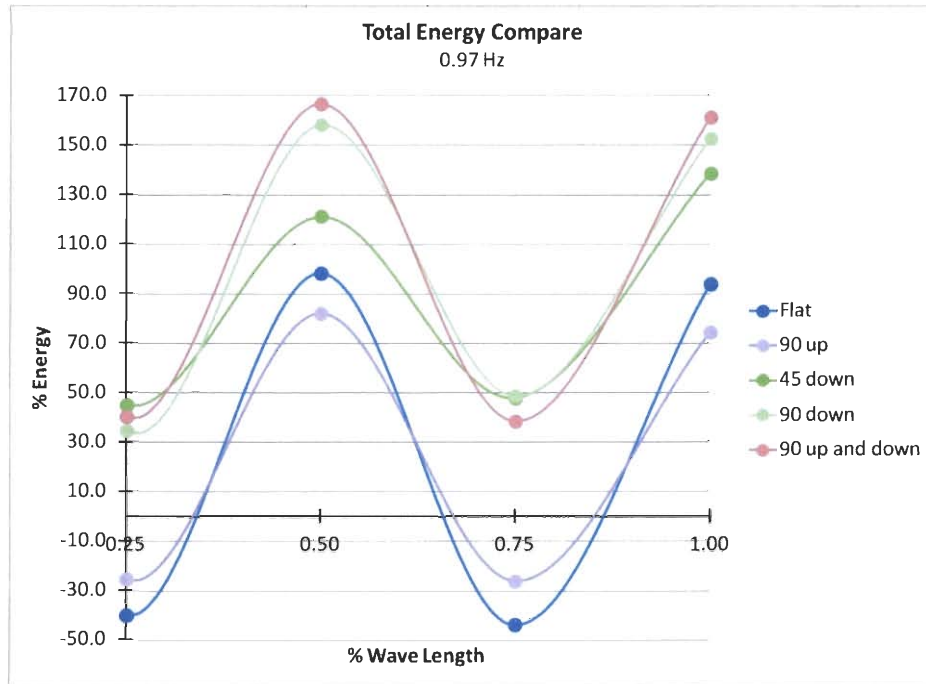


**Figure 4.40 Energy comparisons for 90° bends**

The vertical bend created a reflection of the wave particles along the surface area of the plate as previously described. However, the amplitude of the water particles are

87

the largest at the free surface of the wave and the amount of wing in contact with the free surface was increased with the vertical bends (Figure 4.41). The vertical bends also provide a more direct reflection of the wave particles. Hence, the amount of energy absorbed by the wing increased.
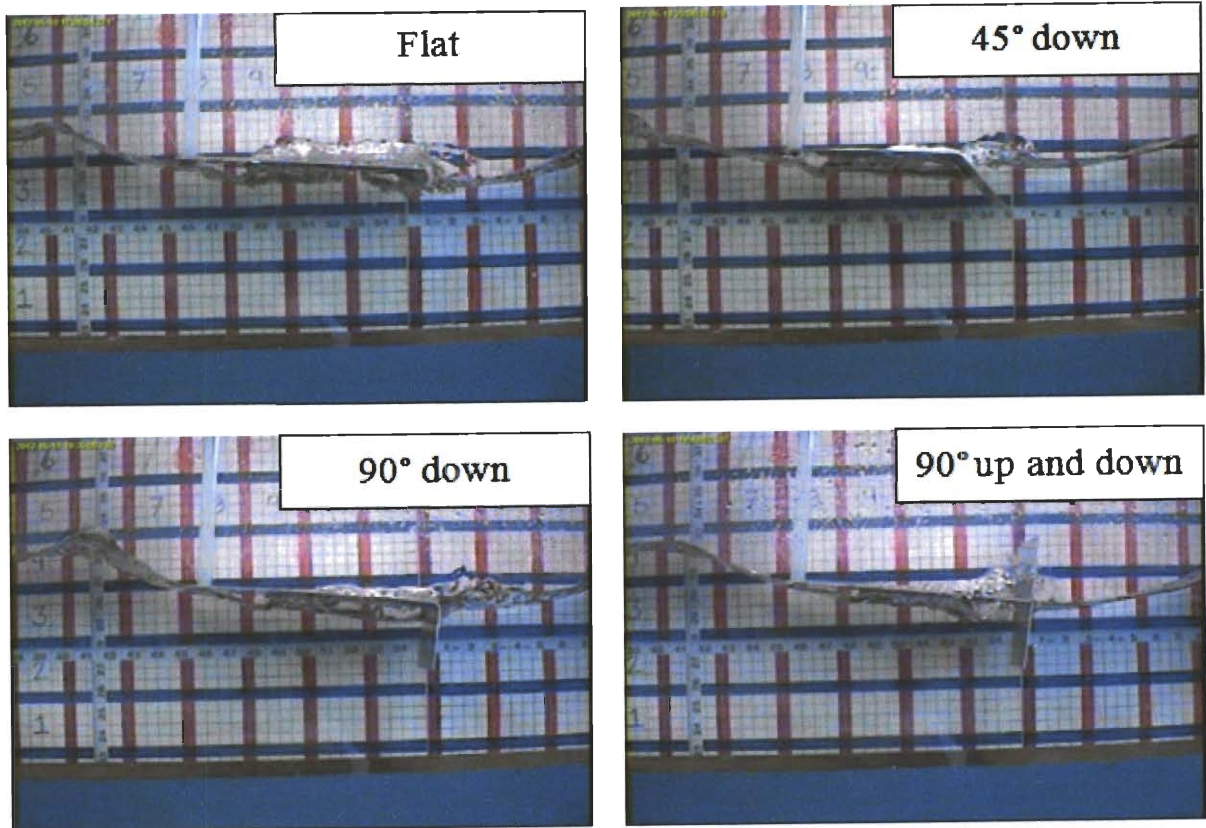


**Figure 4.41 Comparison of the amount of wing in contact with the free surface of the water**

The amount of energy absorbed when the 90° up and down and the 90° down geometries was similar when the trailing edge was placed in anti-node. This showed that the upward bend had little effect on the amount of energy absorbed. Comparing the wave and wing interaction of the 90° down and 90° up and down wing cases supported these results (Figure 4.42).
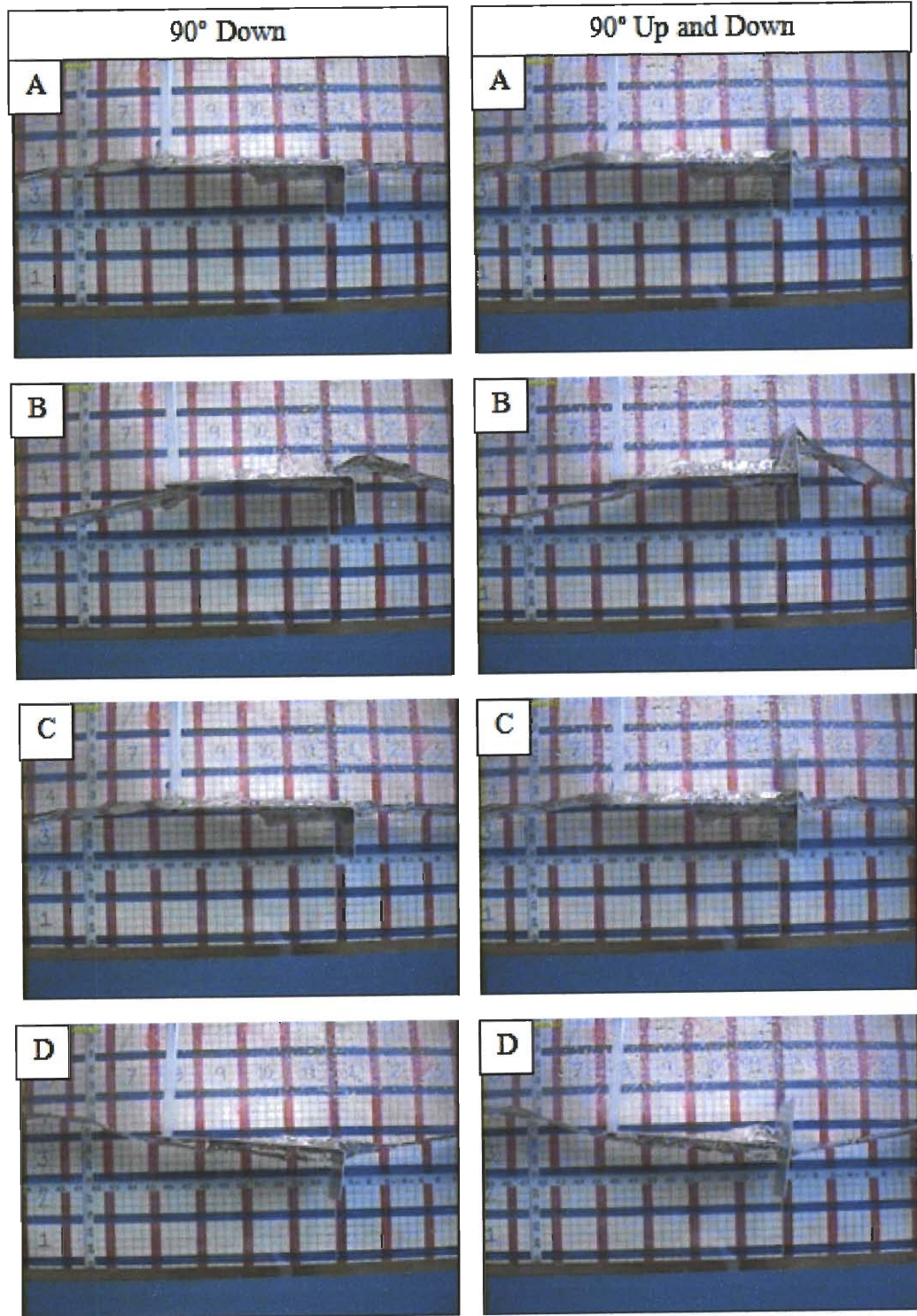
**Figure 4.42 Comparison of wave and wing interaction for the 90° down and 90° up and down wings**

A: Wing is neutral, B: Wave at peak, C: Wave is neutral, D: Wave at trough

In general, as previously discussed, the effect of the upward bend in the wing was detrimental or at most neutral to the amount of energy absorbed. This was supported by the 90° upward geometry when compared to the flat wing.

However, the 90° bend does not follow the same trend that an increase in the degree of the bend decreased the efficiency of the wing. It was seen that the 90° bend absorbed more or the same amount of energy as the 15° wing. This was dependent on the amplitude of the wave.

For the smaller amplitude waves, the 90° case had a greater efficiency because the reflection off the vertical plate increased the volume of water on the plate surface and in turn the amount of positive torque on the plate. However, this effect was decreased as the amplitude of the wave increased because the trailing edge of the 15° wing began to interact with the wave and allowed the wave to break over the wing which increased the positive torque in the same fashion as the reflection off the vertical bend (Figure 4.43).
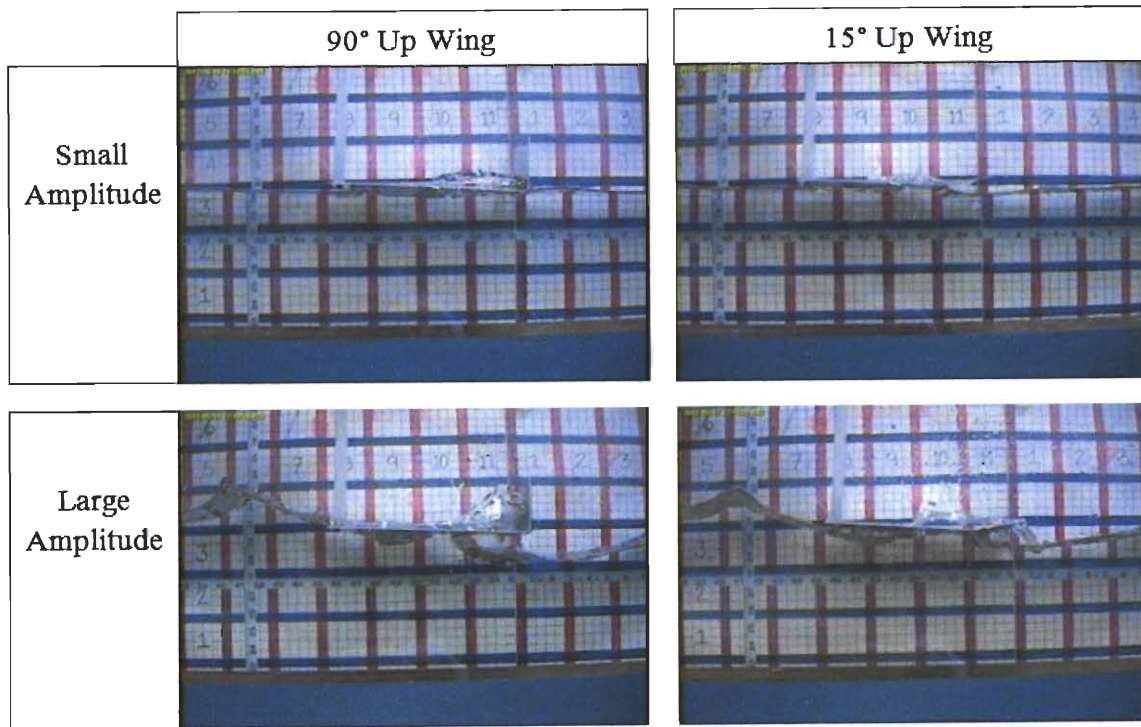
**Figure 4.43** Comparison of small and large amplitude waves on energy absorption of a wing with an upward bend of 90° and 15°

The other point of interest for the 90° upward wing was when the trailing edge was placed in a node there was an increase in the amount of energy absorbed when compared to the flat plate. This trend continues when comparing the energy absorptions of the 90° down and 90° up and down wings.

This was due to the interaction of the wave and the vertical portion of the wing creating a reflection back over the surface of the wing. Since the reaction reduces with the amplitude of the wave, so did the effect of the reflection on energy absorption. As seen in the comparison of the 15° and 90° up comparison in Figure 4.43 above. This was why the 90° up and down wing did not absorb more energy when its trailing edge was placed in a node for 0.97Hz case when compared to 90°down.

91

*Effect on Energy Absorbed with Reflection Plate at 0λ*

Testing for the 0λ case was preformed with the reflection plate shifted back from the trailing edge of the wing by at least 5mm. This shift was done to allow room for the trailing edge of the wing to fully rotate without interfering with the reflection plate (Figure 4.44). The larger degree downward bends required a larger shift to prevent interference. Table 4.7 provides the distance of the shift for each case.
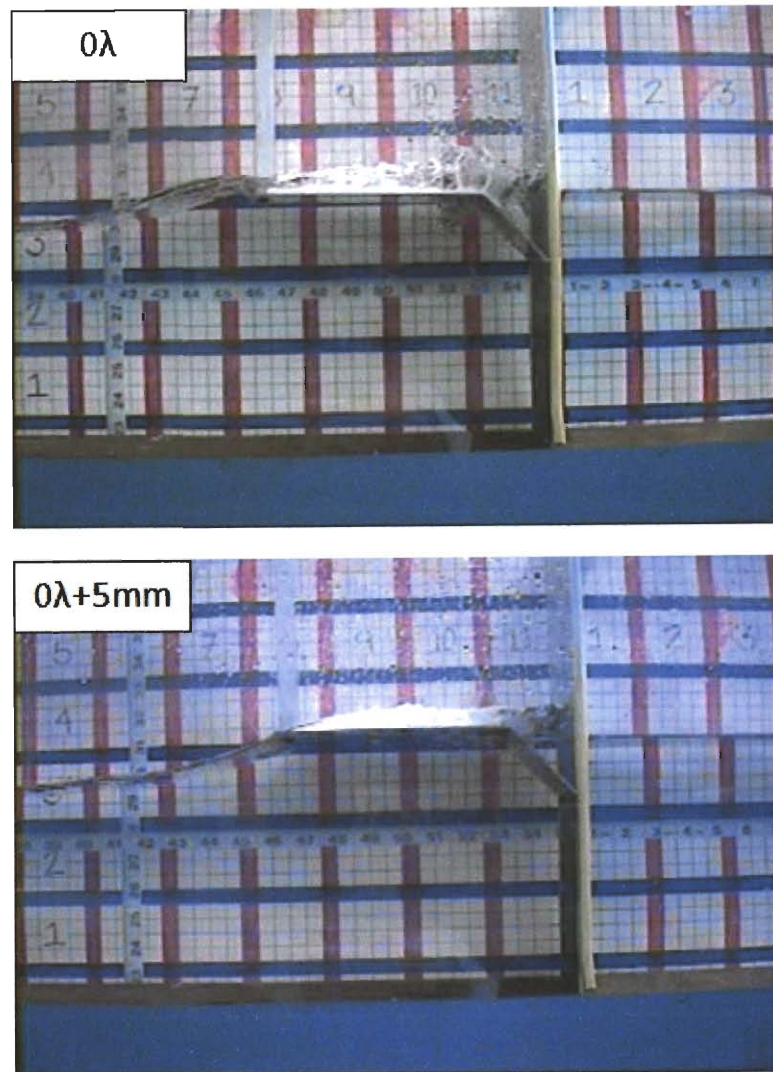


Figure 4.44 The trailing edge of the wing interfering with the reflection plate at 0λ and the trailing edge of the wing allowed to rotate freely 0λ+5mm for the 45° down case

Table 4.7 Distance of reflection plate shift, in mm, for the 0λ location to prevent wing interference

| Geometry | Shift (mm) 0.97 Hz | Shift (mm) 1.56 Hz |
|---|---|---|
| flat | 5 | 5 |
| 15-90° up | 5 | 5 |
| 15° down | 5 | 5 |
| 30° down | 10 | 10 |
| 45° down | 10 | 15 |
| 90° | 10 | 20 |

Comparing the location of the trailing edge of the wing for the 0λ and 0λ+5mm cases showed that when the reflection plate was placed at 0λ the trailing edge was restricted from moving an additional half inch. When the wing was not allowed to rotate freely, the torque created and in turn the energy absorbed was drastically affected (Figure 4.45).
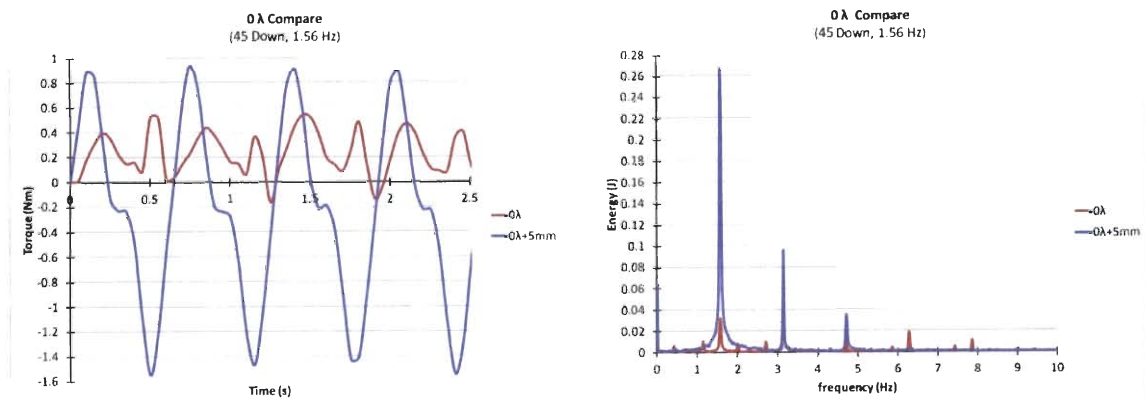


Figure 4.45 Torque and energy comparison for the freely rotating and interfering wing for the 45° down case

The amount of energy absorbed by the wing when the reflection plate was placed at $0\lambda+5$mm so that the trailing edge of the wing can rotate freely was always a maximum. This was to be expected because the trailing edge of the wing was placed in an anti-node. It was also expected that the energy absorbed at this location would be the same as that absorbed when the reflection plate was at 0.5 and $1\lambda$ locations because the trailing edge was in an anti-node. However, this was not the case at this location the energy absorbed was greater than that absorbed at the 0.5 and $1\lambda$ locations (Figure 4.46). This made the $0\lambda$ location a case of special interest and in particular the large5 degree downward bends of 90°.
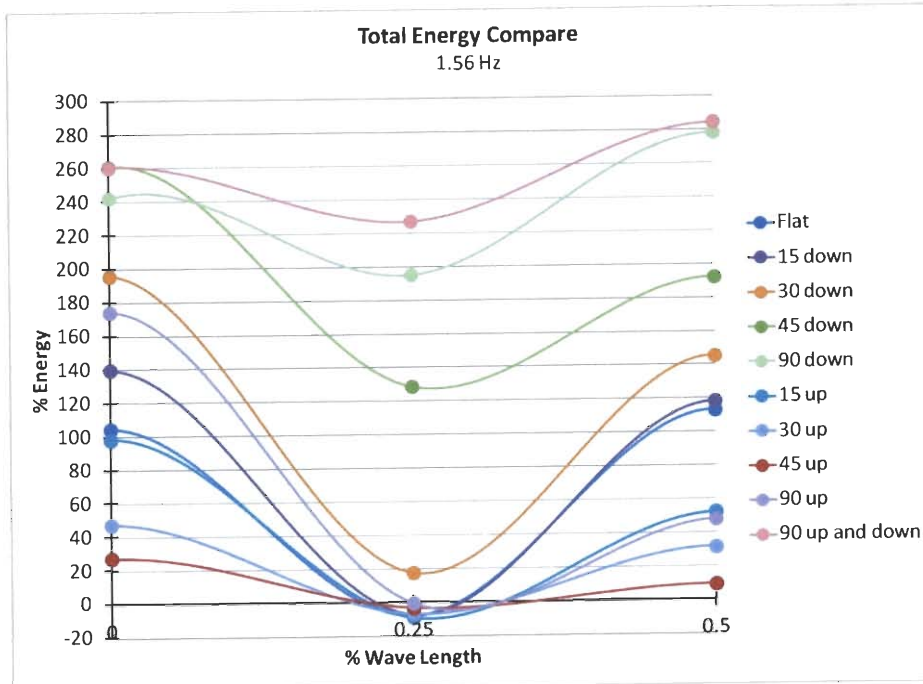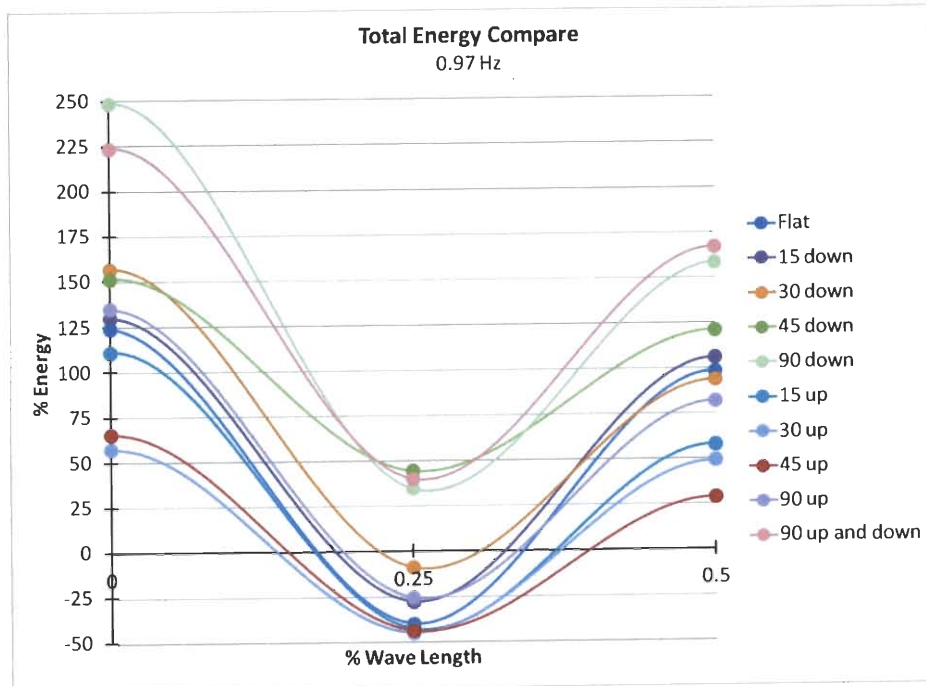
**Figure 4.46 Energy absorbed by the wing for all geometries at 0λ+5mm**

The 0λ location provided the most energy even when compared to the other anti-nodes because the water particles at this location are being directly reflected off the reflection plate and interacting with the trailing edge of the wing. For the other anti-node locations, there was some energy dissipation as the water particles transfer their energy upstream towards the location of the wing. This could be verified by comparing the amplitude of the wave created when the reflection plate was at 0λ to the amplitude of the wave when the reflection plate was placed at 0.5λ (Figure 4.47). It was seen that the amplitude at the anti-node was nearly half an inch more when the reflection plate was placed at 0λ.
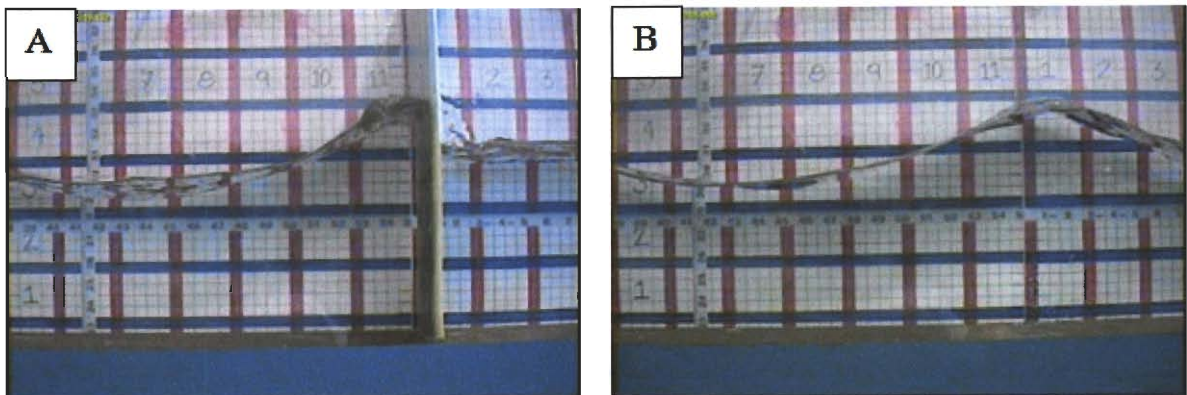


**Figure 4.47 Wave amplitude comparison when the reflection plate was placed at 0λ (A) and 5λ (B), the trailing edge of the wing lies at the anti-node in both cases**

However, since the trailing edge of the wing has to be shifted away from the reflection plate to allow complete rotation, in some cases for example 1.56Hz with 90 down or 90° up and down geometries the amount of energy absorbed at 0λ decreased slightly when compared to the other anti-node locations. By comparing the torque results for these cases, to the case where the trailing edge was shifted 5mm upstream for the flat

96

wing geometry a similar result was observed (Figure 4.48). The curves showed a small decrease in both the negative and positive torque.
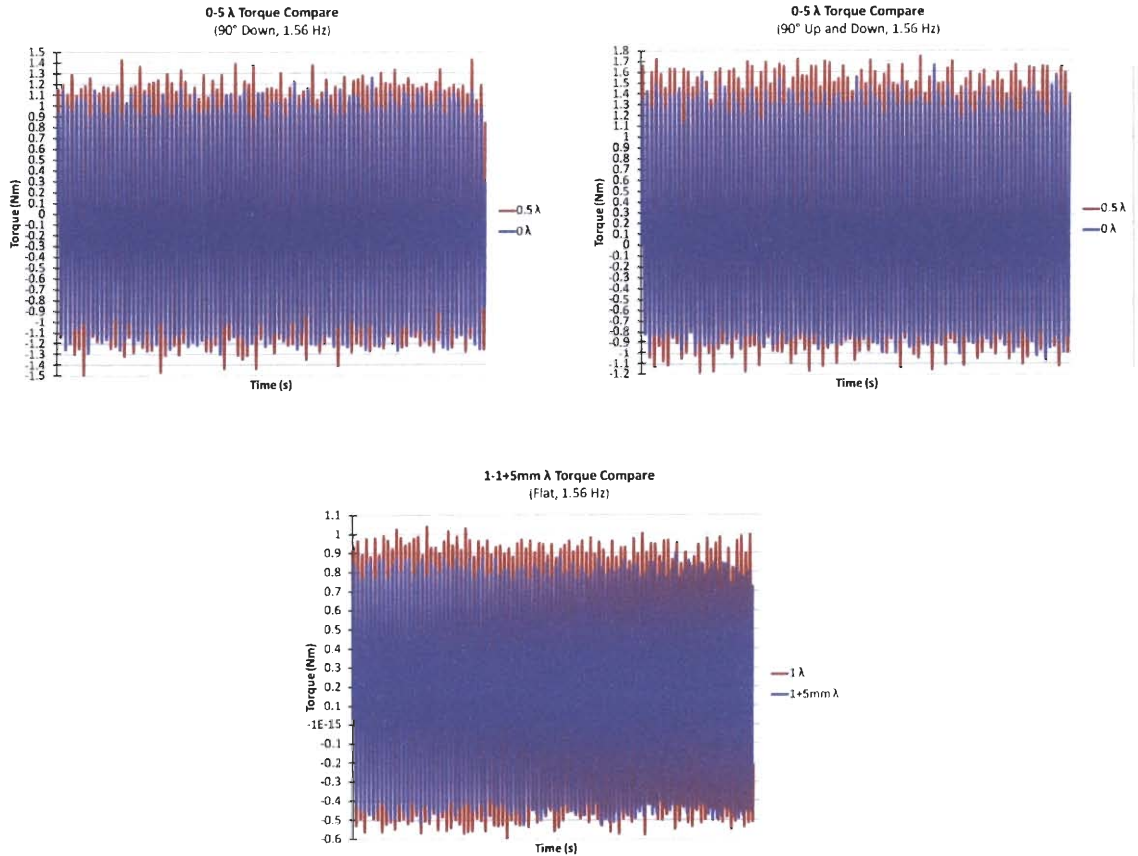


Figure 4.48 Comparison of the effect of shifting the trailing edge of the wing back from the reflection plate

## Efficiency

The efficiency of the wing, $\delta$, Eq. (4.3) was found by comparing the power per unit wave front of the travelling wave, $P'$, Eq. (4.4) to the power absorbed per unit width of the wing, $P_t$, Eq(4.6).

$$\delta = \frac{P_t}{P'} \tag{4.3}$$

$$P' = \frac{\rho g^2 H_{m0}^2 T}{4\pi} \tag{4.4}$$

97

Where $\rho$ is the density of water, $g$ is the acceleration of gravity, $H_{m0}$, Eq. (2.5), is the root mean square of the travelling waves amplitude, and $T$ is the wave period. For the calculation of $P'$, a cosine wave was used Eq. (4.5).

$$h_i = A \cos kx - \omega t \qquad (4.5)$$

Where $h_i$ is the local wave amplitude (refence Figure 2.2), $A$ is the maximum amplitude of the wave, $k$ is the wave number defined in Eq. (2.3), $x$ is the location along the profile of the wave, $\omega$ is the agular frequency, Eq. (2.2) and $t$ is the time in seconds. $A$, $k$, and $\omega$ are from the defintions of the waves produced in the wave tank (Table 4.4), $x$ is varied in 0.01m intervals for one wave peak above the mean surface, and $t$ is held constant.

$$P_t = \frac{E_t}{tw} \qquad (4.6)$$

Where $E_t$ is the total energy measured from the experiments in units of J, t is the test duration in seconds, and w is the width of the wing in m. In order to determine the effect of both reflection plate location and wing geometry on the efficiency, the power avaliable in the travelling wave was chosen for comparison puposes.

The reflection plate location, wing geometry, and wavelength of the wave all had an effect on the effeciency of the wing. The minimum efficency of about 4% for the 0.97 Hz wave was seen when the trailing edge of the wing was placed in a node. The maximum effeciency approaching 40% was seen when the reflection plate was placed at the shifted 0$\lambda$ location for the 90° down and the 90° up and down geometries at the 1.56 Hz case.

The length of the downward bend in relationship to the wavelength of the wing affected the efficency of the wing. This relationship could be seen when comparing the efficency of the 90° down wing for the 0.97 Hz and the 1.56 Hz waves in the travelling

wave condition. The 1.56 Hz wave had double the efficeny of the 0.97 Hz wave. This was because the shorter wavelength of the 1.56 Hz wave allows more of the avaliable energy of the wave to be reflected back over the surface of the wing instead of progressing down the tank because the depth at which water particle motion is negligible decreases with wavelength.

# CHAPTER 5

## CONCLUSION

The addition of a reflection plate to a system of travelling waves produces a standing wave which increases the amplitude of the wave and in turn the available energy. The location of the nodes and antinodes of the standing wave can be controlled by reflection plate location. By adjusting the location of the reflection plate with respect to the trailing edge of the wing, the amount of energy absorbed can be optimized. When the reflection plate was placed at 0, 0.5, 1$\lambda$, an anti-node was created at the trailing edge of the wing. This increased the amount of energy absorbed with respect to a travelling wave. When the trailing edge of the wing was placed in a node, reflection plate placed at 0.25 or 0.75 $\lambda$, the amount of energy absorbed was decreased. The maximum energy was absorbed when the trailing edge of the wing was placed in an anti-node and the minimum when it was in a node. There was an equal amount of energy absorbed when the reflection plate was place at 0.5 $\lambda$ or 1$\lambda$. The same holds true when the reflection plate was placed at 0.25 $\lambda$ or 0.75$\lambda$. The maximum energy was absorbed when the reflection plate was placed at 0$\lambda$.

The geometry of the wing also affected the amount of energy absorbed by the wing. If the wing was bent upward, the energy absorbed compared to a flat wing decreased. For a downward bend, the amount of energy absorbed increased. With an increase in the degree of the bend there was an increase in energy absorption for the downward bend case. However, for the upward bend the opposite was true.

The largest efficiency of the wing was seen when an anti-node was created at the trailing edge and the wing was bent downward to 90°. The efficiency was also affected by the length of the downward bend in relationship to wavelength. The closer the length of the bend was to the where the wave particle amplitude was negligible, $\lambda/2$, the better the efficiency of the system.

It is suggested that the $0\lambda$ reflection plate location is the optimum. This will eliminate the need to monitor the wavelength and only small location adjustments will have to be made to avoid wing inference with the reflection plate. It is also suggested to use the 90° downward wing geometry in this configuration since the 90° up has little effect on energy absorption when the trailing edge is placed in an anti-node.

**Further Work**

Several other properties of the wing need to be optimized to optimize energy absorption and efficiency of the "aqua fly". For better understanding of the physical interaction of the wave and wing, PIV testing or computational modeling should be done. It was found with the Crockrell raft that there was a limit to the energy absorption when the length of the absorber reached a certain length. This should also be investigated with the "aqua fly" to determine the length of the wing. The wavelength to the length of the wing seemed to have little effect on the trend of energy absorption in this study at the optimum reflection plate locations. The length of the downward bend should also be investigated to determine its optimum. It is proposed that a deeper bend may eliminate the need for a reflection plate. This will prevent the wave energy from propagating past

the wing and in turn eliminate the need for the reflection plate and increase the efficiency

of energy absorption.

REFERENCES

Bernhoff, Hans; Sjostedt, Elisabeth; leijon, Mats. "Wave Energy resources in Sheltered Sea Areas: a case the Baltic Sea". Renewable Energy v31, n13, (October 2008); p 221-240.

Brekken, Ted: Jouanne, Annette von: Han, Hai Yue. "Ocean wave Energy Overview and Research at Oregon State University". IEEE Power Electronics and Wind Applications, (2009).

Clement, Alain; McCullen, Pat; Falcao, Antonio; Fiorentino, Antonio; Garder, Fred; Hammarlund, Karin; Lemonis, George; Lewis, Tony; Nielson, Kim; Petroncini, Simona; Pontes, Teresa; Schild, Phillippe; Sjostrom, Bengt-Olov; Sorensen, Hans; Thorpe, Tom. "Wave energy in Europe: current status and perspectives" *Renewable and Sustainable Energy Reviews* V6 (2002):p 405-431.

Cockerell, Sir Christopher; Platts, M.J., Comyns-Carr, R. The Development of the Wave Contouring Raft, Wave Energy Conference, 22-23 November, 1978, Heathrow Hotel, London, England.

Falnes, Johannes. "A Review of Wave Energy Extraction." Marine Structures 20 (2007): p.185-201.

Falnes, Johannes. *Ocean Waves and Oscillating Systems*. New York: Cambridge University Press. 2002. Print.

Falnes, Johannes. "Wave- power conversion by point absorbers". *Norwegian maritime research*, v6, n4 (1978): p.2-11.

Gislason, Kjartan; Fredsoe, Jorgen; Deigaard, Rolf, Mutlu Sumer, B. "Flow Under Standing Waves Part 1. Shear stress distribution, energy flux and stead streaming." *Coastal Engineering* 56(2009):p.341-362.

Henderson, Ross. "Design, Simulation, and Testing of a Novel, Hydraulic Power Take-off System for the Pelamis Wave energy Convertor". Renewable Energy v31, (2006): p.2164-2170.

Huang, Zhenhua. "An experimental study of the surface drift currents in a wave flume."*Ocean Engineering* v34 (2007):p343-352.

IMU-10 Range Motion Sensors. Ship Motion Control. 12 July ,2012 <http://www,shipmotioncontrol.se/imu.html>.

Leijon, Mats: Bostrom, Celcilia; Oska Gustafsson, Stefan; Haikonen, Kalle; Langhamer, Olivia; Stromststeed, Erland: Stalberg, Magnus; Sundberg, Jan; Svensson, Olle; Tyrberg, Simon; Water, Rafael. "Wave Energy from the North Sea: Experiences from Lyseki; Reseach Site". Surveys in Geophusics, v29,n 3, (2008):p 221-240

Luan, haojie; Onar, Omer C.; Khaligh, Alireza. "Dynamic Modeling and Optimum Load Control of a PM Linear Generator for Ocean Wave Energy Harvesting Application". *IEEE* (2009): p.739-743.

McCormick, Micheal E. "Wave-Powered Reverse-Osmosis Desalination". Sea Technology, v42, n12, December (2001): p 37-39.\

Mahmood, Faraz; Huynh, B.P. "Flow about an Oscillating Plate Used to Extract Sea-Wave Energy." ASME 2011 International Mechanical Engineering Congress & Exposition. November 11-17 2011, Denver, Colorado.

Mei, Chiang C. *The Applied Dynamics of Ocean Surface Waves*. Singapore: World Scientific Publishing Co. Pte. Ltd. 1989. Print.

Newman, J.N. "Absorption of wave energy by elongated bodies". *Applied Ocean Research*, v1, n4 (1979): p189-196.

Oh, Jin-Seok; Kim, Jong-Do; Lee, Jong-Ho; Park, Han-Il; Komatsu, Toshimitsu. "Design and analysis of wave energy convertor for a buoy". *Journal of Mechanical Science and Technology*, 21 (2007): p2005-2010.

Orazov, B.; O'Reilly, O.M.; Savas, O. "On the dynamics of a novel ocean wave energy convertor". *Journal of Sound and Vibration*, 329 (2010); p. 5058-5069.

Raftery, M.; Stolkin, R. "Ocean Surface Wave Energy Harnessing Development at Stevens Institute of Technology (SIT)". Oceans Conference Record (IEEE), 2007, Oceans 2007 MTS/IEEE Conference.

Sabzehgar, R. and M. Mooallem. A Review of Ocean Wave Energy Conversion Systems, IEEE Electrical Power & Energy Conference, 2009.

Salter, S.H. "World progress in wave energy-1988." *International Journal of ambient Energy*, v10, n1 (1989): p 3-24.

Taylor, Sir Geoffery. "An experimental study of standing waves" *Proceedings of the Royal Society of London series A* v218, n1132 (1953):p44-59.

Twidell, John, and Tony Weir. *Renewable Energy Resources.* New York: Taylor and
    Francis, 2007. Print.

United States. U.S Department of Energy. Office of Energy Efficiency and Renewable
    Energy. <u>Ocean Energy Technology Overview</u>. Federal Energy Management Program,
    July 2009.

Valerio, Duarte; Beriro, Pedro; Sa da costa, Jose. "Optimisation of Wave Energy
    Extraction with the Archimedes wave Swing". Ocean Engineering v 34 n 17-18,
    December (2007): p 2330.

<u>WaveMATH</u>. Spinka, Kenneth William. 2008. Yale New Haven Teachers Institute. 11
    July, 2012 <www.kwsi.com/ynhti2008/>.

# APPENDIX A
# REPEATABILITY

During initial experiments, data taken for a wave with the same frequency, amplitude, wavelength, and water depth were not returning consistent results. The torque and consequently the absorbed energy were not repeatable between experiments (Figure A.1).
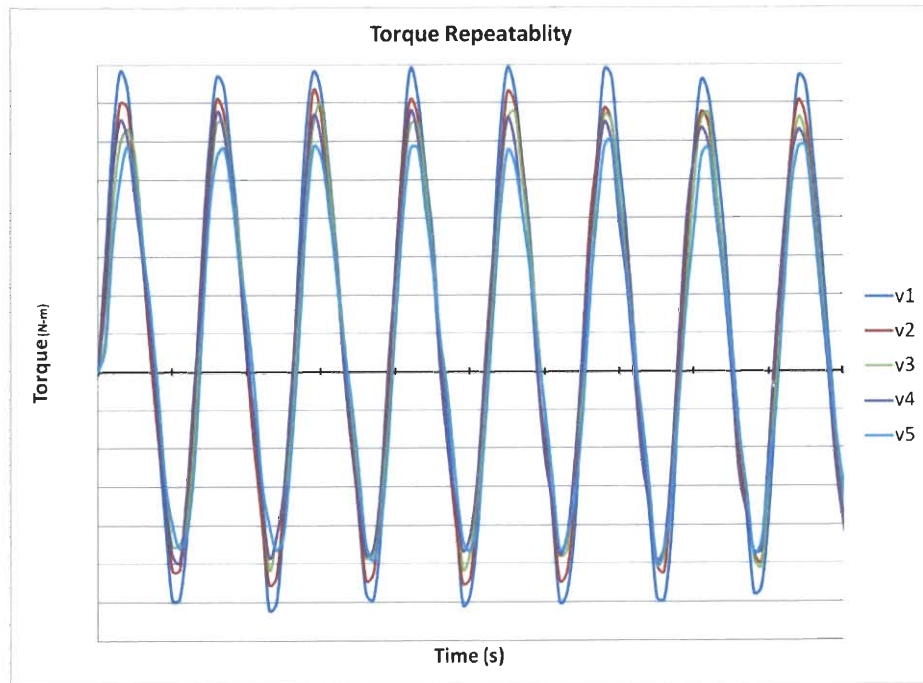


Figure A.1 Early Repeatability problems with torque measurements

Through reviewing journal articles it was found, when a 2-dimensional standing wave in a wave tank has a certain combination of wave amplitude and frequency, the wave peak will reach a 90° angle (Figure A.2).
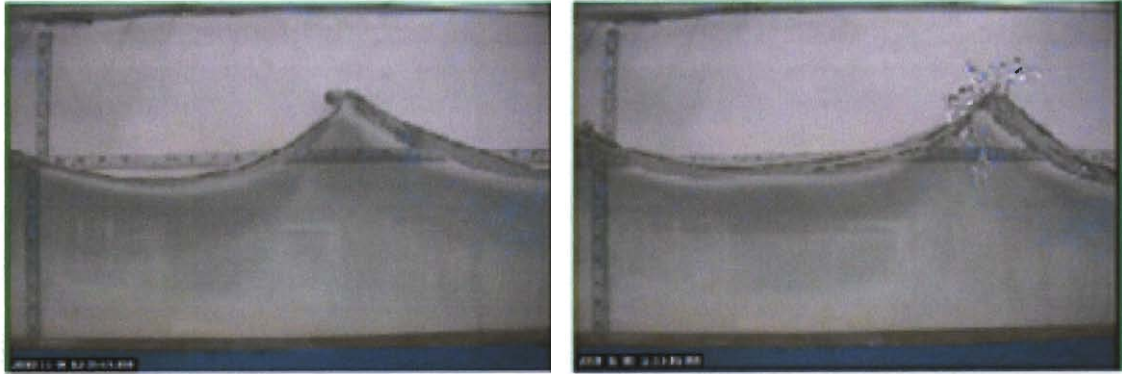
**Figure A.2 Wave peaks of wave in tank in WMU lab**

The wave began to have transverse instability or motion side to side between the tank walls (Figure A.3). This 3-dimensional effect was confirmed analytically by Penny and Price and experimentally by Sir Geoffrey Taylor (Taylor, 1953).
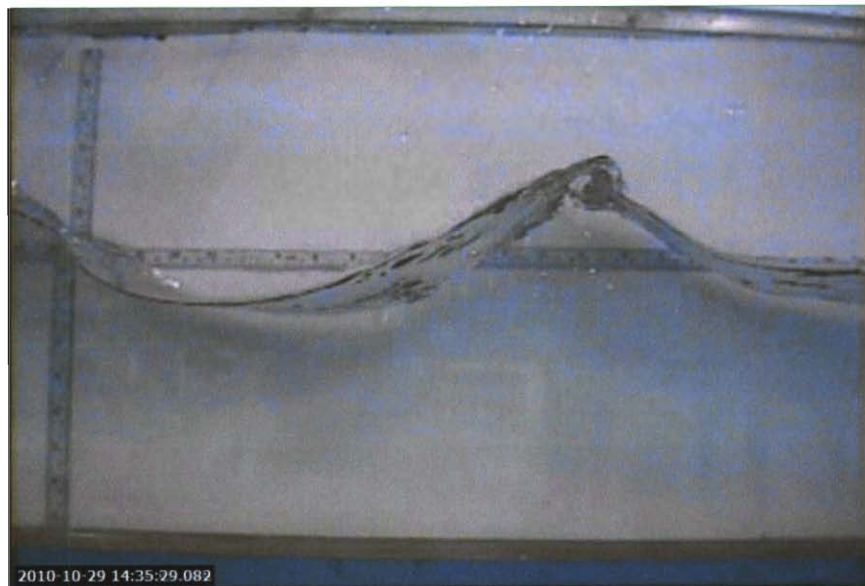

**Figure A.3 3-D effect of the higher frequency waves of waves in WMU wave tank**

Several changes were made to the experimental setup in order to make the experiments repeatable. First, the frequency of the wave was reduced to eliminate the 3-D effect. Secondly, the wave tank was steadied with 2x4 legs in order to eliminate any

109

sway that might also create a 3-D effect (Figure A.4). The hinge on the wave generator was changed in order to eliminate twist in the hinge that also may have added a 3D effect.



**A.4 2x4 legs added to steady the tank**

The 3-D effect of the wave was eliminated with these changes (Figure A.5).
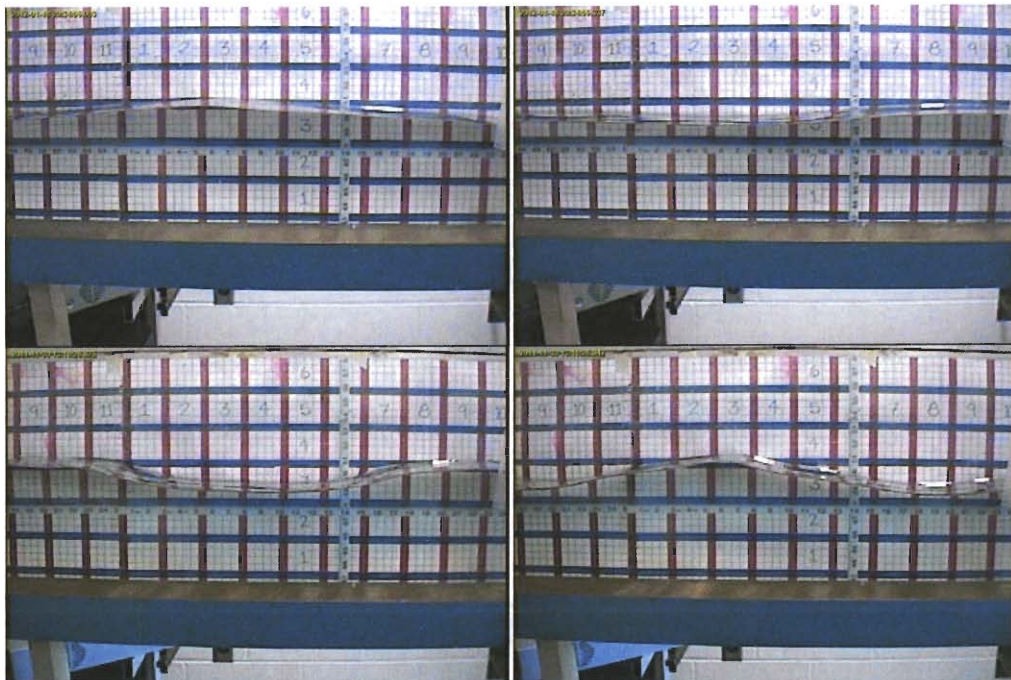


**Figure A.5 Wave without 3-D effect in WMU wave tank**

Also, the stain gauges were insulated to eliminate any effect of room temperature on the strain readings. (Figure A.6).
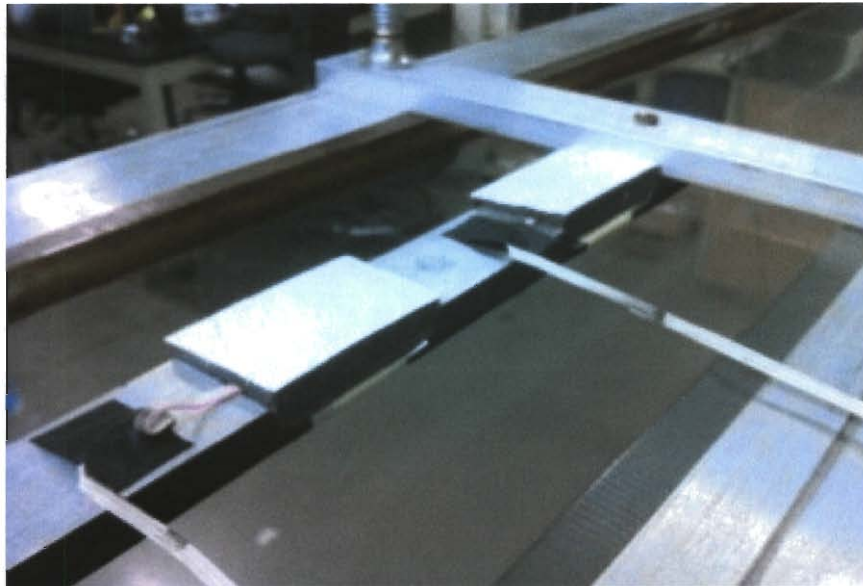


**A.6 Insulated strain gauges**

In order to eliminate that the strain gauges were the source of the error, three strain gauge calibrations were completed. All three calibrations showed that the strain gauge readings were consistent. (Table A.1) This confirmed that the strain gauges were not the source of the error.

**Table A.1. Consistency of calibration readings**

| Calibration Measurements | | | |
|---|---|---|---|
| Force | v1 | v2 | v3 |
| 0 | 0.00 | 0.00 | 0.00 |
| 50 | 0.10 | 0.10 | 0.10 |
| 100 | 0.20 | 0.21 | 0.21 |
| 150 | 0.30 | 0.30 | 0.30 |
| 200 | 0.40 | 0.40 | 0.40 |
| 250 | 0.49 | 0.50 | 0.50 |
| 300 | 0.59 | 0.60 | 0.60 |
| 350 | 0.68 | 0.69 | 0.70 |
| 400 | 0.79 | 0.77 | 0.80 |
| 450 | 0.89 | 0.89 | 0.90 |

111

Finally, the sampling time was increased to eliminate some of the superfluous strain readings that could affect the energy calculations (Figure A.7).
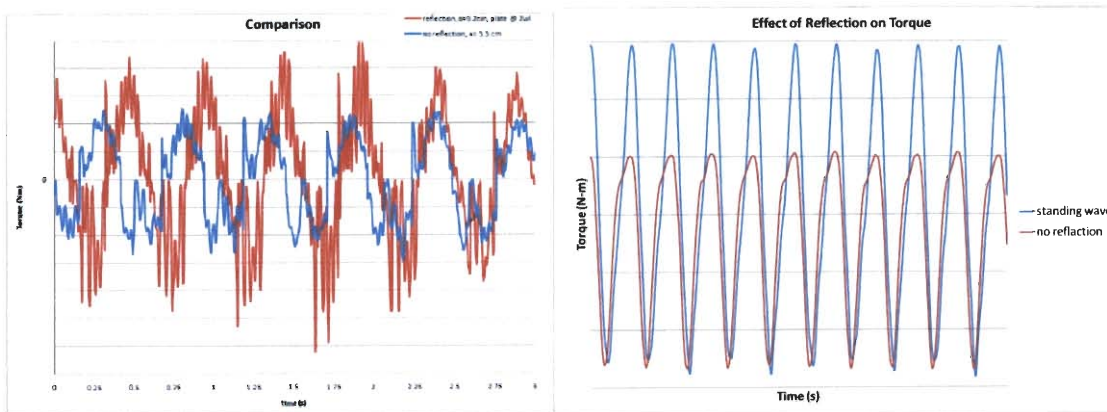


**Figure A.7 Elimination of extraneous strain readings in torque data with changed sampling times**

With all these changes the torque and energy measurements became repeatable (Figure A.8).

.
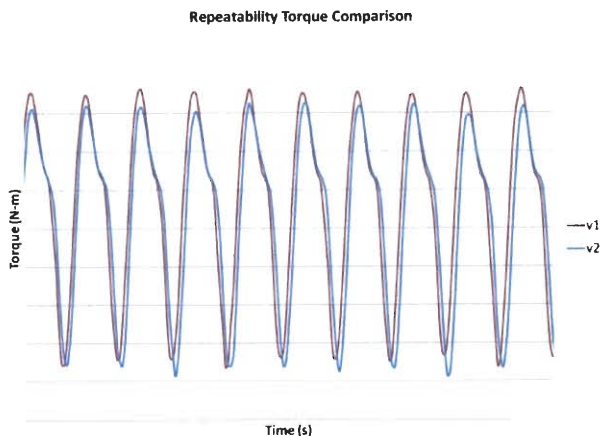


**Figure A.8 Repeatable torque**

# APPENDIX B
# NON-DIMENSIONAL ENERGY

Starting with the dimensional equation for wave energy, $E$, Eq. (B.1)

$$E = \frac{1}{16}\rho g H_{m0}^2 \tag{B.1}$$

Where $H_{m0}$ is the root mean square of the wave amplitude Eq. (B.2)

$$H_{m0} = 4\sqrt{\frac{1}{N}\sum_{i=1}^{N} h_i^2} \tag{B.2}$$

Where $h_i$ is the local wave amplitude using a standing wave Eq. (B.3)

$$h_i = H \cos \omega t \cos kx \tag{B.3}$$

Combining Eq. (B.1)-(B.3) gives the equation for the wave energy of a standing wave Eq. (B.4)

$$E = \rho g \frac{1}{N}\sum_{i=1}^{N} H^2 (\cos \omega t)^2 (\cos kx)^2 \tag{B.4}$$

Table B.1 defines all variables, parameters and there units

**Table B.1 Variables, parameters with the definition and units**

| Variable/ Parameter | Definition | units |
|---|---|---|
| $E$ | energy | $J/m^2$ |
| $\rho$ | densitty | $kg/m^3$ |
| $g$ | gravity | $m/s^2$ |
| $H_{m0}$ | rms amplitude | m |
| $N$ | # of data points | |
| $h_i$ | local amplitude | m |
| $\omega$ | angular frequency | 1/s |
| $t$ | time | s |
| $x$ | position | m |
| $k$ | wave number | m |

First, determine the number of variables and parameters, dimension, and the number of dimensionless quantities needed (Table B.2)

**Table B.2 Parameters/Variables, dimensions, dimensionless quantities**

|  | Value | number |
|---|---|---|
| parameters/ variables | $x, t, E, g, H, \rho, \omega, k$ | 8 |
| dimensions | L, T, M | 3 |
| dimensionless quantities |  | 5 |

Where $L$ is for units of length, $T$ is units of time, and $M$ is units of mass. Using the Buckingham Pi Theorem to solve for the five required dimensionless quantities $E^*, g^*, H^*, x^*, t^*$ (eq B.5-B.9)

$$E = E^* \frac{\rho\omega}{k^3} \tag{B.5}$$

$$g = g^* \frac{\omega^2}{k} \tag{B.6}$$

$$H = \frac{H^*}{k} \tag{B.7}$$

$$x = \frac{x^*}{k} \tag{B.8}$$

$$t = \frac{t^*}{\omega} \tag{B.9}$$

Plugging Eq. (B.5)-(B.9) into Eq. (B.4) yields the non-dimensional energy for a standing wave eq. (B.10)

$$E^* = \frac{1}{N} g^* \sum_{i=1}^{N} H^{*2} (\cos t^*)^2 (\cos x^*)^2 \tag{B.10}$$

A similar procedure is followed to get the equation for non-dimensional energy of a travelling wave Eq. (B.11)

$$E^* = \frac{1}{N} g^* \sum_{i=1}^{N} \left(\frac{H^*}{2}\right)^2 (\cos x^* - t^*)^2 \tag{B.11}$$

115

**APPENDIX C**
**MATLAB CODE: ANALYTICAL**

```
clear
clc

%%%%%inputs%%%%%
g=1.05; %non-dim gravity
H=0.45;%non-dim amplitude
ti=pi/2;%non-dim intial time one period
tf=3*pi/2;%non-dim final time one period
dt=pi/8;%non-dim time step size
xi=0;%non-dim intial position
dx=0.001;%non-dim position step
l=2.36;%non-dim wing length
r=0.25;%non-dim relction plate location


%%%%%define non-dim time (t)%%%%%
c1=(tf-ti)/dt+1;
t=zeros(c1,1);
t(1)=ti;
for i=2:c1
    t(i)=t(i-1)+dt;
end


%%%%%define non-dim wing position (x)%%%%%
Xi=-(xi+2*pi*r);
Xfs=2*pi*r+l;
c2=l/dx+1;
x=zeros(c2,1);
x(1)=Xi;

for j=2:c2
   x(j)=x(j-1)-dx;
end


%%%%%solve for non-dim wave amp (eta)%%%%%
eta=zeros(c2,c1);
for i=1:c1
    for j=1:c2
      eta(j,i)=H^2*(cos(t(i)))^2*(cos(x(j)))^2;
    end
end

etasum=sum(eta,1);
N=c2;
etarms=1/N*etasum;


%%%%%solve for non-dim energy over one period (Et)%%%%%
E=g*etarms;
Et=sum(E);


%%%%%Write to Excel File%%%%%
xlswrite('results',E,'energy_standing_flat')
xlswrite('results',Et,'total energy_standing_flat')
xlswrite('results',eta,'eta_standing_flat')
xlswrite('results',x,'x_standing_flat')
xlswrite('results',t,'t_standing_flat')
```

```matlab
 clear
clc

%%%%%inputs%%%%%
g=1.05; %non-dim gravity
H=0.45;%non-dim amplitude
ti=0;%non-dim intial time one period
tf=pi;%non-dim final time one period
dt=pi/8;%non-dim time step size
xi=0;%non-dim intial position
dx=0.001;%non-dim position step
l=2.36;%non-dim wing length
r=0.25;%non-dim relction plate location

%%%%%define non-dim time (t)%%%%%
c1=(tf-ti)/dt+1;
t=zeros(c1,1);
t(1)=ti;
for i=2:c1
    t(i)=t(i-1)+dt;
end

%%%%%define non-dim wing position (x)%%%%%
Xi=-xi;
Xfs=-l;
c2=l/dx+1;
x=zeros(c2,1);
x(1)=Xi;

for j=2:c2
    x(j)=x(j-1)-dx;
end

%%%%%solve for non-dim wave amp (eta)%%%%%
eta=zeros(c2,c1);
for i=1:c1
    for j=1:c2
      eta(j,i)=(H/2)^2*(sin(x(j)-t(i)))^2;
    end
end

etasum=sum(eta,1);
N=c2;
etarms=1/N*etasum;

%%%%%solve for non-dim energy over one period (Et)%%%%%
E=g*etarms;
Et=sum(E)

%%%%%Write to Excel File%%%%%
xlswrite('results',E,'energy_travelling_flat')
xlswrite('results',Et,'total energy_travelling_flat')
xlswrite('results',eta,'eta_travelling_flat')
xlswrite('results',x,'x_travelling_flat')
xlswrite('results',t,'t_travelling_flat')
```

118

**APPENDIX D**
**MATLAB CODE: DATA PROCESSING**

```matlab
clear
clc

%%%%%%%%%% Load Experimental Data %%%%%%%%%%

%%%%% Data %%%%%
data=load('45up.txt');
T=data(:,1);
V1=data(:,2);
V2=data(:,3);
F1=data(:,4);


%%%%%%%%%% Process Experimental Data %%%%%%%%%%

%%%%% Inputs %%%%%
L1=0.1;
L2=0.211;
C1=0.1796;
C2=0.1805;
n=6001;
d=1201;
ds=0.111;

%%%%% Time %%%%%
i=length(T);
t1=ones(i,1);
for m=1:i
    t1(m)=T(m)-T(1);
end

j=i-n;

t=zeros(n,1);

for m=1:(n)
    t(m)=t1(m)-t1(1);
end

%%%%% Moments: M1 and M2 %%%%%
M1=zeros(n,1);
M2=zeros(n,1);

for m=j:i-1
    M1(m-j+1)=V1(m)*C1;
    M2(m-j+1)=V2(m)*C2;
end

%%%%% Force %%%%%
F=(M2-M1)/ds;

%%%%% Moments: M %%%%%
Ms1=M1-F*L1;
Ms2=M2-F*L2;
```

120

```matlab
Mt=(Ms2+Ms1)/2;

M=zeros(d-1,1);
etotal=zeros(5,1);

for j=1:5

    dt=(d-1)*j-1200;

for i=1:d
    M(i)=Mt(i+dt);
end


%%%%% Solve for energy %%%%%

%%% Step 1 %%%
ynr=fft(M);
xnr=abs(ynr);

%%% Step 2 %%%
s=length(M);
freq=ones(s,1);
freq(1)=1/t(s);

for i=2:s
    freq(i)=freq(i-1)+freq(1);
end

%%% Step 3 %%%
step1=ones(s,1);

for i=1:s
  step1(i)=xnr(i)/s;
end

psd=ones(s,1);

for i=1:s-1
psd(i)=((step1(i)+step1(i+1))/2)/freq(1);
end
psd(s)=step1(s)/2/freq(1);

%%% Step 4 %%%
e=ones(s,1);

for i=1:(s-1)
    e(i)=((psd(i)+psd(i+1))/2)*freq(1);
end

e(s)=psd(s)/2*freq(1);
```

```matlab
%%% Step 5 %%%
etotal(j)=sum(e)/2;
end

disp (etotal)

t=zeros(d,1);

for m=2:d
    t(m)=t(m-1)+0.05;
end

%%%%% Write to Excel %%%%%
xlswrite('new', t, 'time')
xlswrite('new', freq, 'freq')
xlswrite('new', M,'moment')
xlswrite('new', e, 'energy')
xlswrite('new', etotal, 'total energy')
```

# APPENDIX E
# MATLAB CODE: CALIBRATION

```
clear
clc

data=load('LiftCalPoints.dat');
M1=data(:,1);
V1=data(:,2);

M2=data(:,3);
V2=data(:,4);

[coef1,r1]=polyfit_basefn(V1,M1,1)
[coef2,r2]=polyfit_basefn(V2,M2,1)

VV=[-.3:0.02:0.3];
figure(1);
plot(V1,M1,'o',VV,VV*coef1,'-',V2,M2,'>',VV,VV*coef2,'--');
legend('Gauge #1', 'Fit for Gauge #1 (slope = 7321)', 'Gauge #2', 'Fit
for Gauge #2 (slope = 9279)');
xlabel('V (volts)');
ylabel('Moment (g-cm)');
```

```matlab
% Least-squares fit for a set of base functions

function [coef,residual]=polyfit_basefn(xArray,yArray,NoTerm)
A=[];
f=[];
for i=1:length(xArray)
    x=xArray(i);
    y=yArray(i);
%     base(1)=1;
    base(1)=x;
%     base(3)=x^2;
%     base(4)=x^3;
%     base(5)=x^4;
%     base(6)=x^5;

    Aadd=base(1:NoTerm); % NoTerm is the number of terms used
    fadd=yArray(i);
    A=[A;Aadd];
    f=[f;fadd];
end
nematrix=A'*A;


if(rcond(nematrix)>1e-22)
    coef=inv(nematrix)*(A'*f);
    else
    [U,S,V]=svd(nematrix);
    sv=diag(S);
    for i=1:length(sv)
        if sv(i)>max(max(sv))*1e-15
            rsv(i)=1/sv(i);
        else rsv(i)=0;
        end
    end
    S1=diag(rsv);
    coef=V*S1*(U'*(A'*f));
end

zCal=A*coef;
v=zCal-f;
r=length(xArray)-NoTerm;
residual=(v'*v/r)^0.5;
```
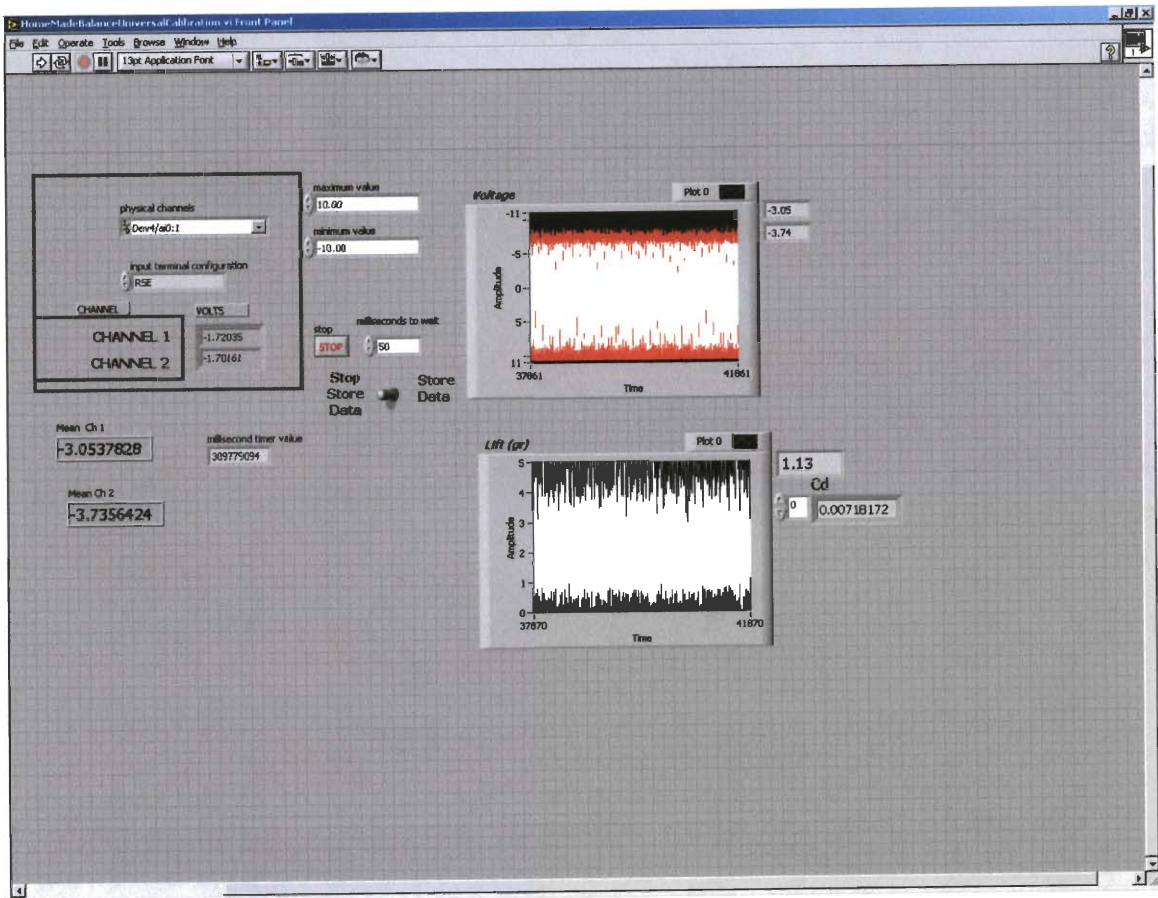
# APPENDIX F
# LABVIEW CODE

Figure F.1 Front page of LABVIEW program
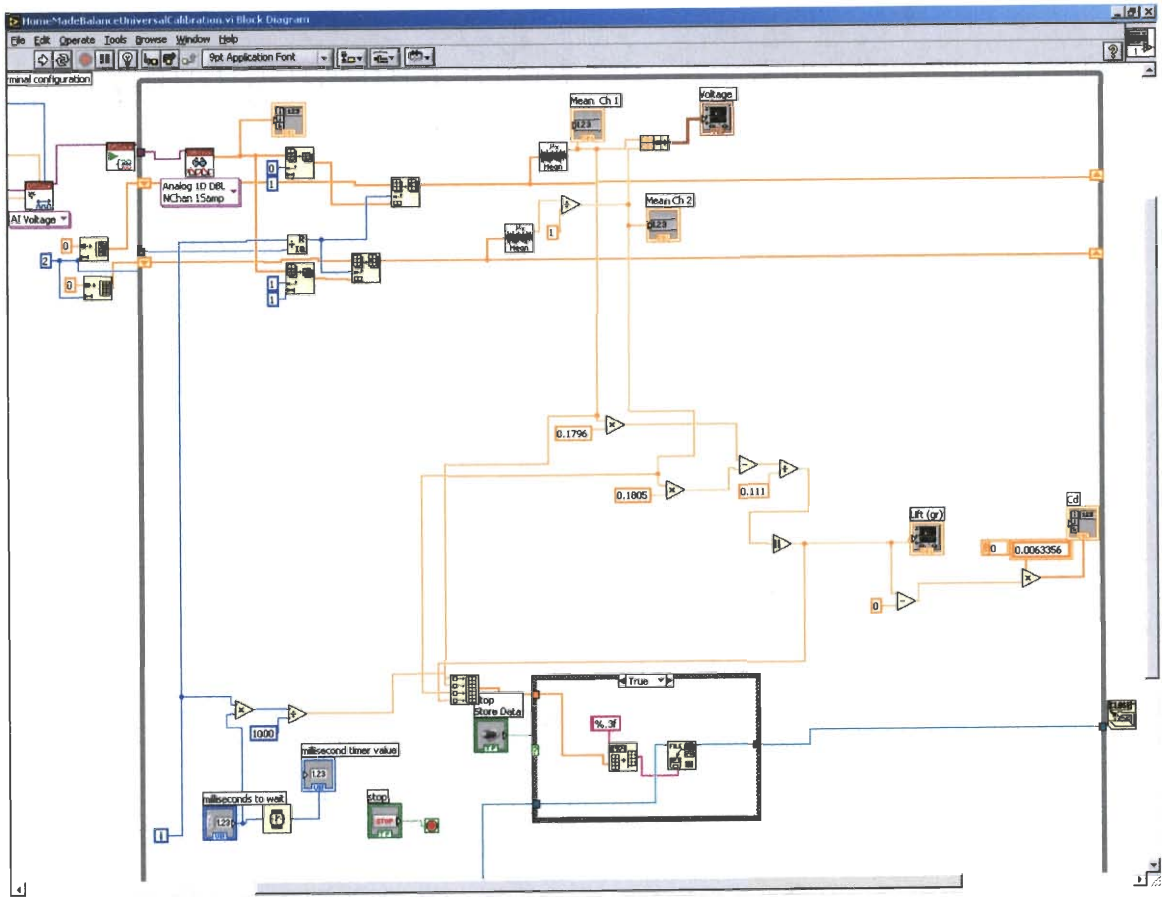
Figure F.2 LABVIEW block diagram

**APPENDIX G**
**WING DIMENSIONS**

Top View  Side View

23 cm

15 cm

0.025 cm
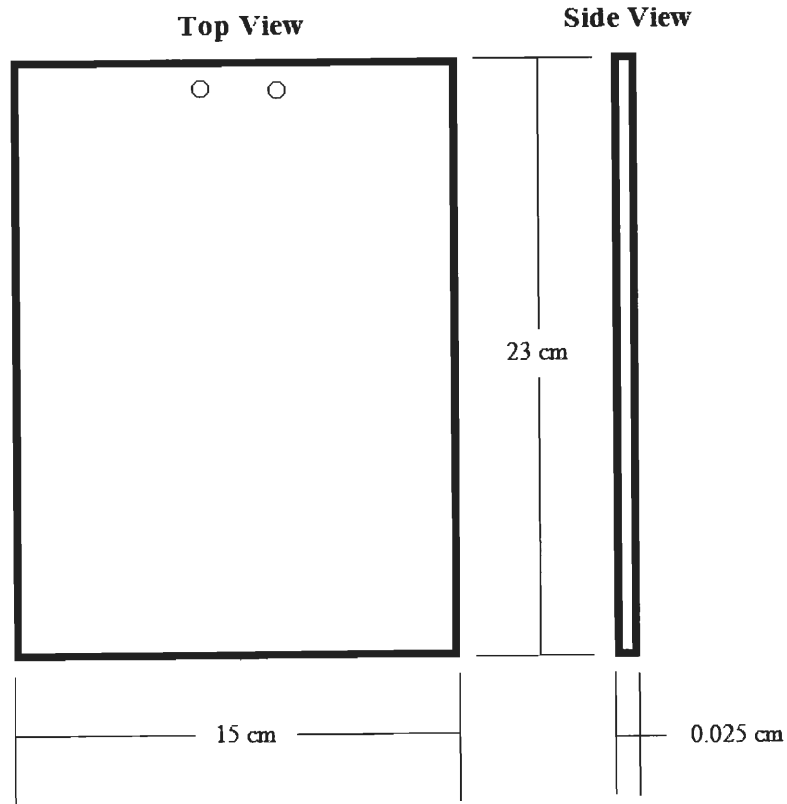
Figure G.1 Top and side view of wing geometry. All plates started with these dimensions and were bent accordingly

Flat Wing

23 cm

16.5 cm  6.3 cm  15° Wing

15°

90° Wing

23 cm

16.5 cm  5.6 cm  30° Wing

30°

90° up and down wing
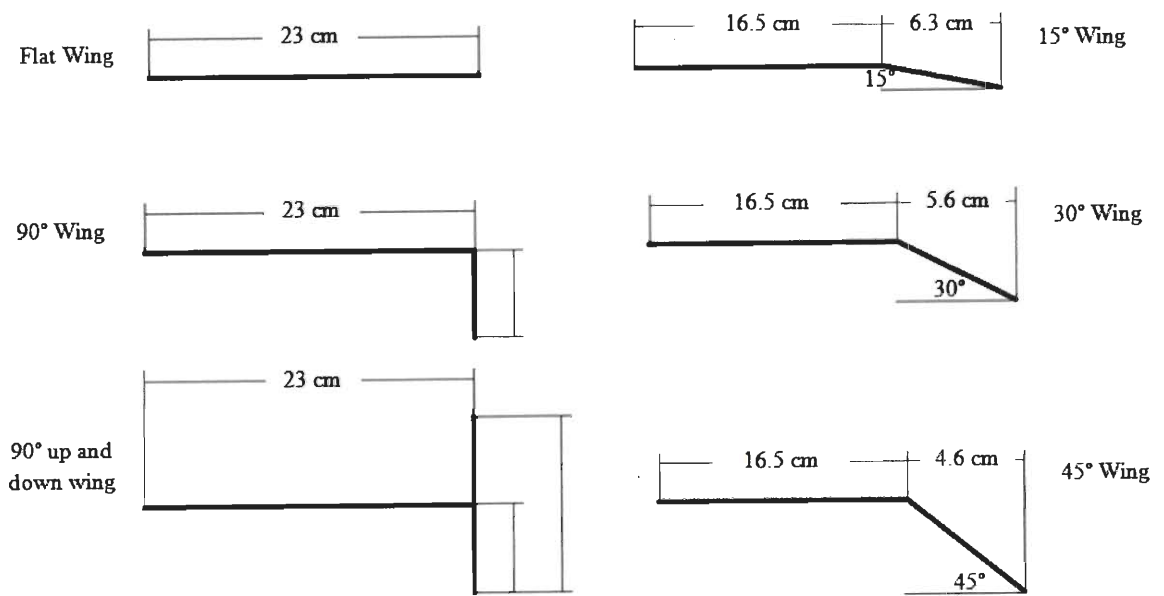
23 cm

16.5 cm  4.6 cm  45° Wing

45°

Figure G.2 Dimensions of wing geometries

130

**APPENDIX H**
**RAW DATA LIST**

## Rachel Durren's Masters Thesis August 2012

| folder | sub folders | document | description | Program |
|---|---|---|---|---|
| Thesis | | MASTER'S THESIS | Copy of the Thesis Document | Word 2007 |
| | | Thesis Defense | Copy of Defense Presentation | Power Point 2007 |
| | | | | |
| Programs | Calibration | fit_M_V | Program for Finding Calibration Coefficients | Matlab M-file |
| | | polyfit_basefn | Sub Program of fit_M_V | Matlab M-file |
| | Analytical | standing | Analytical calculation for energy absorption of a standing wave | Matlab M-file |
| | | travelling | Analytical calculation for energy absorption of a travelling wave | Matlab M-file |
| | Experimental Data Processing | dataprocessing | Program that processes raw data from LABVIEW and outputs torque and energy absorption | Matlab M-file |
| | LABVIEW Data Acquisition | HomeMadeBalanceUniversalCalibration | Program used for data acquisition | LABVIEW |
| | SDVR Viewer | DvrViewer | Program to view video from DVR of the surveillance program | SDVR Viewer |
| | | | | |
| Testing | One folder each for 0.97 Hz and 1.56 Hz | | | |
| | | geometry compare | Results for all 0.97Hz Waves Compared | Excel 2007 |
| | Flat | | Folder containing all raw data and video for the flat wing | video: DAT and IDX files Raw Data: Txt files Processed Data: Excel 2007 |
| | 90 up and down | v1,v2,v3 of raw and processed data video data for all experiments | Folder containing all raw data and video for the 90 up and 90 down wing | |
| | 90 up | | Folder containing all raw data and video for the 90 up wing | |
| | 90 down | | Folder containing all raw data and video for the 90 down wing | |
| | 45 up | | Folder containing all raw data and video for the 45 up wing | |
| | 45 down | | Folder containing all raw data and video for the 45 down wing | |
| | 30 up | | Folder containing all raw data and video for the 30 up wing | |
| | 30 down | | Folder containing all raw data and video for the 30 down wing | |
| | 15 up | | Folder containing all raw data and video for the 15 up wing | |
| | 15 down | | Folder containing all raw data and video for the 15 down wing | |
| | Error | | Folder containing testing on the accuracy of test setup | |
| | Empty Tank | | Folder containing video data of empty tank | |
| | | | | |
| | Error of Measurement System | Error | Calculation of measurement system Error | Excel 2007 |

**Figure H.1 Definition of data provided on a hard drive to Dr. Merati for future researchers**